Recovering the Eikonal Quasinormal Mode Spectrum of the Schwarzschild Black Hole via the Penrose Limit

Masterarbeit der Philosophisch-naturwissenschaftlichen Fakultät
der Universität Bern

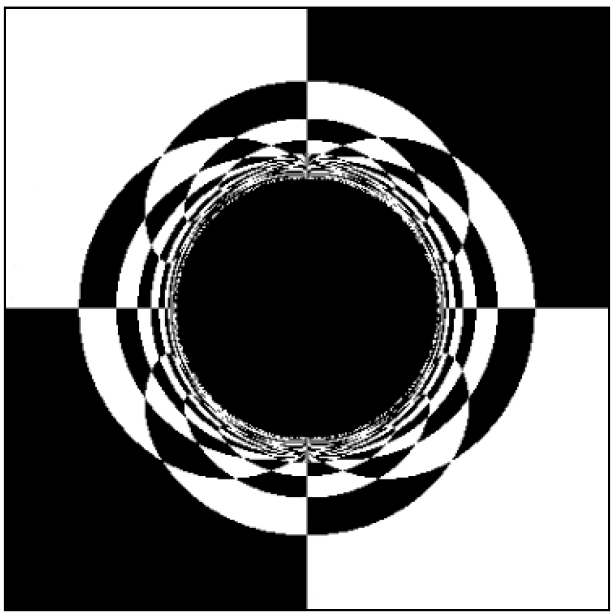

vorgelegt von

Slotboom Niels

2025

Supervisor

Professor M. Blau

Title page: Render of a Schwarzschild black hole in front of a checkerboard background at spatial infinity. Calculated by numerically tracing a family of 400×400 null geodesics with varying initial tangent vectors.

"It is by logic that we prove, but by intuition that we discover. To know how to criticise is good, to know how to create is better."

— Henri Poincaré

Acknowledgements

First and foremost, I would like to express my sincere gratitude to Matthias Blau for supervising my thesis. His wealth of knowledge and experience has been invaluable, allowing me to extend my own abilities and bring these pages to completion.

I am also deeply thankful to my friends, Leonardo Müller and Michael Schöni, for their companionship throughout this process. Whether discussing frustrations or spending time on completely unrelated things, their presence provided the balance and recharge I needed to continue my work.

Finally, I want to express my appreciation for the support of my family. In particular, I am grateful to my father for his time and effort in proofreading this thesis multiple times. As part of the extended family, I must also mention my cat, who spent hours lying in my room—completely oblivious to my work, yet somehow still a source of energy.

Contents

Acknowledgements 4
1 Preliminaries 7
1.1 Introduction 7
1.2 Plane Wave Metrics 10
1.2.1 Motivation 10
1.2.2 Rosen and Brinkmann Coordinates 11
1.2.3 Curvature 13
1.2.4 Geodesics 13
1.2.5 Symmetries 14
2 Penrose Limit 16
2.1 Adapted Coordinate Construction 16
2.2 The Hamilton-Jacobi Equation and Null Geodesic Congruences 17
2.3 Parallel Transport and Orthonormal Frames 19
2.3.1 Parallel Transport 19
2.3.2 Orthonormal Frames 19
2.4 Introduction to Geodesic Deviation and Congruences 21
2.4.1 The Transverse Geodesic Deviation Equation 21
2.4.2 Expansion of Congruences 23
2.5 Covariant Construction 25
3 Penrose Limit of Schwarzschild along the Photon Ring 28
3.1 Geodesics and Congruences 28
3.1.1 Geodesic Lagrangian and Conserved Quantities 28
3.1.2 The Photon Ring 29
3.1.3 Hamilton-Jacobi for Schwarzschild 29
3.2 Penrose Limit 32
3.2.1 Covariant Derivation 32
3.2.2 Relating Schwarzschild and Brinkmann Coordinates 34
3.2.3 Identifying Geometric Quantities in the Wave Profile 35
3.2.4 Explicit Form of the Isometry Algebra 36
4 Quasinormal Modes, Geometric Optics and WKB 37
4.1 Wave Equations and WKB 37
4.1.1 Quasinormal Mode Problem for Schwarzschild 37
4.1.2 The WKB Approximation 39
4.1.3 Schwarzschild QNMs from WKB 40
4.2 Geometric Optics Approximation and the Near Ring Region 43
4.2.1 Geometric Optics Approximation 43
4.2.2 QNM Boundary Conditions for Geometric Optics 44
4.2.3 The Near-Ring Region 45
4.2.4 Eikonal QNM Spectrum from Geometric Optics 47
4.2.5 Conserved Quantities from Emergent Symmetries 49
5 QNM Spectrum from the Penrose Limit Wave Equation 51
5.1 Penrose Limit and Near Ring Region 51
5.2 Quasinormal Mode Spectrum from Brinkmann Wave Equation 52
5.2.1 Stable Angular Direction 54
5.2.2 Unstable Radial Direction 55
5.2.3 Summary 56
5.3 Plane Wave Isometries and (Emergent) Symmetries in Schwarzschild 57

5.3.1 Scaling Limit of Spherical Harmonics and Ladder Operators 57
5.3.2 Emergent Symmetries of the Near-Ring Wave Equation 59
5.3.3 Completing the Isometry Algebra 62
5.4 Summary 64
Appendix A - Argument for the WKB Schutz-Will Method 66
Appendix B - Spectrum of the Inverted Harmonic Oscillator 66
Appendix C - Review: Spherical Harmonics 68
C.1 Algebraic Structure and Eigenvalues 68
C.2 Explicit Forms of the Eigenfunctions 70
Bibliography 71

1 Preliminaries

1.1 Introduction

Quasinormal modes (QNMs) describe the characteristic response of a black hole to small external perturbations, acting as the gravitational equivalent of a damped oscillator around an equilibrium state [1]. These perturbations can arise from various astrophysical processes, such as the accretion of matter, the scattering of gravitational waves, or the ringdown phase following a black hole merger. Once perturbed, the black hole begins to oscillate while emitting gravitational waves, resulting in a complex QNM frequency spectrum, where the imaginary part encodes the damping rate of the oscillation. QNMs play a crucial role in gravitational wave astronomy, as their detection by interferometers such as LIGO and Virgo provides a means to probe the fundamental properties of black holes and test general relativity in the strong-field regime. For the analysis of gravitational wave measurements, accurate theoretical predictions of QNM frequencies are essential, which has driven the development of various approximation methods. This thesis reviews two standard approaches and examines a more recent method based on the Penrose limit, aiming to understand why this approach yields the same results.

In more mathematical terms, (scalar) quasinormal modes are solutions to the massless wave equation

$$\Box_g \Phi = 0 \tag{1.1.1}$$

in the unperturbed background defined by the spacetime metric g. Since QNM solutions describe only the *reaction* to an external perturbation, they are required to have no incoming component, and hence must satisfy purely outgoing boundary conditions. More concretely, this means that the wave must propagate exclusively towards spatial infinity far from the black hole, and by causality, only towards the horizon near the black hole. In this thesis, we consider the QNMs of the Schwarzschild spacetime, with line element

$$ds^2 = -f(r)\,dt^2 + f(r)^{-1}\,dr^2 + r^2\,d\theta^2 + r^2\sin^2\theta\,d\varphi^2, \tag{1.1.2}$$

where $f(r) = 1 - \frac{2M}{r}$. Introducing the tortoise coordinate via $dr = f(r)\,dr_*$, the spherical and time-translation symmetries of the Schwarzschild spacetime allow the solutions of the wave equation to be decomposed into modes of the form

$$\Phi_{\omega\ell m}(x) = e^{-i\omega t}\frac{\psi_{\omega\ell}(r)}{r}Y_{\ell m}(\theta,\varphi). \tag{1.1.3}$$

Here, $Y_{\ell m}(\theta,\varphi)$ are spherical harmonics, and $\psi_{\omega\ell}(r)$ satisfies the radial wave equation

$$0 = \partial_{r_*}^2\psi_{\omega\ell} + [\omega^2 - \mathcal{V}_\ell(r_*)]\psi_{\omega\ell}, \quad \mathcal{V}_\ell(r_*) = f(r)\left[\frac{\ell(\ell+1)}{r^2} + \frac{2M}{r^3}\right]. \tag{1.1.4}$$

The outgoing boundary conditions are then implemented by requiring $\psi(r_*) \sim e^{\pm i\omega r_*}$ as $r_* \to \pm\infty$, ensuring purely outgoing behavior at spatial infinity, $r_* = \infty$, and purely infalling behavior at the horizon ($r_* = -\infty$).

Unfortunately, the Schrödinger-like radial wave equation (1.1.4) is not amenable to analytical solutions, increasing the difficulty of finding frequencies ω for which quasinormal mode solutions exist. Because of this, various approximation methods have been developed, a selection of which are presented in this thesis—two "standard" approximation methods,

the WKB [2] and geometric optics approximations, as well as a more recent approach involving the Penrose limit [3], [4]. Each of these methods ultimately leads to the so-called *eikonal QNM spectrum*, given by

$$\omega_{n\ell} = \frac{1}{3\sqrt{3}M}\left(\ell + \frac{1}{2}\right) - \frac{i}{3\sqrt{3}M}\left(n + \frac{1}{2}\right). \tag{1.1.5}$$

The first approximation method, WKB, was first applied to the quasinormal mode problem by Schutz and Will in 1985 [5]. As a first step, we will reproduce their findings. In essence, WKB solutions of equation (1.1.4)—subject to the quasinormal mode boundary conditions —can exist for ω and ℓ such that the single minimum of the function $Q(r_*) = \omega^2 - \mathcal{V}_\ell(r_*)$ takes on a small negative value, remaining positive everywhere on $\mathbb{R}$ except for a narrow region containing the minimum. Within this narrow region, the function $Q(r_*)$ can be expanded to second order around the minimum, leading to an inverted harmonic oscillator equation, ultimately giving rise to the quantisation condition

$$i\frac{Q_0}{\sqrt{2Q_0''}} = n + \frac{1}{2}, \quad n \in \mathbb{N}_0, \tag{1.1.6}$$

where Q_0 and Q_0'' denote the values of $Q(r_*)$ as well as its second derivative with respect to r_* at the position of the minimum. Since ω appears in the expression for Q_0, this quantisation condition can be solved for the approximate quasinormal mode frequencies. Therefore, approximating the quasinormal mode frequencies can be achieved with just two pieces of information about the spacetime—the value of the potential $\mathcal{V}_\ell$ and its second derivative at its maximum, located near the characteristic Schwarzschild photon sphere at $r = 3M$. In other words, the quasinormal mode spectrum is already determined approximately by the local properties of the spacetime around the potential's maximum, with outgoing asymptotic behaviour of the solutions being ensured automatically through WKB matching.

Given that the eikonal QNM spectrum is determined by the local properties of the spacetime near $r = 3M$, we then employ the geometric optics approximation, which interprets wave solutions in terms of null geodesic congruences[1] generated by a Hamilton-Jacobi function S. More concretely, geometric optics employs the ansatz $\Phi = Ae^{iS}$, where A is a scalar amplitude function that varies slowly with respect to the Hamilton-Jacobi principal function S appearing in the oscillatory term. In this approximation framework, quasinormal mode boundary conditions translate into conditions on the radial geodesic motion. Specifically, they require the presence of a double root in the radial geodesic equation

$$\dot{r}^2 = E^2 - f(r)\frac{L^2}{r^2}, \tag{1.1.7}$$

leading to $r = 3M$ and $L = 3\sqrt{3}ME$. This configuration of geodesic parameters causes the null geodesic congruence associated with the principal function S to embed photon ring geodesics—unstable null orbits with $r = 3M$, $\dot{r} = 0$. Following the approach of [6], we then restrict our attention to the near-ring region, which selects geodesics that remain close to the photon ring. This approximation isolates the contributions from the vicinity of the photon ring at $r = 3M$, which was identified to be sufficient to determine the eikonal QNM

[1] A geodesic congruence is a family of geodesic curves such that each point in spacetime is traversed by exactly one geodesic within the family.

spectrum with the WKB approach. By expanding S in the near-ring region and solving the transport equation for A, we obtain a geometric optics solution of the wave equation corresponding to the $n = 0$ mode of the eikonal QNM spectrum (1.1.5).

Due to the structure of the amplitude transport equation for A, new solutions can be generated from existing ones by multiplying A by powers of a conserved quantity q, i.e., a quantity transported along the geodesic congruence associated with the principal function S. Following [4], we derive such a quantity, which accounts for the $n > 0$ overtone modes in the spectrum (1.1.5). One standard way to construct such conserved is by acting on S with a Killing vector K, defining $q = K[S]$. However, the derived quantity does not fall into this pattern. Instead, it can be expressed as the action of a non-Killing vector X on S, that is, $q = X[S]$. This suggests the existence of *emergent symmetries*—vector fields that, while not true Killing symmetries of the full spacetime, nonetheless generate new solutions —within a specific region in spacetime—from certain existing ones.

In a recent publication, Fransen [3] demonstrated that the eikonal QNM spectrum (1.1.5) can be derived from the wave equation in a Penrose limit of the Schwarzschild metric. This result was later extended in a more detailed analysis by Kapec and Sheta [4]. The Penrose limit, broadly speaking, associates a limiting plane wave spacetime to a given spacetime metric and a null geodesic. This limiting plane wave has a much simpler structure than the original spacetime and can be understood as a simultaneous boost onto and "zoom" into the selected null geodesic while preserving local geodesic deviation properties. Consequently, it serves as an approximation of the original spacetime in the vicinity of the chosen null geodesic. When this limit is applied to a photon ring geodesic in the Schwarzschild spacetime, the resulting line element,

$$ds^2 = 2\,du\,dv + \frac{1}{3M^2}(x_1^2 - x_2^2)\,du^2 + d\boldsymbol{x}^2, \tag{1.1.8}$$

provides an effective description of the Schwarzschild spacetime near the photon sphere—the specifics of this somewhat loose statement will be examined in detail throughout this thesis. Furthermore, we will show that the wave modes in the Schwarzschild spacetime that remain non-singular under this Penrose limit correspond precisely to the near-ring modes studied with the geometric optics approximation.

This motivates the study of wave solutions in the Penrose-limiting spacetime, as they are expected to correspond to solutions ("lifts") in the full Schwarzschild spacetime. The significantly simpler form of the plane wave metric allows the corresponding wave equation to be solved analytically, enabling a complete classification of its quasinormal modes. This classification reveals a double-ladder structure, where the isometry generators of the plane wave spacetime act as ladder operators (called $a_\pm$ and $b_\pm$) on a fundamental mode. These operators generate a two-dimensional harmonic structure: one stable direction, corresponding to the angular θ-direction in Schwarzschild, and one unstable (inverted) direction, corresponding to the radial coordinate r.

These plane wave mode solutions can be lifted to the Schwarzschild spacetime, yielding a corresponding double-ladder structrue composed of near-ring modes. These modes scale into the plane wave solutions under the Penrose limit. The most straightforward way of making this identification is to determine lifts of the fundamental mode as well as the ladder operators that act on it to obtain higher order modes. As a first step in this analysis, one can expand the radial wave equation (1.1.4) around the near-ring region, turning it into an inverted harmonic oscillator equation. Its "ground" state is then found to scale into the

radial contribution to the fundamental mode. Moreover, in the limit $\ell \to \infty$ simultaneous to the Penrose scaling limit, the remainder of the Schwarzschild mode solution (1.1.3) reproduces both the u, v and the angular dependence of the wave mode solution in the plane wave spacetime.

Having identified the fundametal mode's lift, we then seek vector fields in Schwarzschild spacetime that scale into the ladder operators $a_\pm$ and $b_\pm$. The Schwarzschild isometry generators $J_\pm$, which act as raising and lowering operators on the spherical harmonics, naturally scale into $a_\mp$. However, the operators $b_\pm$, which act on the radial direction, cannot originate from Schwarzschild Killing symmetries. Instead analysing the near-ring approximation of the radial wave equation (1.1.4) reveals a decomposition in terms of new ladder operators $X_\pm$, which act as emergent symmetries of the Schwarzschild near-ring region. These $X_\pm$ operators scale into $b_\pm$, completing the identification and demonstrating that emergent symmetries in Schwarzschild can be promoted to exact Killing symmetries in the Penrose limit. Furthermore, this identification confirms that the quasinormal mode spectrum obtained in the plane wave spacetime aligns with the eikonal spectrum of Schwarzschild, (1.1.5).

Thesis Overview: This thesis is structured as follows: We begin by reviewing the necessary theoretical background, covering plane wave metrics that result from taking a Penrose limit in Section 1.2, and both the original and covariant constructions of the Penrose limit in Section 2, introducing required concepts such as orthonormal frames and parallel transport where necessary.
In Section 3, we compute relevant objects related to the Schwarzschild spacetime—such as geodesic congruences, Hamilton-Jacobi functions and a specific Penrose limit onto the equatorial photon ring—which will be essential for the remainder of the thesis.
Next, Section 4.1 introduces the scalar quasinormal mode problem of the Schwarzschild black hole and the WKB approximation, which we then use to derive the approximate eikonal quasinormal mode spectrum. Building on this, Section 4.2 applies insights from the WKB procedure to a second approximation scheme—the geometric optics approximation, applied in the so-called near-ring region. After introducing geometric optics in a general setting, this allows us to identify the geometric quantities that appear in the eikonal quasinormal mode spectrum—quantities that also emerge in the wave profile of the Penrose limit, hinting at a connection between the two.
Finally, Section 5 provides a complete classification of the quasinormal mode solutions of the wave equation in the plane wave spacetime obtained from the Penrose limit, linking them to its isometry algebra. Furthermore, we derive lifts to the Schwarzschild spacetime of the functions and ladder operators involved in this classification, revealing an analogous double-ladder structure of near-ring Schwarzschild wave solutions. This ultimately explains how the eikonal quasinormal mode spectrum of the Schwarzschild spacetime can be recovered from its equatorial photon ring Penrose limit.

1.2 Plane Wave Metrics

1.2.1 Motivation

The simplest model used to describe gravitational waves assumes that the metric can be written as a small perturbation around flat Minkowski space,

$$g_{\mu\nu} = \eta_{\mu\nu} + h_{\mu\nu}, \tag{1.2.1}$$

where $h_{\mu\nu}$ is assumed to be small. At leading order in h, the Einstein equations linearise, and in an appropriate coordinate gauge, a plane-fronted wave propagating in the z-direction has the form

$$ds^2 = -dt^2 + dz^2 + d\boldsymbol{x}^2 + h_{ij}(z-t)\,dx^i\,dx^j \tag{1.2.2}$$

in coordinates (t, z, x^i), $i = 1, 2$. Introducing the lightcone coordinates

$$U = \frac{1}{\sqrt{2}}(z-t), \quad V = \frac{1}{\sqrt{2}}(z+t), \tag{1.2.3}$$

the metric takes the form

$$ds^2 = 2\,dU\,dV + g_{ij}(U)\,dx^i\,dx^j, \quad \text{where} \quad g_{ij}(U) = \delta_{ij} + h_{ij}(U). \tag{1.2.4}$$

This is the prototypical form of a *plane wave metric in Rosen coordinates*. However, instead of requiring a weak perturbation h_{ij} around δ_{ij}, plane wave metrics are exact solutions to Einstein's equations, and therefore allow, in principle, for arbitrary wave profiles $g_{ij}(U)$. They hence extend the concept of gravitational waves beyond the linearised approximation.

Due to their simple form, plane wave metrics serve as an important toy model for exploring various theoretical concepts. In particular, they exhibit a high degree of symmetry —the Rosen form above has the manifest Killing vectors ∂_V and ∂_i, along with a further, less obvious Killing vector for each of the transverse dimensions enumerated by i. This symmetry simplifies calculations in the corresponding spacetime, including solving the geodesic and scalar wave equations. Furthermore, plane wave metrics have a significantly sparser curvature structure compared to more familiar spacetimes like Schwarzschild, with many components of the Riemann tensor vanishing.

Unfortunately, however, the Rosen coordinates introduced above have a high degree of residual coordinate gauge freedom, meaning different choices of coordinates can retain the same form of the metric but obscure physical features. Further, they are often plagued by coordinate singularities, making them inconvenient for a global description of the spacetime. A more suitable choice, alleviating both of these issues, is provided by *Brinkmann coordinates*, which will be introduced in the next section. Using this formulation, we will then analyse the curvature, geodesics and symmetries of plane wave spacetimes in more detail, based on [7], adapted to suit this thesis.

1.2.2 Rosen and Brinkmann Coordinates

As introduced in the previous section, a generic plane wave metric in $D = d + 2$ dimensions has the line element

$$d\bar{s}^2 = 2\,dU\,dV + \bar{g}_{ij}(U)\,dY^i\,dY^j \tag{1.2.5}$$

in Rosen coordinates $Y^\mu = (U, V, Y^i)$, where $i = 1, ..., d$ enumerates the transverse directions. In the following, we will typically use bars, as with $\bar{g}_{ij}$, to indicate plane wave quantities. This distinction will be crucial in the context of the Penrose limit, which associates a plane wave spacetime to any pair consiting of a spacetime and a null geodesic. To illustrate both the residual gauge freedom and the coordinate singularities often prevalent in this form, consider the two line elements

$$ds^2 = 2\,dU\,dV + U^2\,d\boldsymbol{Y}^2, \quad d\tilde{s}^2 = 2d\tilde{U}d\tilde{V} + d\tilde{\boldsymbol{y}}^2. \tag{1.2.6}$$

Both are plane wave metrics of the Rosen form, with the latter simply being the Minkowski line element. The former has a coordinate singularity at $U = 0$, where the determinant of the metric is zero. Nonetheless, the two metrics are related by the change of coordinates

$$\tilde{U} = U, \quad \tilde{y}^i = U y^i, \quad \tilde{V} = V - \frac{1}{2} U^{-1} \tilde{\boldsymbol{y}}^2, \tag{1.2.7}$$

exemplifying residual coordinate gauge freedom and explicitly showing that $U = 0$ is merely a coordinate singularity of the former metric.

Having motivated the need for a better coordinate system, we now introduce the *Brinkmann form* of a plane wave metric, which is given by

$$d\bar{s}^2 = 2\,du\,dv + A_{ab}(u) x^a x^b\, du^2 + d\boldsymbol{x}^2. \tag{1.2.8}$$

Here, $X^\alpha = (u, v, x^a)$, $a = 1, ..., d$ are called *Brinkmann coordinates* and $A_{ab}(u)$ is a u-dependent symmetric matrix called the *wave profile*. Before showing that any plane wave metric can be brought from Rosen into Brinkmann form, let us analyse its coordinate singularities and residual gauge freedom. We have $\det g = -1$, meaning that the Brinkmann form is non-singular everywhere. Concerning gauge freedom, the $2\,du\,dv$ term restricts reparametrisations of u and v while retaining this form without producing additional terms. In addition, the transverse coordinates x^a enter g_{uu} only quadratically, which restricts possible redefinitions of x^a while preserving the metric's form. As an added bonus to the absence of coordinate singularities and low residual gauge freedom, we will see later on that the curvature of this metric directly incorporates A_{ab}—it is rare that functions appearing in the components of the metric have an immediate geometric interpretation.

It remains to show that any plane wave metric in the Rosen form (1.2.5) can be brought into the Brinkmann form (1.2.8) by an appropriate change of coordinates. The Brinkmann form features a particularly simple transverse structure, $d\boldsymbol{x}^2$, which can be achieved by introducing a U-dependent $d \times d$ matrix $\bar{E}^i_a(U)$ such that

$$\bar{g}_{ij}(U) \bar{E}^i_a(U) \bar{E}^j_b(U) = \delta_{ab}. \tag{1.2.9}$$

This transforms the transverse Rosen metric $g_{ij}(U)$ into its normal form. We further require this matrix to satisfy the symmetry condition

$$\dot{\bar{E}}_{ai} \bar{E}^i_b = \dot{\bar{E}}_{bi} \bar{E}^i_a \tag{1.2.10}$$

where the overdot denotes differentiation with respect to U, and indices are raised and lowered using δ_{ab} and g_{ij}, respectively. Such *parallel-transported vielbeins*, a concept that we will introduce in Section 2.3, always exist and automatically satisfy this condition. We will demonstrate this in Section 2.5, where we will have established the necessary theoretical background. The new coordinates $X^\alpha = (u, v, x^a)$ are then defined by

$$U = u, \quad V = v + \frac{1}{2} \dot{\bar{E}}_{ai} \bar{E}^i_b x^a x^b, \quad Y^i = \bar{E}^i_a x^a. \tag{1.2.11}$$

This transformation brings the Rosen form (1.2.5) into the desired Brinkmann form (1.2.8). The resulting wave profile A_{ab} is given by

$$A_{ab}(u) = \ddot{\bar{E}}_{ai}(u) \bar{E}^i_b(u). \tag{1.2.12}$$

In essence, the coordinate transformation (1.2.11) performs U-dependent linear transformations on the coordinate directions Y^i to bring g_{ij} into its normal form δ_{ab}, while the shift from V to v ensures the emergence of the desired lightcone structure and simultaneously removes potential $du\,dx^a$ terms.

1.2.3 Curvature

The curvature of plane wave spacetimes is particularly simple, with many components of the Riemann tensor vanishing identically. Explicitly, the non-zero components of the Riemann tensor in Rosen coordinates are given by

$$\bar{R}_{iUjU} = -\frac{1}{2}\partial_U^2 \bar{g}_{ij} + \frac{1}{4}\bar{g}^{k\ell}\left[\partial_U \bar{g}_{jk}\partial_U \bar{g}_{i\ell}\right]. \tag{1.2.13}$$

In Brinkmann coordinates, the Riemann tensor has an even simpler form, with the wave profile A_{ab} making an explicit appearance as

$$\bar{R}_{aubu} = -A_{ab}. \tag{1.2.14}$$

The Ricci tensor then only has a single non-trivial component,

$$\bar{R}_{uu} = -\delta^{ab}A_{ab}, \tag{1.2.15}$$

from which we infer that a plane wave spacetime is a vacuum solution if and only if the wave profile is traceless. For plane wave metrics, all scalar curvature invariants (Ricci scalar, Kretschmann scalar etc.) vanish identically as $g^{u\alpha} = \delta^\alpha_v$.

For the covariant construction of the Penrose limit in Section 2.5, we further note that the non-zero Rosen and Brinkmann components of the Riemann tensor are related by

$$\begin{aligned}\bar{R}_{aubu} &= J^\mu_a J^\nu_u J^\rho_b J^\sigma_u \bar{R}_{\mu\nu\rho\sigma} \\ &= \bar{E}^i_a \bar{E}^j_b \Big(\delta^\nu_U + \dot{\bar{E}}^k_a x^a \delta^\nu_k\Big)\Big(\delta^\sigma_U + \dot{\bar{E}}^\ell_b x^b \delta^\sigma_\ell\Big)\bar{R}_{i\nu j\sigma} = \bar{E}^i_a \bar{E}^j_b \bar{R}_{iUjU}\end{aligned} \tag{1.2.16}$$

where $J^\mu_\alpha = \frac{\partial Y^\mu}{\partial X^\alpha}$ is the Jacobian of the transformation (1.2.11). The first step made use of $\bar{R}_{V\alpha\beta\gamma} = 0$. All other terms vanish due to $\bar{R}_{ijk\alpha} = 0$ as is evident from (1.2.13)—the $\bar{R}_{UiUj}$ are the only non-zero components.

1.2.4 Geodesics

Although we will not need it in the following, studying the geodesics of a spacetime is often a useful way to develop intuition about its structure. Since this thesis primarily deals with null geodesics, we focus on those.

A generic plane wave spacetime in Brinkmann coordinates has the geodesic Lagrangian

$$\mathcal{L} = \frac{1}{2}g_{\mu\nu}\dot{X}^\mu\dot{X}^\nu = \dot{u}\dot{v} + \frac{1}{2}A_{ab}(u)x^a x^b \dot{u}^2 + \frac{1}{2}\dot{\boldsymbol{x}}^2 \tag{1.2.17}$$

where $X^\mu(\tau) = (u, v, x^a)$ is the coordinate embedding of the geodesic parameterised by the affine parameter τ. Since the Lagrangian is independent of v, we have a conserved momentum

$$p_v = \frac{\partial\mathcal{L}}{\partial\dot{v}} = \dot{u}. \tag{1.2.18}$$

Through a reparametrisation of τ, we can set $p_v = 1$, implying $u(\tau) = \tau$, up to an additive constant. With this, the null geodesic Lagrangian simplifies to

$$\mathcal{L} = \dot{v} + \frac{1}{2}A_{ab}(u)x^a x^b + \frac{1}{2}\dot{\boldsymbol{x}}^2. \tag{1.2.19}$$

The Euler-Lagrange equations then yield the transverse equations of motion,

$$\ddot{x}^a = A_{ab}(\tau)x^b, \tag{1.2.20}$$

which describe a set of harmonic oscillator equations for the transverse directions x^a.

It remains to find an equation for the coordinate v. For a null geodesic, we impose $\mathcal{L} = 0$, from which we derive the first integral of the equation of motion for $v(\tau)$,

$$\dot{v} = -\frac{1}{2}A_{ab}(u)x^a x^b + \frac{1}{2}\dot{\boldsymbol{x}}^2. \tag{1.2.21}$$

Once the transverse coordinate embeddings $x^a(\tau)$ are determined, the function $v(\tau)$ can be obtained by integrating this equation. We note here that one particular geodesic that always exists is the one given by $u(\tau) = \tau$, $v(\tau) = x^a(\tau) = 0$.

1.2.5 Symmetries

As mentioned before, plane wave spacetimes have a high degree of symmetry. This section presents their generic Killing vectors in both Rosen and Brinkmann coordinates and touches upon the corresponding Heisenberg isometry algebra.

In Rosen coordinates and $D = d + 2$ dimensions, there are $d + 1$ manifest Killing vectors,

$$Z = \partial_V \quad \text{and} \quad Q_i = \partial_i, \quad i = 1, ..., d, \tag{1.2.22}$$

which are Killing as a consequence of the V- and Y^i-independence of the Rosen form of any given plane wave metric. It is straightforward to verify that the vectors

$$P^i = y^i \partial_V - C^{ij}\partial_j \quad \text{where} \quad \dot{C}^{ij} = g^{ij} \tag{1.2.23}$$

also satisfy the Killing equation. Here, an overdot refers to a derivative with respect to the coordinate U. These complete the isometry algebra of the plane wave metric, which takes the form

$$[Q_i, Z] = 0, \quad [P^i, Z] = 0, \quad [Q_i, P^j] = \delta^i_j Z, \tag{1.2.24}$$

which is a $(2d + 1)$-dimensional Heisenberg algebra with central element Z.

In Brinkmann coordinates, we only have a single manifest Killing vector, $Z = \partial_v$, since the metric explicitly depends on both u and x^a. However, since the dimension (and structure) of the isometry algebra is coordinate-independent, an additional set of $2d$ Killing vectors must exist. These are given by

$$X_f = f_a \partial_a - \dot{f}_a x^a \partial_v \tag{1.2.25}$$

where $f_a(u)$ solves the harmonic oscillator equation $\ddot{f}_a = A_{ab} f_b$. This second-order linear differential equation in d dimensions admits $2d$ linearly independent solutions, which define $2d$ linearly independent Killing vectors, yielding the expected total of $2d + 1$, together

with Z. An appropriate choice of linear combinations ensures that they satisfy the same commutation relations as in the Rosen case, with $Z = \partial_v = \partial_V$ as the central element.

It is worth emphasising that the Heisenberg algebra appearing here is directly related to the algebra of the Schrödinger equation for the (inverted) harmonic oscillator in quantum mechanics, which emerges when solving the wave equation in a plane wave spacetime. As we will see later on, the isometry algebra acts as a set of ladder operators on solutions of the wave equation, allowing for a systematic construction of mode solutions.

2 Penrose Limit

The following delineates the concept of the *Penrose limit*, as first introduced by Sir Roger Penrose in 1976 [8]. The Penrose limit (PL) maps a spacetime manifold M and a chosen null geodesic γ to a corresponding limiting plane wave spacetime manifold M_γ. This limiting spacetime can be interpreted as the result of simultaneously zooming[2] into an infinitesimal neighbourhood of γ while applying a boost along its direction.

We begin by reviewing Penrose's original definition, which relies on adapted coordinates. Subsequently, we develop the necessary theory of null geodesic congruences, parallel transport, and orthonormal frames, enabling a more modern and covariant formulation of the Penrose limit as first presented in [9]. This provides the foundation for deriving the Penrose limit of the Schwarzschild geometry along a specific class of null geodesics, which we will undertake in Section 3.

2.1 Adapted Coordinate Construction

The original construction of the Penrose limit relies on the introduction of a coordinate system adapted to the chosen null geodesic. This section specifies the conditions these coordinates must satisfy and demonstrates how the introduction of a positive parameter λ implements a simultaneous parameterised large volume limit and boost onto the geodesic γ. We then investigate how this leads to a meaningful plane wave metric in Rosen coordinates in the limit $\lambda \to 0$.

The central idea is to embed the geodesic γ in a null geodesic congruence, i.e., a family of null geodesics such that each point in the spacetime is traversed by precisely one geodesic. We introduce the coordinate U as an affine parameter along this null congruence. The corresponding tangent vector field ∂_U must then be both null and geodesic, implying

$$g_{UU} = 0, \quad \nabla_U \partial_U = 0. \tag{2.1.1}$$

The latter condition is equivalent to requiring $\Gamma_{\alpha UU} = 0$, which due to

$$\Gamma_{\alpha UU} = \frac{1}{2}\big(2g_{\alpha U,U} - \underbrace{g_{UU,\alpha}}_{=0}\big) = \partial_U g_{\alpha U} \tag{2.1.2}$$

is equivalent to $g_{\alpha U}$ being U-independent. Since a congruenc in a D-dimensional manifold is parameterised by $D-1$ independent coordinates, we can use its parameters as the remaining coordinates, denoted by (V, Y^i) with $i = 1, ..., D-2$. A particularly simple way to enforce the U-independence of $g_{\alpha U}$ is to choose

$$g_{\alpha U} = \delta^V_\alpha. \tag{2.1.3}$$

This choice leads to a metric in what we call the *adapted coordinate form*,

$$\begin{aligned} ds^2 = {} & 2\,dU\,dV + a(U,V,Y^i)\,dV^2 + b_i(U,V,Y^i)\,dV\,dY^i \\ & + g_{ij}(U,V,Y^i)\,dY^i\,dY^j. \end{aligned} \tag{2.1.4}$$

Correspondingly, we call the coordinates (U, V, Y^i) *adapted coordinates*. As we will see, this form of the metric is suited for taking the Penrose limit. Additionally, it reveals the roles of

[2] More formally, this is a large volume limit.

U and V as lightcone coordinates, with Y^i serving as transverse spacelike coordinates to γ. In the next section, we explicitly construct adapted coordinates using the Hamilton-Jacobi principal function, demonstrating their existence for any spacetime and null geodesic.

We now introduce a parameter $\lambda > 0$ to parameterise both the boost and the large volume limit. In lightcone coordinates, a boost is performed by rescaling U and V as

$$(U, V) \to (\lambda^{-1}U, \lambda V) \tag{2.1.5}$$

while leaving the transverse coordinates Y^i unchanged. The large volume limit entails rescaling all coordinates by λ, i.e. $X^\alpha \to \lambda X^\alpha$, while simultaneously rescaling the line element as $ds^2 \to \lambda^{-2} ds^2$. Combined, the action of the boost and the large volume limit result in the coordinate and line element rescaling

$$(U, V, Y^i) \to (U, \lambda^2 V, \lambda Y^i), \quad ds^2 \to \lambda^{-2} ds^2. \tag{2.1.6}$$

Applying this to the adapted coordinate form (2.1.4) of the metric yields

$$\begin{aligned} ds^2 \to\ & 2\,dU\,dV + \lambda^2 a(U, \lambda^2 V, \lambda Y^i)\,dV^2 + \lambda b_i(U, \lambda^2 V, \lambda Y^i)\,dV\,dY^i \\ & + g_{ij}(U, \lambda^2 V, \lambda Y^i)\,dY^i\,dY^j. \end{aligned} \tag{2.1.7}$$

The Penrose limit can now be taken as the limit $\lambda \to 0$, resulting in the *Penrose limit line element* or simply *Penrose limit*

$$d\bar{s}^2 = 2\,dU\,dV + \bar{g}_{ij}(U)\,dY^i\,dY^j \tag{2.1.8}$$

where

$$\bar{g}_{ij}(U) = g_{ij}(U, 0, 0) \tag{2.1.9}$$

is the restriction of the transverse metric to the null geodesic γ. Notice here that the condition (2.1.3) on the components of the metric in adapted coordinates is necessary to prevent singular behaviour—U-components other than g_{UV} would result in at least $\mathcal{O}(\lambda^{-1})$ divergence in the limit $\lambda \to 0$, as for example, $dU\,dY^i \to \lambda^{-1}\,dU\,dY^i$. We close this section by remarking that equation (2.1.3) is the line element of a plane wave metric in Rosen coordinates, which can be brought into the more convenient Brinkmann form by the coordinate transformation from Section 1.2.2.

2.2 The Hamilton-Jacobi Equation and Null Geodesic Congruences

This section introduces the Hamilton-Jacobi (HJ) equation in the context of general relativity, and demonstrates how it can be used to find so-called null geodesic congruences. Explicitly, we consider the central *null Hamilton-Jacobi equation*,

$$g^{\mu\nu}\partial_\mu S \partial_\nu S = 0, \tag{2.2.1}$$

where $S(x)$ is a scalar called the *principal* or *Hamilton-Jacobi* function and $g^{\mu\nu}$ denotes the inverse metric of the D-dimensional spacetime. Note that equation (2.2.1) effectively states that the gradient $\ell_\mu \equiv \partial_\mu S$ of the principal function is null, i.e. $\ell_\mu \ell^\mu = 0$. By analogy, one can also formulate spacelike and timelike HJ equations; however, they are not relevant to this thesis. Therefore, we will omit the null specifier when referring to equation (2.2.1).

A consequence of the HJ-equation is that the contravariant gradient ℓ^μ is geodesic, meaning that $\ell^\mu \nabla_\mu \ell^\nu = 0$. By exploiting the symmetry of second covariant derivatives of scalars, the geodesic property can be shown succinctly as

$$\ell^\mu \nabla_\mu \ell_\nu = g^{\mu\lambda}\partial_\lambda S \nabla_\mu \partial_\nu S = g^{\mu\lambda}\partial_\lambda S \nabla_\nu \partial_\mu S = \frac{1}{2}\partial_\nu \underbrace{\left(g^{\mu\lambda}\partial_\mu S \partial_\lambda S\right)}_{=0} = 0. \tag{2.2.2}$$

Therefore, the integral lines along the flow of ℓ^μ, i.e. curves parameterised by $x^\mu(u)$ satisfying

$$\dot{x}^\mu(u) = \ell^\mu(x(u)) = g^{\mu\nu}\partial_\nu S(x(u)), \tag{2.2.3}$$

are null geodesic curves with tangent vector ℓ^μ. Thus, ℓ^μ is the tangent field of a *(null) geodesic congruence*, i.e. a $(D-2)$-parameter family of null geodesic curves such that each point in spacetime is traversed by exactly one geodesic.

In the remainder of this thesis, HJ principal functions and their corresponding null geodesic congruences will appear frequently. The principal function is an efficient tool for finding the flow fields of particular congruences—integrating them as in eq. (2.2.3) to find parameterised geodesic curves is often unnecessary. Although finding a general solution to the HJ-equation in e.g. the Schwarzschild geometry is typically impossible, imposing additional restrictions motivated by symmetries of the given spacetime often leads to useful solutions. We will encounter this for Schwarzschild in Section 3.1.3.

One important application of the principal function is the construction of adapted coordinates. Suppose S generates a null congruence with tangent field

$$\ell^\mu = g^{\mu\nu}\partial_\nu S \tag{2.2.4}$$

which embeds the chosen null geodesic γ. Let U be an affine parameter along the congruence, and define $V = S$. Then, we have

$$\partial_U = \ell^\mu \partial_\mu = g^{\mu\nu}\partial_\mu S \partial_\nu. \tag{2.2.5}$$

Since

$$0 = g^{\mu\nu}\partial_\mu S \partial_\nu S = \partial_U V, \tag{2.2.6}$$

it follows that V is a constant of integration along all geodesics in the congruence generated by $S = V$. The remaining $D-2$ independent constants of integration of equation (2.2.3) can be used as the transverse coordinates Y^i—they complete (U, V, Y^i) into an adapted coordinate system, since

$$\begin{aligned} 1 &= \partial_U U = g^{\mu\nu}\partial_\mu V \partial_\nu U = g^{VU}, \\ 0 &= \partial_U V = g^{\mu\nu}\partial_\mu V \partial_\nu V = g^{VV}, \\ 0 &= \partial_U Y^i = g^{\mu\nu}\partial_\mu V \partial_\nu Y^i = g^{Vi}. \end{aligned} \tag{2.2.7}$$

More compactly, this can be written as $g^{V\mu} = \delta^\mu_U$, which is equivalent[3] to $g_{U\mu} = \delta^V_\mu$—as required by the form (2.1.3) of the metric components. Since we may assume without loss of generality that the integration constants of γ satisfy $V = Y^i = 0$, this completes the construction.

[3]This is shown by $g_{U\mu} = g_{\rho\mu}\delta^\rho_U = g_{\rho\mu}g^{V\rho} = \delta^V_\mu$.

2.3 Parallel Transport and Orthonormal Frames

Parallel transport and orthonormal frames are two fundamental concepts in differential geometry that we will need for the upcoming covariant construction of the Penrose limit. This section briefly introduces them in a general setting.

2.3.1 Parallel Transport

The general idea of parallel transport is as follows: we take an object, such as a vector, at a point p on a manifold, and transport it along a curve γ to another point q. During this process, we ensure that the object remains "parallel" to itself, meaning that its direction and magnitude do not change relative to the connection on the manifold. In more formal terms, we call a tensor T *parallel transported* or simply *parallel along* γ if

$$\nabla_{\dot\gamma} T = \dot x^\mu \nabla_\mu T = 0, \tag{2.3.1}$$

assuming that γ is affinely parameterised by $x^\mu(u)$ and an overdot indicates a derivative with respect to u.

The most familiar example of a parallel transported vector is the tangent field $\ell = \ell^\mu \partial_\mu = \dot x^\mu \partial_\mu$ of a geodesic parameterised by $x^\mu(u)$. Specifically, the tangent of a geodesic γ is parallel along γ—to see this, consider

$$\begin{aligned} \nabla_\ell \ell = \ell^\mu \nabla_\mu (\ell^\nu \partial_\nu) &= \underbrace{(\ell^\mu \partial_\mu \ell^\nu)}_{=\frac{d}{du}} \partial_\nu + \ell^\mu \ell^\nu \Gamma^\lambda{}_{\mu\nu} \partial_\lambda \\ &= \left[\frac{d}{du} \ell^\lambda + \Gamma^\lambda{}_{\mu\nu} \ell^\mu \ell^\nu \right] \partial_\lambda = 0, \end{aligned} \tag{2.3.2}$$

where the last equality holds by the geodesic equation.

2.3.2 Orthonormal Frames

For any D-dimensional manifold M with local coordinates $\{x^\mu\}$, the coordinate vector fields

$$\{\partial_\mu\} = \left\{ \frac{\partial}{\partial x^\mu} \right\} \tag{2.3.3}$$

form a basis of the tangent space T_pM at each point $p \in M$, and the corresponding one-forms $\{dx^\mu\}$ form a basis of the cotangent space T_p^*M. However, any other set of linearly independent vector fields can just as well serve as a basis of TM, and likewise for T^*M. More generally, given a smooth matrix field $E_a^\mu(x)$ taking values in $\mathrm{GL}(D)$, with inverse $E_\mu^a(x)$, we can define an alternative local basis

$$\{E_a\} = \{E_a^\mu \partial_\mu\}, \quad \{E^a\} = \{E_\mu^a \, dx^\mu\} \tag{2.3.4}$$

of TM and T^*M, respectively. Such bases are called (co)frames, and allow one to express any tensor in terms of its *frame components* in place of its *coordinate components*. For example, a $(1,1)$-tensor T can be written as

$$\begin{aligned} T &= T^\mu{}_\nu [\partial_\mu \otimes dx^\nu] = T^\mu{}_\nu [E_\mu^a E_a \otimes E_b^\nu E^b] \\ &= E_\mu^a E_b^\nu T^\mu{}_\nu [E_a \otimes E^b] \equiv T^a{}_b [E_a \otimes E^b]. \end{aligned} \tag{2.3.5}$$

Here, $T^{\mu}{}_{\nu}$ are the *coordinate components*, while $T^{a}{}_{b} = E^{a}_{\mu} E^{\nu}_{b} T^{\mu}{}_{\nu}$ are the *frame components* with respect to the frame E_a. The lowercase Latin indices $a, b, ...$ used here are referred to as *frame indices*, which differ from coordinate indices in that they do not transform under coordinate changes but rather under local $\mathrm{GL}(D)$-transformations of the (co)tangent space bases. As a result, the frame components $T^{a}{}_{b}$ remain invariant under coordinate transformations.

In any spacetime, a particularly important tensor is the metric tensor, whose frame components are given by

$$g_{ab} = E^{\mu}_{a} E^{\nu}_{b} g_{\mu\nu}. \tag{2.3.6}$$

This transformation can be viewed as a two-sided matrix transformation of the metric, analogous to $g \to E^{\top} g E$. There always exists a choice of frame such that the metric takes its Sylvester normal form, i.e. a diagonal matrix with entries given by the metric's signature. In particular, for a Lorentzian metric, there exist matrix-valued functions $E^{\mu}_{a}(x)$ with inverses $E^{a}_{\mu}(x)$, called *vielbeins* or *orthonormal frames*, such that

$$E^{\mu}_{a}(x) E^{\nu}_{b}(x) g_{\mu\nu} = \eta_{ab}, \tag{2.3.7}$$

where $\eta = \mathrm{diag}(-1, 1, ..., 1)$ is the D-dimensional Minkowski metric. From special relativity, we know that such orthonormal frames are unique up to local Lorentz transformations, as the Minkowski metric is invariant under them.

In this thesis, so-called *pseudo-orthonormal frames* $\{E_A\}$, with $A = +, -, a$, and $a = 1, ..., D-2$ will appear frequently. These are analogous to orthonormal frames, as they bring the metric into Minkowskian form,

$$E^{\mu}_{A}(x) E^{\nu}_{B}(x) g_{\mu\nu} = \eta_{AB}, \tag{2.3.8}$$

but here, η_{AB} refers to the Minkowski metric in lightcone coordinates, which has the nonzero components

$$\eta_{+-} = 1, \quad \eta_{ab} = \delta_{ab}. \tag{2.3.9}$$

This structure implies that the vectors $E_{\pm}$ are null, while the E_a are spacelike. An equivalent condition to equation (2.3.8) is that the line element be cast into

$$ds^2 = E^{+} E^{-} + \delta_{ab} E^{a} E^{b}. \tag{2.3.10}$$

The distinction between an orthonormal and a pseudo-orthonormal frame will not always be made explicitly in the following but should be clear from context, particularly from the use of uppercase Roman indices $A, B, ...$. It is importent to note that the raising and lowering of indices of orthonormal and pseudo-orthonormal frames can be performed using the respective metrics, e.g. the inverse frame can be computed as

$$E^{A}_{\mu} = \eta^{AB} g_{\mu\nu} E^{\nu}_{B}. \tag{2.3.11}$$

To conclude our terminology, we introduce *parallel frames*. For a curve γ, we call a frame $\{E_a\}$ *parallel along* γ if

$$\nabla_{\dot{\gamma}} E_a = 0, \tag{2.3.12}$$

i.e. if all frame legs are parallel along the curve. In the following, we will frequently deal with parallel pseudo-orthonormal frames, which are unique up to *global* Lorentz-transformations.

2.4 Introduction to Geodesic Deviation and Congruences

2.4.1 The Transverse Geodesic Deviation Equation

In this section, we derive the transverse geodesic deviation equation—a linear differential equation dictating the evolution of a geodesic deviation vector along a congruence of null geodesics. The presented derivation closely follows Section 12.3 of [10]. The geodesic deviation matrix that appears in this equation will later be shown to encode the covariant information preserved under the Penrose limit.

We begin by considering a null geodesic congruence with tangent field ℓ, parameterised by an affine parameter u, satisfying

$$\nabla_\ell \ell = 0, \quad \ell^\alpha \ell_\alpha = 0. \tag{2.4.1}$$

Additionally, let ξ be a geodesic deviation vector field, which must satisfy the condition

$$\nabla_\ell \xi = \nabla_\xi \ell. \tag{2.4.2}$$

This condition follows naturally from the following construction: consider a one-parameter family of curves, labeled by s and parameterised by u, with coordinate embedding $x^\alpha(u, s)$. We define the tangent vector ℓ and geodesic deviation vector ξ as

$$\ell^\alpha = \frac{\partial}{\partial u} x^\alpha(u, s), \quad \xi^\alpha = \frac{\partial}{\partial s} x^\alpha(u, s). \tag{2.4.3}$$

Differentiating ξ along ℓ, we obtain

$$\nabla_\ell \xi^\beta = \frac{\partial}{\partial u} \xi^\beta + \Gamma^\beta{}_{\alpha\gamma} \ell^\alpha \xi^\gamma. \tag{2.4.4}$$

Similarly, differentiating ℓ along ξ yields

$$\nabla_\xi \ell^\beta = \frac{\partial}{\partial s} \ell^\beta + \Gamma^\beta{}_{\alpha\gamma} \xi^\alpha \ell^\gamma. \tag{2.4.5}$$

Due to the symmetry of the Christoffel symbols in the lower indices and the fact that

$$\frac{\partial}{\partial s} \ell^\beta = \frac{\partial^2}{\partial s \partial u} x^\beta = \frac{\partial}{\partial u} \xi^\beta, \tag{2.4.6}$$

we recover the geodesic deviation condition (2.4.2).

As a first step in deriving the geodesic deviation equation we show that the components of ξ along the congruence's tangent ℓ and an auxiliary null vector n are constant and can thus be discarded. Here, the auxiliary vector n satisfies the conditions

$$\ell_\alpha n^\alpha = 1, \quad n^\alpha n_\alpha = 0. \tag{2.4.7}$$

We first consider a contribution $\xi = c\ell$, where c is a scalar function. For ξ to be a valid geodesic deviation vector, condition (2.4.2) needs to be satisfied, implying that we must have

$$0 = c\nabla_\ell \ell = \nabla_{c\ell}\ell = \nabla_\xi \ell \overset{!}{=} \nabla_\ell \xi = (\nabla_\ell c)\ell + c\nabla_\ell \ell = \left(\frac{d}{du}c\right)\ell. \tag{2.4.8}$$

Therefore, $c = \text{const.}$ and may be set to zero without loss of generality, as it does not contribute to any interesting dynamics. Since the ℓ-component of ξ is isolated by $c = n_\alpha \xi^\alpha$, this result is equivalent to requiring $n_\alpha \xi^\alpha = 0$.

Next, we examine the component $\xi^\alpha \ell_\alpha$. Differentiating along ℓ, we find

$$\frac{d}{du}(\xi^\alpha \ell_\alpha) = (\nabla_\ell \xi)^\alpha \ell_\alpha = \big(\nabla_\xi \ell\big)^\alpha \ell_\alpha = \frac{1}{2}\nabla_\xi(\ell^\alpha \ell_\alpha) = 0, \tag{2.4.9}$$

which informs us that $\xi^\alpha \ell_\alpha = \text{const.}$ and we may hence set it to zero. Since $\xi^\alpha \ell_\alpha$ isolates the n-component of ξ, we infer that ξ has no interesting dynamics in the n-direction. In summary, we have shown that, without loss of generality, the geodesic deviation vector ξ satisfies the transversality conditions

$$\xi^\alpha n_\alpha = 0, \quad \xi^\alpha \ell_\alpha = 0. \tag{2.4.10}$$

We now introduce the *deformation matrix* $B_{\alpha\beta}$ of our null congruence as

$$B_{\alpha\beta} \equiv \nabla_\beta \ell_\alpha. \tag{2.4.11}$$

This allows us to express the geodesic deviation condition (2.4.2) in component form as

$$\nabla_\ell \xi^\alpha = B^\alpha{}_\beta \xi^\beta \tag{2.4.12}$$

which is a first-order linear evolution equation for the deviation vector ξ, with evolution matrix $B^\alpha{}_\beta$. Taking a second covariant derivative along ℓ, we find

$$\nabla_\ell^2 \xi^\alpha = \big(\nabla_\ell B^\alpha{}_\beta\big)\xi^\beta + B^\alpha{}_\beta\big(\nabla_\ell \xi^\beta\big) = \big[\nabla_\ell B^\alpha{}_\beta + B^\alpha{}_\gamma B^\gamma{}_\beta\big]\xi^\beta. \tag{2.4.13}$$

We now examine the bracketed expression in more detail. Substituting the definition of the deformation matrix, we find

$$\begin{aligned}
\nabla_\ell B^\alpha{}_\beta + B^\alpha{}_\gamma B^\gamma{}_\beta &= \ell^\gamma \nabla_\gamma \nabla_\beta \ell^\alpha + \nabla_\gamma \ell^\alpha \nabla_\beta \ell^\gamma \\
&= \ell^\gamma \nabla_\gamma \nabla_\beta \ell^\alpha - \ell^\gamma \nabla_\beta \nabla_\gamma \ell^\alpha + \nabla_\beta \underbrace{\big(\ell^\gamma \nabla_\gamma \ell^\alpha\big)}_{=0} \\
&= \ell^\gamma \big[\nabla_\gamma, \nabla_\beta\big]\ell^\alpha = R^\alpha{}_{\delta\gamma\beta}\ell^\delta \ell^\gamma,
\end{aligned} \tag{2.4.14}$$

where $[\cdot,\cdot]$ denotes the commutator. Thus, we conclude that ξ satisfies the *transverse null geodesic deviation equation*,

$$\nabla_\ell^2 \xi^\alpha = R^\alpha{}_{\delta\gamma\beta}\ell^\delta \ell^\beta \xi^\delta. \tag{2.4.15}$$

To express this equation in a form better suited for the covariant construction of the Penrose limit, we rewrite it in terms of a pseudo-orthonormal frame,

$$E_+ = \ell = \ell^\alpha \partial_\alpha, \quad E_- = n = n^\alpha \partial_\alpha, \quad E_a = E_a^\alpha \partial_\alpha \tag{2.4.16}$$

We assume this frame to be parallel transported along the flow of ℓ, meaning

$$\nabla_\ell E_A = 0, \quad A = +, -, a. \tag{2.4.17}$$

Here, the vectors E_a are necessarily spacelike vectors and complete the vectors ℓ and n to form a pseudo-orthonormal frame.

From the transversality conditions $\xi^\alpha \ell_\alpha = 0$ and $\xi^\alpha n_\alpha = 0$, we infer that the geodesic deviation vector ξ only contains components along E_a, or more concretely,

$$\xi = \xi^a E_a. \tag{2.4.18}$$

The equation (2.4.15) then implies that the transverse frame components ξ^a satisfy

$$\frac{d^2}{du^2}\xi_a = E_a^\alpha R_{\alpha\delta\gamma\beta} E_+^\delta E_+^\gamma E_b^\beta \xi^b = -R_{a+b+}\xi^b \tag{2.4.19}$$

Here, we note that the covariant derivatives ∇_ℓ may be replaced by ordinary derivatives $\frac{d}{du}$ when working with parallel frame components[4].

To summarise, we have derived the following results:

- The geodesic deviation vector can be expressed as a linear combination of the transverse frame legs,

$$\xi = \xi^a E_a, \tag{2.4.20}$$

  where $\{E_A\}$, $A = +, -, a$ forms a parallel pseudo-orthonormal frame, with E_+ aligned with the tangent field ℓ of the geodesic congruence.

- The transverse componens ξ^a satisfy the transverse geodesic deviation equation

$$\frac{d^2}{du^2}\xi_a = -R_{a+b+}\xi^b \equiv A_{ab}\xi^b. \tag{2.4.21}$$

- The required Riemann tensor components, which constitute the geodesic deviation matrix $A_{ab} = -R_{a+b+}$, can alternatively be computed using the frame components of the deformation matrix, $B_{ab} = E_a^\alpha E_b^\beta B_{\alpha\beta}$, provided a congruence is available. This can be done using the relation

$$\begin{aligned} A_{ab} = -R_{a+b+} &= R_{\alpha\delta\gamma\beta} E_a^\alpha E_+^\delta E_+^\gamma E_\beta^\delta = \left[R_{\alpha\delta\gamma\beta}\ell^\delta \ell^\gamma\right] E_a^\alpha E_b^\beta \\ &= \left[\nabla_\ell B_{\alpha\beta} + B_{\alpha\gamma}B^\gamma{}_\beta\right] E_a^\alpha E_b^\beta = \frac{d}{du}B_{ab} + B_{ac}B^c{}_b. \end{aligned} \tag{2.4.22}$$

2.4.2 Expansion of Congruences

Every geodesic congruence is associated with a characteristic scalar known as its *expansion*, Θ. Since it will appear briefly in a later section, we define it here and provide a short discussion of its geometric interpretation.

The *expansion* of a geodesic congruence with tangent field ℓ and deformation matrix $B_{\alpha\beta} = \nabla_\beta \ell_\alpha$ is defined as the trace

$$\Theta = g^{\alpha\beta} B_{\alpha\beta}. \tag{2.4.23}$$

To interpret its geometric meaning, we introduce a projector onto the transverse directions. Similar to the previous section, we define an auxiliary null vector n satisfying

[4]Due to $\nabla_\ell \xi = \nabla_\ell(\xi^a E_a) = (\partial_u \xi^a)E_a + \xi^a \underbrace{\nabla_\ell E_a}_{=0} = (\partial_u \xi^a)E_a$.

$$n^\alpha \ell_\alpha = -1, \quad n^\alpha n_\alpha = 0, \tag{2.4.24}$$

and use it to construct the projector

$$s_{\alpha\beta} = g_{\alpha\beta} + \big(\ell_\alpha n_\beta + n_\alpha \ell_\beta\big). \tag{2.4.25}$$

It is straightforward to verify that $B_{\alpha\beta}$ is transverse in the sense that

$$\ell^\alpha B_{\alpha\beta} = B_{\alpha\beta}\ell^\beta = 0. \tag{2.4.26}$$

As a result, we may express the expansion Θ as

$$\begin{aligned}\Theta &= s^{\alpha\beta}B_{\alpha\beta} = s^{\alpha\beta}\nabla_\alpha \ell_\beta = \frac{1}{2}s^{\alpha\beta}\big[\nabla_\alpha \ell_\beta + \nabla_\beta \ell_\alpha\big] \\ &= \frac{1}{2}s^{\alpha\beta}\mathcal{L}_\ell g_{\alpha\beta} = \frac{1}{2}s^{\alpha\beta}\mathcal{L}_\ell s_{\alpha\beta},\end{aligned} \tag{2.4.27}$$

where $\mathcal{L}_\ell$ denotes the Lie derivative along the tangent ℓ. The replacement of $g_{\alpha\beta}$ with $s_{\alpha\beta}$ in the last step follows from

$$\mathcal{L}_\ell g_{\alpha\beta} = \mathcal{L}_\ell\big(s_{\alpha\beta} - \ell_\alpha n_\beta - n_\alpha \ell_\beta\big) = \mathcal{L}_\ell s_{\alpha\beta} - \ell_\alpha \mathcal{L}_\ell n_\beta - (\mathcal{L}_\ell n_\alpha)\ell_\beta. \tag{2.4.28}$$

Here, the terms with $\mathcal{L}_\ell \ell = [\ell, \ell] = 0$ drop out, and the remaining terms other than $\mathcal{L}_\ell s_{\alpha\beta}$ are proportional to ℓ and hence vanish when contracting with $s^{\alpha\beta}$. This leads to the final expression

$$\Theta = \frac{1}{2}s^{\alpha\beta}\mathcal{L}_\ell s_{\alpha\beta}. \tag{2.4.29}$$

This result closely resembles the formula for the variation of the determinant,

$$\frac{1}{\sqrt{s}}\mathcal{L}_\ell \sqrt{s} = \frac{1}{2}s^{\alpha\beta}\mathcal{L}_\ell s_{\alpha\beta}. \tag{2.4.30}$$

Since $s_{\alpha\beta}$ projects onto the transverse spacelike directions of the congruence, this suggests an intuitive interpretation of Θ as describing the logarithmic rate of expansion or contraction of a transverse volume element $\sqrt{s}$ as it evolves along the congruence.

Although this interpretation is valid, there is a subtlety to address. Since $s_{\alpha\beta}$ is a projector onto the $D-2$ transverse directions, it does not have full rank, and hence its determinant vanishes. The mathematically rigorous way of interpreting Θ as measuring the rate of change in the magnitude of a transverse volume element involves defining the induced metric on the transverse submanifolds, where the determinant can be properly taken. However, as the purpose of this section is to provide only an intuitive understanding of expansion, the considerations outlined above are sufficient.

To conclude this section, let us examine the expression for the expansion of a geodesic congruence generated by a HJ principal function S. For such a congruence, the cotangent field is given by $\ell_\alpha = \partial_\alpha S$. Consequently, the expansion is computed as

$$\Theta = g^{\alpha\beta}B_{\alpha\beta} = g^{\alpha\beta}\nabla_\beta \partial_\alpha S = \Box_g S. \tag{2.4.31}$$

This means that a HJ principal function satisfies a wave equation with the expansion as its source term.

2.5 Covariant Construction

In Section 2.1, we introduced the Penrose limit following its original construction by Penrose. Unfortunately, it is not immediately clear which covariant properties of the original spacetime are preserved in the limit $\lambda \to 0$. Furthermore, the resulting plane wave metric naturally emerges in Rosen coordinates, which must then be transformed into the more convenient Brinkmann form.

To address these issues, Blau et al. [9] provide a fully covariant characterisation of the Penrose limit, which we review in this section. In essence, the covariant information preserved in the limit is encoded in the geodesic deviation matrix along the chosen null geodesic γ onto which the limit is taken. Specifically, the matrix elements are given by the frame components of the restriction of the Riemann tensor to γ, evaluated in a parallel pseudo-orthonormal frame—let us now derive these claims.

Before presenting the covariant construction of the Penrose limit, we first clarify the notation used throughout this section. Since we will be dealing with two distinct spacetimes and multiple coordinate systems, a careful distinction is necessary to avoid confusion. Our starting point is an arbitrary metric expressed in adapted coordinates[5] $x^\alpha = (U, V, Y^i)$, with the line element

$$ds^2 = 2\,dU\,dV + a(U,V,Y)\,dV^2 + b_i(U,V,Y)\,dV\,dY^i + g_{ij}(U,V,Y)\,dY^i\,dY^j. \quad (2.5.1)$$

In these coordinates, the selected null geodesic γ is parameterised by

$$x^\alpha(u) = (U = u, 0, 0). \quad (2.5.2)$$

From Section 2.1, we recall that the Penrose limit associated with the pair (ds^2, γ) results in the plane wave metric

$$d\bar{s}^2 = 2\,dU\,dV + \bar{g}_{ij}(U)\,dY^i\,dY^j \quad (2.5.3)$$

in Rosen coordinates, where

$$\bar{g}_{ij}(U) = g_{ij}(U, 0, 0) \quad (2.5.4)$$

is the restriction of the transverse metric in the original spacetime (2.5.1) to γ. We may bring this plane wave metric into Brinkmann form, which we denote by

$$d\bar{s}^2 = 2\,du\,dv + \bar{A}_{ab}(u)x^a x^b\,du^2 + d\boldsymbol{x}^2. \quad (2.5.5)$$

Throughout the following, we use the convention that a barred quantity, such as $\bar{R}_{\alpha\beta\gamma\delta}$, refers to an object in the Penrose limiting plane wave spacetime, whereas its unbarred counterpart, e.g. $R_{\alpha\beta\gamma\delta}$, denotes the corresponding object in the original spacetime.

We begin the covariant construction by relating the curvature tensors of the plane wave and the original spacetime. From Section 1.2.3, we recall that the plane wave metric (2.5.4) has the non-trivial Riemann tensor components

$$\bar{R}_{iUjU}(U) = -\frac{1}{2}\partial_U^2 \bar{g}_{ij} + \frac{1}{4}\bar{g}^{k\ell}\left[\partial_U \bar{g}_{jk}\partial_U \bar{g}_{i\ell}\right], \quad (2.5.6)$$

[5]Although this construction alludes to adapted coordinates, the final results will be valid in any coordinate system. Only the existence of adapted coordinates is relevant, not their actual construction for specific examples.

which depend only on the coordinate U. Curiously, computing the same Riemann tensor components in the original spacetime (2.5.1) gives

$$R_{iUjU}(U,V,Y) = -\frac{1}{2}\partial_U^2 g_{ij} + \frac{1}{4}g^{k\ell}\left[\partial_U g_{jk}\partial_U g_{i\ell}\right], \tag{2.5.7}$$

which has precisely the same form as its plane wave counterpart. Since the transverse metric in the Penrose limit is simply the restriction $\bar{g}_{ij} = g_{ij}|_\gamma$, and the above expression involves only U-derivatives of g_{ij}, we conclude that

$$\bar{R}_{iUjU} = R_{iUjU}|_\gamma. \tag{2.5.8}$$

Thus, the Penrose limit preserves certain components of the Riemann tensor along γ, while all others vanish.

Next, we introduce a γ-aligned parallel pseudo-orthonormal frame E_A, with indices $A = +, -, a$ and $a = 1, ..., D-2$, along the null geodesic γ in the original spacetime. This frame satisfies

$$\nabla_{\dot{\gamma}} E_A = 0, \quad E_+ = \partial_U, \tag{2.5.9}$$

i.e. E_+ is aligned with the tangent vector of the geodesic. Since the transverse frame vectors E_a are orthogonal to E_+, i.e.

$$g(E_+, E_a) = 0, \tag{2.5.10}$$

due to the structure of the metric it follows that they have no ∂_V-component and can be expressed as

$$E_a = E_a^U \partial_U + E_a^i \partial_i. \tag{2.5.11}$$

The transverse geodesic deviation matrix along γ, introduced in Section 2.4.1, is then given by

$$A_{ab} = -R_{a+b+} = -R_{\alpha\beta\gamma\delta}E_a^\alpha E_+^\beta E_b^\gamma E_+^\delta = -R_{iUjU}E_a^i E_b^j. \tag{2.5.12}$$

This relation shows that the Riemann tensor components R_{iUjU}—which are precisely the components preserved under the Penrose limit—encode the geodesic deviation around the null geodesic γ in the original spacetime.

We can push this analysis further and derive an explicit expression for the wave profile matrix $\bar{A}_{ab}(u)$ in the Brinkmann form (2.5.5) of the limiting plane wave. First, note that as a direct consequence of $E_a^V = 0$, the transverse frame components E_a^i diagonalise the transverse metric g_{ij}, meaning that

$$\delta_{ab} = g_{ij}E_a^i E_b^j \tag{2.5.13}$$

Since $\bar{g}_{ij}$ is simply the restriction of g_{ij} to γ, the same diagonalisation property holds for $\bar{g}_{ij}$. Furthermore, the symmetry condition (1.2.10) required for the coordinate transformation from Rosen to Brinkmann coordinates follows automatically as a consequence of parallel transport. To see this explicitly, we note that parallel transport implies

$$\nabla_U E_a^i = 0 \quad \Longrightarrow \quad \partial_U E_a^i = -\Gamma^i{}_{U\gamma}E_a^\gamma = -\Gamma^i{}_{Uj}E_a^j, \tag{2.5.14}$$

having made use of $\Gamma^i{}_{UU} = E^V_a = 0$. From this, we derive

$$\begin{aligned}\dot{E}_{ai}E^i_b &= \partial_U\left[g_{ij}E^j_a\right]E^i_b = \underbrace{\partial_U\left[g_{ij}E^j_aE^i_b\right]}_{=\partial_U\delta_{ab}=0} - g_{ij}E^j_a\partial_U E^i_b \\ &= \Gamma_{iUj}E^i_aE^j_b = \frac{1}{2}\left[\partial_U g_{ij}\right]E^i_aE^j_b,\end{aligned} \tag{2.5.15}$$

which is manifestly symmetric in a, b. This symmetry ensures that we can use E^i_a as the vielbein for the transformation from Rosen to Brinkmann coordinates, allowing us to set

$$\bar{E}^i_a = E^i_a|_\gamma. \tag{2.5.16}$$

From equation (1.2.16), we know the relationship of the nontrivial components of the plane wave Riemann tensor between Rosen and Brinkmann coordinates, which allows us to conclude

$$\begin{aligned}\bar{A}_{ab} &= -\bar{R}_{aubu} = -\bar{R}_{iUjU}\bar{E}^i_a\bar{E}^j_b = -R_{iUjU}E^i_aE^j_b|_\gamma \\ &= -R_{\alpha\beta\gamma\delta}E^\alpha_aE^\beta_+E^\gamma_bE^\delta_+|_\gamma = -R_{a+b+}|_\gamma = A_{ab}|_\gamma.\end{aligned} \tag{2.5.17}$$

This is a profound result. We have now established that the transverse geodesic deviation matrix A_{ab} along γ in the original spacetime is *exactly* the wave profile $\bar{A}_{ab}$ of the limiting plane wave. Furthermore, this provides a fully covariant expression for $\bar{A}_{ab}$,

$$\bar{A}_{ab} = -R_{a+b+}|_\gamma. \tag{2.5.18}$$

This result highlights an important conceptual advantage of the covariant approach to the Penrose limit—rather than relying on explicit coordinate constructions, we obtain a direct and manifestly covariant relation between the wave profile of the Penrose limit and the frame components of the Riemann tensor in the original spacetime. Moreover, since $\bar{A}_{ab} = -\bar{R}_{aubu}$ is the null geodesic deviation matrix for the null geodesic $x^\alpha(\tau) = (u = \tau, v = 0, y^a = 0)$ in the Penrose limit, we see that the limit retains information about the geodesic deviation properties of an infinitesimal neighbourhood around γ—a fact that is entirely obscured by the adapted coordinate construction.

As a final remark, recall from Section 2.4.1 that the transverse null geodesic deviation matrix can be computed from the frame components of the deformation matrix defined by a congruence which embeds γ,

$$B_{ab} = B_{\alpha\beta}E^\alpha_aE^\beta_b. \tag{2.5.19}$$

Using equation (2.4.22), we find that the wave profile is then given by

$$\bar{A}_{ab} = R_{+a+b} = \frac{d}{d\tau}B_{ab} + B_{ac}B^c{}_b. \tag{2.5.20}$$

Although we will not use it in this thesis, this alternative formula is sometimes useful when an embedding congruence is available.

3 Penrose Limit of Schwarzschild along the Photon Ring

Later in this thesis, we will compute the quasinormal mode spectrum of the Schwarzschild black hole using WKB and geometric optics approximations to the Schwarzschild wave equation, as well as the wave equation of its Penrose limit. These calculations will rely on certain results derived in this section.

3.1 Geodesics and Congruences

3.1.1 Geodesic Lagrangian and Conserved Quantities

In this section, we derive the information about null geodesics and null geodesic congruences in the Schwarzschild spacetime that we will need in the following. We denote the Schwarzschild line element by

$$ds^2 = -f(r)\,dt^2 + f(r)^{-1}\,dr^2 + r^2\,d\theta^2 + r^2\sin^2\theta\,d\varphi^2, \tag{3.1.1}$$

where $f(r) = 1 - \frac{2M}{r}$ is the metric function with mass parameter M. We make use of the usual interpretation for the Schwarzschild coordinates $x^\mu = (t, r, \theta, \varphi)$.

It is typically argued that it suffices to only consider equatorial geodesics with $\theta = \frac{\pi}{2}$, since all other geodesics can be obtained by rotations of these, owing to the spherical symmetry of the problem. To produce global geodesic congruences, however, it is much more convenient to assume geodesics to run in polar planes, i.e. at fixed values of φ. This implies $\dot\varphi = 0$ and allows us to write the geodesic Lagrangian as

$$\mathcal{L} = -\frac{1}{2}f(r)\dot t^2 + \frac{1}{2}f(r)^{-1}\dot r^2 + \frac{1}{2}r^2\dot\theta^2, \tag{3.1.2}$$

where an overdot indicates a derivative with respect to the affine parameter u along the geodesic. The Lagrangian is independent of t and θ, which leads to the conserved quantities

$$\begin{aligned} E &\equiv -\frac{\partial\mathcal{L}}{\partial\dot t} = f(r)\dot t \quad &\Rightarrow \quad \dot t = f(r)^{-1}E, \\ L &\equiv \frac{\partial\mathcal{L}}{\partial\dot\theta} = r^2\dot\theta \quad &\Rightarrow \quad \dot\theta = \frac{L}{r^2}. \end{aligned} \tag{3.1.3}$$

Plugging these into the Lagrangian (3.1.2) and employing the null condition $\mathcal{L} = 0$ necessary to find null geodesics yields another first integral,

$$\dot r^2 = E^2 - f(r)\frac{L^2}{r^2} \equiv E^2 - 2V_{\text{eff}}(r), \qquad V_{\text{eff}}(r) = f(r)\frac{L^2}{2r^2}, \tag{3.1.4}$$

where we call $V_{\text{eff}}(r)$ the *effective (radial, geodesic) potential*. Differentiating with respect to u once more leads to the equation

$$\ddot r = -V'_{\text{eff}}(r), \tag{3.1.5}$$

with a prime denoting a derivative of V_{eff} with respect to r. For a particular choice of E and L, solving the equations for $\dot t, \dot r, \dot\theta$ with initial conditions $x^\mu(u_0) = (t_0, r_0, \theta_0, \varphi_0)$ gives us a geodesic. By appropriately varying three of the four initial coordinate values[6], we produce

[6]Since $\dot\varphi = 0$, we necessarily have to vary φ_0 to produce a congruence, as otherwise the family of curves will only be able to fill a three-dimensional submanifold of the four-dimensional spacetime.

a *geodesic congruence*, i.e. a three-parameter family of geodesics with the property that each point in a subset of the spacetime manifold is traversed by exactly one geodesic. By the above, its tangent field is given by

$$\dot{x}^\mu(t,r,\theta,\varphi) = \left(f(r)^{-1}E, \pm\sqrt{E^2 - 2V_{\text{eff}}(r)}, \frac{L}{r^2}, 0\right). \tag{3.1.6}$$

In some instances that we will specify in the following section, we will also need equatorial geodesics, i.e. geodesics with $\theta = \frac{\pi}{2}$. An analogous derivation to the above yields the first integrals

$$\dot{t} = f(r)^{-1}E, \quad \dot{\varphi} = \frac{L}{r^2}, \quad \dot{\theta} = 0, \quad \dot{r}^2 = E^2 - 2V_{\text{eff}}(r). \tag{3.1.7}$$

Notice that now, $L = \frac{\partial \mathcal{L}}{\partial \dot{\varphi}}$ is an angular momentum associated to the coordinate φ instead of θ. Nonetheless, the dynamics of t and r are the same as in the polar case, as one expects from spherical symmetry.

3.1.2 The Photon Ring

In the remainder of the thesis, a geodesic class of particular interest—along with its associated Penrose limits, for reasons that will be discussed later—are the bound unstable photon orbits characteristic of the Schwarzschild geometry. We proceed with the setup from Section 3.1.1 and require $\dot{r} = \ddot{r} = 0$ to obtain the circular orbit. This is equivalent to demanding that $V_{\text{eff}}(r_0) = \frac{1}{2}E^2$, $V'_{\text{eff}}(r_0) = 0$, where r_0 is the constant value of r along the circular geodesic. Explicitly solving these equations leads to the radius $r_0 = 3M$ as well as the impact parameter $L/E = 3\sqrt{3}M$. For the so-called *photon sphere* hypersurface at $r = 3M$, we further note that $f(3M) = \frac{1}{3}$. There are two particularly simple parametrisations of photon ring geodesics—firstly, we have the *polar* photon ring geodesics, parameterised by

$$t_\gamma(u) = 3Eu + t_0, \quad r_\gamma(u) = 3M, \quad \theta_\gamma(u) = 3\Omega E u + \theta_0, \quad \varphi_\gamma(u) = \varphi_0. \tag{3.1.8}$$

Here, $\Omega = \left(3\sqrt{3}M\right)^{-1}$ is the orbital frequency with respect to t, $\Omega = \frac{d}{dt}\theta_\gamma = \dot{\theta}_\gamma/\dot{t}_\gamma$. By the rotational symmetry, any origin-centered circle with radius $3M$ is an unstable circular orbit, and hence we also have *equatorial* photon ring geodesics, parameterised by

$$t_\gamma(u) = 3Eu + t_0 \quad r_\gamma(u) = 3M, \quad \theta_\gamma(u) = \frac{\pi}{2}, \quad \varphi_\gamma(u) = 3\Omega E u + \varphi_0. \tag{3.1.9}$$

Here, $\Omega = \frac{d}{dt}\varphi_\gamma = \dot{\varphi}_\gamma/\dot{t}_\gamma$—nonetheless, it takes on the same value as for the polar case.

In the subsequent sections, we will make use of both polar and equatorial geodesics, as depending on the context, one may be easier to deal with than the other. In particular, it is much simpler to find a globally defined Hamilton-Jacobi function for which the associated congruence embeds polar photon ring geodesics, which we will need when dealing with geometric optics. Conversely, the association between Schwarzschild coordinates and the Brinkmann coordinates of the Penrose limit is much clearer if the limit is taken onto an equatorial photon ring geodesic.

3.1.3 Hamilton-Jacobi for Schwarzschild

In this section, we derive an adequately but not completely general solution to the Hamilton-Jacobi equation

$$g^{\mu\nu}\partial_\mu S\partial_\nu S = 0 \tag{3.1.10}$$

for the Schwarzschild geometry. Similar to Section 3.1.1, we leverage the symmetries of the spacetime to restrict the form of the Hamilton-Jacobi function S.

As a first step, let us take a step back and review Killing vectors and tensors as well as their associated conserved geodesic quantities. A Killing vector $K = K^\mu\partial_\mu$ is a vector satisfying

$$\mathcal{L}_K g_{\mu\nu} = 0 \quad \Leftrightarrow \quad \nabla_\mu K_\nu + \nabla_\nu K_\mu = 0, \tag{3.1.11}$$

where the latter equality is referred to as the *Killing equation*. The symbol $\mathcal{L}_K$ denotes the Lie-derivative along K—the former equation thus effectively states that K generates an isometry of the metric. Given a Killing vector and a geodesic parameterised by $x^\mu(u)$, the quantity $Q = K_\mu\dot{x}^\mu$ is conserved, where an overdot indicates the derivative d/du. Indeed, we can check

$$\frac{d}{du}Q = \dot{x}^\mu\nabla_\mu(K_\nu\dot{x}^\nu) = K_\nu\underbrace{\dot{x}^\mu\nabla_\mu\dot{x}^\nu}_{=0} + \dot{x}^\mu\dot{x}^\nu\nabla_\mu K_\nu = \dot{x}^\mu\dot{x}^\nu\underbrace{\nabla_{(\mu}K_{\nu)}}_{=0} = 0 \tag{3.1.12}$$

and hence Q is conserved along the geodesic. Higher rank Killing tensors generalise this concept. By definition, a rank r Killing tensor is a symmetric tensor $K_{\mu_1\ldots\mu_r} = K_{(\mu_1\ldots\mu_r)}$ that satisfies the generalised Killing equation

$$\nabla_{(\nu}K_{\mu_1\ldots\mu_r)} = 0. \tag{3.1.13}$$

The case of rank $r = 1$ reproduces the (vectorial) Kiling equation. By a one-line proof analogous to (3.1.12), one can show that the quantity

$$Q = K_{\mu_1\ldots\mu_r}\dot{x}^{\mu_1}\ldots\dot{x}^{\mu_r} \tag{3.1.14}$$

is conserved along any given geodesic. Killing tensors are also referred to as *hidden symmetries* in some contexts. We conclude this review by noting that the sum as well as the tensor product of two Killing tensors is a Killing tensor as well. In particular, if $K = K^\mu\partial_\mu$ is a Killing vector, then $K_\mu K_\nu$ is a Killing tensor.

We now return to the Hamilton-Jacobi formalism. Suppose S is a solution to the Hamilton-Jacobi equation (3.1.10) and K a Killing vector of the spacetime with an associated conserved quantity we denote by Q_K. Then, $\partial_\mu S$ is the cotangent field of a geodesic congruence (cf. Section 2.2), and the function

$$K[S] \equiv K^\mu\partial_\mu S = K^\mu\dot{x}_\mu = Q_K \tag{3.1.15}$$

evaluated at a point x yields the value of Q_K for the unique geodesic in the congruence that passes through x. In principle, the value of Q_K can be different for each geodesic. However, we can also turn this around—we can impose that S not only be a solution to the Hamilton-Jacobi equation, but should additionally satisfy the first integral

$$Q_K = K[S], \tag{3.1.16}$$

where Q_K is now a constant fixed to the same value for all geodesics in the congruence. This is akin to how we used conserved quantities to get first integrals of the geodesic equation in Section 3.1.1.

By the same token, we can impose additional conditions on S using conserved quantities associated to higher rank Killing tensors. For example, for a rank 2 Killing tensor $T_{\mu\nu}$, we can impose

$$T^{\mu\nu}\partial_\mu S \partial_\nu S = Q_T \tag{3.1.17}$$

for a global constant Q_T. Although the imposition of such conditions restricts the solution space of the Hamilton-Jacobi equation and hence results in a loss of generality, they allow us to find certain solutions in a more systematic and physically motivated manner.

Let us now proceed to derive a solution of the Hamilton-Jacobi equation for the Schwarzschild geometry, which has the Killing vectors

$$\begin{aligned} K_{(0)} &= \partial_t, \\ K_{(1)} &= \sin\varphi\,\partial_\theta + \cot\theta\cos\varphi\,\partial_\varphi, \\ K_{(2)} &= -\cos\varphi\,\partial_\theta + \cot\theta\sin\varphi\,\partial_\varphi, \\ K_{(3)} &= \partial_\varphi. \end{aligned} \tag{3.1.18}$$

The first Killing vector encodes the time-translation symmetry of the metric, whereas the $K_{(a)}$ for $a = 1, 2, 3$ generate the $\mathfrak{so}(3)$-algebra associated to its spherical symmetry[7]. The vector $K_{(0)}$ defines an associated conserved energy $E = -K^{(0)}_\mu \dot{x}^\mu$ while the $K_{(a)}$ are linked to conserved angular momenta $L_a = K^{(a)}_\mu \dot{x}^\mu$ aligned with the directions of the "cartesian" coordinates

$$x^1 = r\sin\theta\cos\varphi, \quad x^2 = r\sin\theta\sin\varphi, \quad x^3 = r\cos\theta. \tag{3.1.19}$$

We demand our Hamilton-Jacobi function to have the same energy E and angular momentum component L_3 for each of the geodesics in its corresponding congruence, i.e. we impose

$$K_{(0)}[S] = -E, \quad K_{(3)}[S] = L_3. \tag{3.1.20}$$

This already simplifies the form of $S(x)$ to

$$S(t, r, \theta, \varphi) = -Et + \tilde{S}(r, \theta) + L_3\varphi. \tag{3.1.21}$$

To further restrict the form of our solution, we impose an additional constraint, for which we define the Killing tensor

$$T = \delta_{ab}\Big(K_{(a)} \otimes K_{(b)}\Big) = \partial_\theta \otimes \partial_\theta + \frac{1}{\sin^2\theta}\partial_\varphi \otimes \partial_\varphi. \tag{3.1.22}$$

Since this tensor is formed as a tensor product of Killing vectors, it is evidently a Killing tensor. Its associated conserved quantity is the squared magnitude of the angular momentum vector,

$$T_{\mu\nu}\dot{x}^\mu\dot{x}^\nu = \delta_{ab}K^{(a)}_\mu K^{(b)}_\nu \dot{x}^\mu\dot{x}^\nu = \delta_{ab}L_aL_b = \boldsymbol{L}^2, \qquad \boldsymbol{L} = (L_1, L_2, L_3). \tag{3.1.23}$$

[7]In particular, we have $\big[K_{(a)}, K_{(b)}\big] = -\varepsilon_{abc}K_{(c)}$; for a more detailed discussion of these Killing vectors, see [10] section 9.5. The Schwarzschild metric has a rank 2 isometry group, which allows us to impose two independent first integrals of the form $K[S] = Q_K = \text{const.}$ for two commuting Killing vectors without overrestricting the solution.

Thence, we can impose the third condition

$$\boldsymbol{L}^2 = T^{\mu\nu}\partial_\mu S \partial_\nu S \tag{3.1.24}$$

which fixes the $\boldsymbol{L}^2$ of all geodesics in the congruence to the same value. Imposing this third condition further restricts the form of (3.1.21) to

$$S(t, r, \theta, \varphi) = -Et + S_r(r) + \int \sqrt{\boldsymbol{L}^2 - \frac{L_3^2}{\sin^2\theta}}\, d\theta + L_3\varphi. \tag{3.1.25}$$

Finally, inserting this into the Hamilton-Jacobi equation leads us to

$$0 = g^{\mu\nu}\partial_\mu S \partial_\nu S = f(r)^{-1}E^2 + f(r)(S_r'(r))^2 + \frac{\boldsymbol{L}^2}{r^2} \tag{3.1.26}$$

which implies

$$S_r(r) = \int \varepsilon(r) f(r)^{-1}\sqrt{E^2 - f(r)\frac{\boldsymbol{L}^2}{r^2}}\, dr = \int \varepsilon(r)\sqrt{E^2 - 2V_{\text{eff}}(r)}\, dr_*, \tag{3.1.27}$$

where $\varepsilon(r) \in \{-1, 1\}$ is a sign used to make the integrand differentiable across roots of the square root.

To summarise, we have achieved the following: By making use of the symmetries of the Schwarzschild metric, we have derived a solution to the Hamilton-Jacobi equation. The congruence it defines is such that all geodesics in it share the same energy E, angular momentum component L_3 as well as magnitude $\boldsymbol{L}^2$. Notice that we recover the polar congruence from Section 3.1.1 by setting $\boldsymbol{L}^2 = L^2$ and $L_3 = 0$.
Here, we also encounter an issue when we attempt to embed a polar geodesic with $\boldsymbol{L} = (0, 0, L_3)$, $L_3 \neq 0$ into the generated congruence. In this scenario, we have $\boldsymbol{L}^2 = L_3^2$. Therefore the $d\theta$ integral in equation (3.1.25) is defined only for $\theta = \frac{\pi}{2}$, leading to a Hamilton-Jacobi function that is defined only in the equatorial plane. Of course, there exist Hamilton-Jacobi functions and corresponding congruences that embed polar geodesics, but they are much harder to find since the S derived here is the most general separable solution, i.e. the most general S of the form

$$S(t, r, \theta, \varphi) = S_t(t) + S_r(r) + S_\theta(\theta) + S_\varphi(\varphi). \tag{3.1.28}$$

More general solutions are no longer separable, which significantly increases the complexity of finding them.

3.2 Penrose Limit

3.2.1 Covariant Derivation

In this section, we derive the Penrose limit of the Schwarzschild metric along the equatorial photon ring geodesic (3.1.9). As we have noted before, finding an embedding congruence is tedious—because of this, we opt to compute the wave profile matrix A_{ab} directly from the geodesic deviation using the Riemann tensor's frame components,

$$A_{ab} = -R_{+a+b}|_\gamma \tag{3.2.1}$$

where + and a refer to the legs of a parallel pseudo-orthonormal frame E_A, $A = +, -, a$ along the geodesic. Such a frame is given by

$$\begin{aligned} E_+ &= E_+^\alpha \partial_\alpha = \partial_u = 3\partial_t + \frac{1}{\sqrt{3}M}\partial_\varphi, \\ E_- &= E_-^\alpha \partial_\alpha = \frac{1}{6}\left(1 - \frac{u^2}{9M^2}\right)\partial_u - \partial_t + \frac{u}{9M}\partial_r, \\ E_1 &= E_1^\alpha \partial_\alpha = -\frac{u}{3\sqrt{3}M}\partial_u + \frac{1}{\sqrt{3}}\partial_r, \\ E_2 &= E_2^\alpha \partial_\alpha = \frac{1}{3M}\partial_\theta. \end{aligned} \tag{3.2.2}$$

Here we have set the geodesic energy to $E = 1$, which can always be achieved by a reparametrisation of the geodesics and hence does not result in a loss of generality. Notice that the frame components

$$R_{+a+b}|_\gamma = R_{\alpha\beta\gamma\delta} E_+^\alpha E_a^\beta E_+^\gamma E_b^\delta|_\gamma \tag{3.2.3}$$

are independent of the ∂_u- or equivalently E_+-components of the E_a, as $R_{+++A} = 0$ by symmetry of the Riemann tensor. Moreover, equation (2.5.16) is also independent of any ∂_u components of the transverse frame legs, which allows us to drop them and rather work with the simpler frame[8]

$$\begin{aligned} E_+ &= \partial_u = 3\partial_t + \frac{1}{\sqrt{3}M}\partial_\varphi, \\ E_1 &= \frac{1}{\sqrt{3}}\partial_r, \\ E_2 &= \frac{1}{3M}\partial_\theta. \end{aligned} \tag{3.2.4}$$

The relevant nonzero components of the Riemann tensor, restricted to the photon ring geodesic (3.1.9), read[9]

$$\begin{aligned} R_{trtr} &= -\frac{2}{27M^2}, \quad & R_{\varphi r\varphi r} &= -1, \\ R_{t\theta t\theta} &= \frac{1}{9}, & R_{\varphi\theta\varphi\theta} &= 6M^2. \end{aligned} \tag{3.2.5}$$

With these, we compute the frame components

$$\begin{aligned} R_{+1+1}|_\gamma &= R_{trtr}(E_1^r)^2(E_+^t)^2 + R_{\varphi r\varphi r}(E_1^r)^2(E_+^\varphi)^2 = -\frac{1}{3M^2}, \\ R_{+2+2}|_\gamma &= R_{t\theta t\theta}\big(E_2^\theta\big)^2(E_+^t)^2 + R_{\varphi\theta\varphi\theta}\big(E_2^\theta\big)^2(E_+^\varphi)^2 = \frac{1}{3M^2}. \end{aligned} \tag{3.2.6}$$

The off-diagonal components $R_{+1+2}|_\gamma = R_{+2+1}|_\gamma$ are zero because of $R_{trt\theta} = R_{\varphi r\varphi\theta} = 0$. Thus, the nonzero components of the wave profile are

[8] We omit writing down E_- since we do not need it.

[9] These components were computed using [11], a symbolic tensor calculus library I developed in Python to check analytical calculations and ensure accuracy in computations related to my thesis work.

$$A_{11} = -A_{22} = \frac{1}{3M^2} \tag{3.2.7}$$

and the Penrose limit of the Schwarzschild metric along the equatorial photon ring is given by

$$ds^2 = 2\,du\,dv + \frac{1}{3M^2}(x_1^2 - x_2^2)\,du^2 + d\boldsymbol{x}^2. \tag{3.2.8}$$

As a closing remark, we note that due to the spherical symmetry of the Schwarzschild metric, this result is universal in the sense that any photon ring geodesic (polar, equatorial or any other) leads to this Penrose limit, although of course, the interpretation of x_1 and x_2 will differ when relating back to Schwarzschild coordinates.

3.2.2 Relating Schwarzschild and Brinkmann Coordinates

In this section, we follow [4] to derive an association between the Schwarzschild coordinates (t, r, θ, φ) and the Brinkmann coordinates (u, v, x^a) of the Penrose limit (3.2.8). This association is essential for identifying relationships between wave solutions of the plane wave spacetime and the original Schwarzschild spacetime, such as imposing consistent boundary conditions.

As mentioned before, the Penrose limit of the Schwarzschild metric onto a photon ring geodesic, for our context, is most conveniently performed using the equatorial photon ring geodesic (3.1.9). This is because the coframe legs associated to the pseudo-orthonormal frame (3.2.4), reading

$$\begin{aligned} E^- &= (E_+)^\flat = -dt + 3\sqrt{3}M\,d\varphi, \\ E^1 &= (E_1)^\flat = \sqrt{3}\,dr, \\ E^2 &= (E_2)^\flat = 3M\,d\theta, \end{aligned} \tag{3.2.9}$$

are exact[10] and hence (locally) define a coordinate basis. More precisely, integrating this frame motivates the definition of the coordinates

$$v = -t + \underbrace{3\sqrt{3}M}_{=\Omega^{-1}}\varphi, \quad \rho = \sqrt{3}(r - 3M), \quad \psi = 3M\Big(\theta - \frac{\pi}{2}\Big). \tag{3.2.10}$$

This can be extended to a full coordinate system by introducing $t = 3u$, motivated by the t-coordinate parametrisation (3.1.9) of the equatorial photon ring.
To solidify the association between this coordinate system (u, v, ρ, ψ) and (u, v, x^1, x^2), we briefly recompute the Penrose limit. To this end, in the spirit of the rescalings of the adapted coordinate construction[11], we rescale $v \to \lambda^2 v$, $\psi \to \lambda\psi$, $\rho \to \lambda\rho$ for a positive parameter λ. We may then express the Schwarzschild coordinates as

[10] A differential p-form ω is exact if there exists a differential $(p-1)$-form η such that $\omega = d\eta$.

[11] Under the Penrose limit rescaling $U \to U$, $V \to \lambda^2 V$, $Y \to \lambda Y$ consistent with the Rosen-to-Brinkmann coordinate transformation which is (figuratively) given by $u = U$ $v = V + \frac{1}{2}\dot{E}Ex^2$, $x = EY$.

$$
\begin{aligned}
t &= 3u, \\
r &= \frac{\lambda}{\sqrt{3}}\rho + 3M, \\
\theta &= \frac{\lambda}{3M}\psi + \frac{\pi}{2}, \\
\varphi &= 3\Omega u + \Omega\lambda^2 v.
\end{aligned}
\tag{3.2.11}
$$

Using the expansions

$$
\begin{aligned}
f(r) &= \frac{1}{3} + \frac{2}{3}\lambda\Omega\rho - \frac{2}{3}\lambda^2\Omega^2\rho^2 + \mathcal{O}(\lambda^3), \\
f(r)^{-1} &= 3 + \frac{2\lambda}{\sqrt{3}M}\rho + \frac{2\lambda^2}{3M^2}\rho^2 + \mathcal{O}(\lambda^3), \\
\sin^2\theta &= \cos^2\frac{\lambda}{3M}\psi = 1 - \lambda^2\frac{\psi^2}{9M^2} + \mathcal{O}(\lambda^4),
\end{aligned}
\tag{3.2.12}
$$

we express the Schwarzschild line element as

$$
ds^2 = \lambda^2\left(2\,du\,dv + \frac{1}{3M^2}(\rho^2 - \psi^2)\,du^2 + d\rho^2 + d\psi^2\right) + \mathcal{O}(\lambda^3). \tag{3.2.13}
$$

Taking the Penrose limit now amounts to performing the limit $d\bar{s}^2 = \lim_{\lambda\to 0}\lambda^{-2}\,ds^2$, which is equivalent to isolating the λ^2-terms in equation (3.2.13) and setting $\lambda = 1$. This recovers the Penrose limit (3.2.8) under the association $\rho = x^1$, $\psi = x^2$.

3.2.3 Identifying Geometric Quantities in the Wave Profile

So far, the geometric interpretation of the wave profile matrix components A_{ab} of the Penrose limit (3.2.8) is rather intransparent. We only know the explicit expressions (3.2.7), but their origin in the Schwarzschild spacetime is unclear, other than being geodesic deviation information. To identify their origin, we refer to a more general result of the Penrose limit as presented by [7], which derives the wave profile for the Penrose limit along a general polar geodesic with the radial coordinate parameterised by $r(u)$. The result is the diagonal matrix

$$
\begin{aligned}
A_{11}(u) &= -\frac{3}{r}V'_{\text{eff}}(r(u)) - V''_{\text{eff}}(r(u)), \\
A_{22}(u) &= -\frac{1}{r}V'_{\text{eff}}(r(u)) - \frac{L^2}{r(u)^4}.
\end{aligned}
\tag{3.2.14}
$$

By spherical symmetry, the Schwarzschild metric is invariant under rotations and hence, this result derived for polar geodesics also holds for equatorial geodesics, with appropriate redefinitions of L. It is defined relative to the normal vector of of the geodesic's plane of motion, and rotating the geodesic rotates this plane. Thus, while [7] uses $L = \frac{\partial\mathcal{L}}{\partial\dot{\theta}}$ for polar geodesics, in the equatorial plane, it corresponds to $L = \frac{\partial\mathcal{L}}{\partial\dot{\varphi}} = \dot{\varphi}r^2$.

For our specific case of an equatorial photon ring geodesic (cf. equation (3.1.9)), we have $r(u) = 3M$ as well as $V'_{\text{eff}}(r(u)) = 0$. This simplifies the wave profile above to

$$
A_{11} = -V''_{\text{eff}}(3M), \quad A_{22} = -\frac{L^2}{r^4} = -\dot{\varphi}^2. \tag{3.2.15}
$$

We recognise $\dot{\varphi}$ as the orbital frequency (normalised to the affine parameter u), which is related to Ω via $\dot{\varphi} = 3\Omega$, consistent with our result $A_{22} = -1/3M^2$. Moreover, from equation (3.1.5) we infer that

$$A_{11} = -V''_{\text{eff}}(3M) = \partial_r \ddot{r}|_{r=3M}, \tag{3.2.16}$$

which describes the radial geodesic deviation in an infinitesimal neighbourhood of the photon ring, capturing the (in)stability properties of the photon ring. The configuration $V'_{\text{eff}}(3M) = 0$, $V''_{\text{eff}}(3M) < 0$ indicates that the potential $V_{\text{eff}}(r)$ takes on a local maximum at $r = 3M$, yielding an unstable orbit since small radial perturbations around it lead to growing deviations. This will be examined in greater detail at the end of Section 4.2.3. Lastly, the value $-V''_{\text{eff}}(3M) = 1/3M^2$ is consistent with our previous result.

3.2.4 Explicit Form of the Isometry Algebra

We now focus on determining the explicit forms of the vectors that generate the isometry algebra of the Penrose limit (3.2.8). We will need these results in later parts of the thesis.

From Section 1.2.5 we already know that there exists a Heisenberg isometry algebra which can be constructed from solutions of the harmonic oscillator equation

$$\ddot{f}_a = A_{ab} f_b. \tag{3.2.17}$$

Since A is u-independent and diagonal, the solutions can be derived straightforwardly. Denoting $\beta^2 = A_{11} = -A_{22}$, a set of linearly independent solutions is given by

$$f_a^{\pm} = \big(e^{\pm\beta u}, 0\big), \quad g_a^{\pm} = \big(0, e^{\pm i\beta u}\big) \tag{3.2.18}$$

Using expression (1.2.25) we construct the Killing vectors

$$\begin{aligned} a_{\pm} &\equiv \mp\frac{1}{\sqrt{2\beta}} X_{g^{\mp}} = \frac{1}{\sqrt{2\beta}} e^{\mp i\beta u}(\mp\partial_2 - i\beta x_2 \partial_v), \\ b_{\pm} &\equiv \mp\frac{1}{\sqrt{2\beta}} X_{f^{\mp}} = \frac{1}{\sqrt{2\beta}} e^{\mp\beta u}(\mp\partial_1 - \beta x_1 \partial_v). \end{aligned} \tag{3.2.19}$$

Moreover, since the plane wave metric (3.2.8) is u- and v-independent, we have the additional Killing vectors

$$Z = -i\partial_v, \quad H = \frac{i}{\beta}\partial_u \tag{3.2.20}$$

The choice of normalisations is such that the non-vanishing commutators of the generated isometry algebra read

$$[a_-, a_+] = Z, \quad [b_-, b_+] = -iZ, \quad [H, a_{\pm}] = \pm a_{\pm}, \quad [H, b_{\pm}] = \mp i b_{\pm}. \tag{3.2.21}$$

4 Quasinormal Modes, Geometric Optics and WKB

This section provides an in-depth discussion of the quasinormal mode (QNM) problem for the Schwarzschild geometry, focusing on two central approximation methods for addressing the analytically intractable radial potential. Quasinormal modes are solutions to the wave equation that satisfy outgoing boundary conditions in the radial direction, occurring at a discrete set of complex frequencies known as the QNM spectrum.

The first approximation method we explore is the Wentzel-Kramers-Brillouin (WKB) approach [2], which we apply to the radial wave equation of the Schwarzschild geometry following a method introduced by Schutz and Will [5]. This analysis demonstrates that the QNM spectrum can be approximated using a quadratic expansion of the radial potential around its maximum. This is because a wave with an outgoing profile, leaving the region where the quadratic approximation holds, will maintain its outgoing nature as it propagates to the horizon and spatial infinity.

Building on this understanding, we employ the geometric optics approximation, in the limit of the so-called near-ring region. This approach not only reproduces the spectrum derived using the WKB method, but also serves as the foundation for establishing a correspondence with the Penrose limit, which we will show to provide a geometric framework for the QNM spectrum.

4.1 Wave Equations and WKB

Here, we consider the wave equation and the associated quasinormal mode (QNM) problem in the Schwarzschild geometry. We introduce the Wentzel–Kramers–Brillouin (WKB) approximation, and subsequently employ it to approximate the QNM frequencies, following the approach of Schutz and Will [5]. This analysis will highlight the pivotal role of the maximum of the radial wave potential $\mathcal{V}(r_*)$ in determining the QNM frequencies.

4.1.1 Quasinormal Mode Problem for Schwarzschild

Although a rigorous definition of quasinormal modes is beyond the scope of this thesis, this section provides an introduction to them in the setting of the Schwarzschild geometry. Quasinormal modes can be understood as characteristic oscillations of a black hole that describe how it responds to perturbations. As discussed by Kokkotas [1], they describe the behaviour of a weakly perturbed black hole returning to equilibrium. A black hole may be perturbed by accretion of matter or by scattering incoming gravitational waves, causing it to deviate temporarily from equilibrium before settling back by radiating gravitational waves.

Since quasinormal modes describe only the *reaction* of the black hole to external perturbations, they are solutions with no incoming components. Consequently, they must be purely outgoing, with components propagating away from the black hole—towards spatial infinity at large distances and, by causality, only *towards* the event horizon near the black hole.

In a stationary spacetime, the dependence on the time coordinate t of a mode is given by a factor $e^{-i\omega t}$, with complex frequencies $\omega = \omega_R + i\omega_I$. The sign of the imaginary part ω_I informs us about the stability of a given mode, as a negative sign leads to exponential decay, whereas an imaginary part greater than zero causes exponential growth. A spacetime in which all quasinormal mode frequencies satisfy $\omega_I < 0$ is called *mode-stable*.

Scalar quasinormal modes are a class of solutions to the scalar wave equation

$$0 = \Box_g \Phi(x) = \frac{1}{\sqrt{g}} \partial_\mu [\sqrt{g} g^{\mu\nu} \partial_\nu \Phi(x)] \tag{4.1.1}$$

that obey outgoing boundary conditions which are specified in the following. For the Schwarzschild metric, the wave equation takes on a convenient form when introducing the *tortoise coordinate* r_* via $dr = f(r)\, dr_*$. Explicitly, for Schwarzschild, it is given by

$$r_* = r + 2M \log(r - 2M) \quad \Leftrightarrow \quad r = 2MW\left(\frac{e^{r_*/2M}}{2Me}\right) + 2M \tag{4.1.2}$$

where $W(x)$ is the Lambert W-function, i.e. the principal solution to $W(x)e^{W(x)} = x$. The tortoise coordinate turns the Schwarzschild line element into

$$ds^2 = f(r)(-dt^2 + dr_*^2) + r^2\, d\theta^2 + r^2 \sin^2\theta\, d\varphi^2, \tag{4.1.3}$$

and using the general formula (4.1.1) for the wave operator, it is derived that the corresponding expression for Schwarzschild is

$$0 = -\partial_t^2 \Phi + \frac{1}{r^2} \partial_{r_*} \left(r^2 \partial_{r_*} \Phi \right) + f(r) \frac{1}{r^2} \Delta_{S^2} \Phi. \tag{4.1.4}$$

Here, Δ_{S^2} denotes the Laplacian of the 2-sphere. This Laplacian, together with the t-translation symmetry, motivates the decomposition of the solution Φ into modes of the form

$$\Phi_{\omega\ell m}(t, r_*, \theta, \varphi) = e^{-i\omega t} \frac{\psi_{\omega\ell}(r_*)}{r} Y_{\ell m}(\theta, \varphi), \tag{4.1.5}$$

where $Y_{\ell m}$ are the spherical harmonics which satisfy $\Delta_{S_2} Y_{\ell m} = -\ell(\ell+1) Y_{\ell m}$ (cf. Appendix C). The radial equation for $\psi_{\omega\ell}(r_*)$ arising from equation (4.1.4), dropping the $\omega\ell$ subscript, reads

$$0 = \partial_{r_*}^2 \psi + [\omega^2 - \mathcal{V}(r_*)]\psi, \quad \mathcal{V}(r_*) = f(r) \left[\frac{\ell(\ell+1)}{r^2} + \frac{2M}{r^3} \right]. \tag{4.1.6}$$

Note that the radial wave potential $\mathcal{V}(r_*)$ approaches zero towards both the horizon, $r \to 2M$, and spatial infinity, $r \to \infty$, and has a maximum in the vicinity of $r = 3M$. The tortoise coordinate r_* maps spatial infinity to $r_* = \infty$ and the horizon to $r_* = -\infty$, which effectively renders equation (4.1.6) a time-independent one-dimensional Schrödinger equation for an asymptotically free particle on $\mathbb{R}$ with eigenvalue ω^2 and a potential barrier at $r \approx 3M$.

Because of $\lim_{r_* \to \pm\infty} \mathcal{V}(r_*) = 0$, the solutions $\psi(r_*)$ of equation (4.1.6) are linear combinations of $e^{\pm i\omega r_*}$ asymptotically, i.e. of waves moving towards and away from spatial infinity, and analogously, towards and away from the horizon. The amplitudes and phases of the asymptotic waves for the $r_* \to \pm\infty$ directions are related by how they interact with the bulk of the potential around $r \approx 3M$.
A *quasinormal mode* at the *quasinormal mode frequency* ω, in this context, is a solution of equation (4.1.6) with outgoing boundary conditions, i.e.

$$\psi(r_*) \sim \begin{cases} e^{i\omega r_*}, & r_* \to \infty, \\ e^{-i\omega r_*}, & r_* \to -\infty. \end{cases} \tag{4.1.7}$$

This means that the asymptotic behaviour of $\psi(r_*)$, which is generally a linear combination of right- and left-moving waves, simplifies for a quasinormal mode to include only components moving away from the potential barrier. In other words, a quasinormal mode solution is a solution that is moving solely towards spatial infinity for large positive r_* and moving solely towards the horizon for large negative r_*.
As is discussed by [1] and [12], these boundary conditions are non-hermitean and lead to a discrete, complex spectrum for the quasinormal mode frequencies $\omega = \omega_R + i\omega_I$.

In summary, QNMs are a class of solutions to the wave equation of a black hole geometry which satisfy purely outgoing boundary conditions at spatial infinity and the horizon. These solutions usually exist at a discrete set of QNM frequencies termed the *quasinormal mode spectrum*. Since the analytic solution of equation (4.1.6) is not feasible in practice, the determination of the QNM spectrum typically relies on approximation methods, which we will discuss in the following.

4.1.2 The WKB Approximation

The WKB approximation, which has its origin in quantum mechanics and is discussed in greater detail in [2], is a solution approximation scheme applicable to one-dimensional Schrödinger-type equations, i.e. equations of the form

$$\psi''(x) + Q(x)\psi(x) = 0, \tag{4.1.8}$$

in which Q is a "slowly varying" function compared to the local wavelength $\sqrt{Q}$. More precisely, it is assumed that

$$|Q'(x)| \ll |Q(x)|^{3/2}, \tag{4.1.9}$$

This follows from dimensional analysis: from equation (4.1.8), we see that $[Q] = 2$, $[Q'] = 3$, and thus $\left[|Q|^{3/2}\right] = 3$, allowing us to make the comparison (4.1.9). For the specific case of the radial wave potential (4.1.6), the function Q takes the form $Q(r_*) = \omega^2 - \mathcal{V}(r_*)$.

To derive the WKB approximation, we introduce a parameter $\delta > 0$. Although at the end of the derivation, we will set it to 1, its introduction allows for a systematic expansion. We multiply the second derivative in the Schrödinger equation (4.1.8) with δ^2, and subsequently recast it using the substitution

$$\psi(x) = e^{i\varphi(x)/\delta} \tag{4.1.10}$$

into the form

$$i\delta\varphi''(x) - (\varphi'(x))^2 + Q(x) = 0. \tag{4.1.11}$$

This Riccati differential equation for φ' can be solved by a series expansion in δ,

$$\varphi(x) = \varphi_0(x) + \delta\varphi_1(x) + \delta^2\varphi_2(x) + \mathcal{O}(\delta^3). \tag{4.1.12}$$

When inserted into equation (4.1.11), the expansion enables the comparison of coefficients in δ, leading to the equations

$$\begin{aligned} \mathcal{O}(\delta^0): &\quad (\varphi_0')^2 = Q \quad \Rightarrow \quad \varphi_0(x) = \pm\int^x \sqrt{Q(z)}\,dz, \\ \mathcal{O}(\delta^1): &\quad 2\varphi_0'\varphi_1' = i\varphi_0'' \quad \Rightarrow \quad \varphi_1(x) = \frac{i}{4}\log Q(x) + C. \end{aligned} \tag{4.1.13}$$

Inserting the expansion for φ, truncated to $\mathcal{O}(\delta)$, back into its relationship to ψ leads to

$$\psi(x) = \frac{A}{|Q(x)|^{\frac{1}{4}}} \exp\left(\pm i \int^x \sqrt{Q(z)}\, dz\right), \quad A \in \mathbb{C}, \tag{4.1.14}$$

after setting $\delta = 1$. In the following, we will refer to this as the *WKB approximation* of the solution to equation (4.1.8).

This truncation is a valid approximation provided that equation (4.1.12) converges rapidly, i.e. that φ_2 is negligible compared to φ_1 and φ_0. At order $\mathcal{O}(\delta^2)$, comparing coefficients in equation (4.1.11) yields

$$i\varphi_1'' - \left(2\varphi_0'\varphi_2' + (\varphi_1')^2\right) = 0 \quad \Longrightarrow \quad \varphi_2' = \frac{i\varphi_1'' - (\varphi_1')^2}{2\varphi_0'}. \tag{4.1.15}$$

We can see that φ_2 is small if $|\varphi_1'| \ll |\varphi_0'|$. Inserting the expressions for φ_0 and φ_1 from equation (4.1.13) into this inequality, we recover the validity condition (4.1.9).

Before moving on to use the WKB approximation in the context of QNMs, it is worth making the following observation. Depending on the sign of Q, the behaviour of the approximate solution (4.1.14) will differ significantly. In regions where Q is positive, the exponential has a purely imaginary argument—hence, the solution oscillates, with the direction of propagation given by the choice of sign. Conversely, for negative values of Q, the solution will behave exponentially. This distinction will be crucial in the following.

4.1.3 Schwarzschild QNMs from WKB

In this section, we follow a procedure introduced by Schutz and Will in 1985 [5] to use the WKB approximation as a tool to find approximate quasinormal solutions of the radial wave equation (4.1.6).

For the Schwarzschild geometry, the radial wave equation is of the same type as equation (4.1.8) discussed in the previous section, with the identifications

$$x = r_*, \quad Q(x) = \omega^2 - \mathcal{V}(r_*). \tag{4.1.16}$$

Up to a possible constant imaginary offset from ω^2, the function $Q(x)$ is real-valued, and, since $\mathcal{V}$ has a single maximum, the function $Q(x)$ has a single minimum. If $Q(x)$ is positive everywhere, then the WKB solution is a linear combination of two oscillating components, asymptotically behaving as $e^{\pm i\omega r_*}$ (cf. eq. (4.1.14), recalling that $Q(x) \to \omega^2$ as $x \to \pm\infty$). Such a superposition cannot satisfy the purely outgoing QNM boundary conditions and is therefore irrelevant to the present discussion.
We now consider the case where ω^2 is chosen such that the function $Q(x)$ is negative in a region (x_1, x_2) around its minimum at x_0, and negative on its complement, as illustrated in Figure 1. This separates the real line into three regions—two for which the solution of the radial wave equation is oscillatory, called regions I and III, as well as an exponential region II in the neighbourhood (x_1, x_2) of the minimum at x_0.

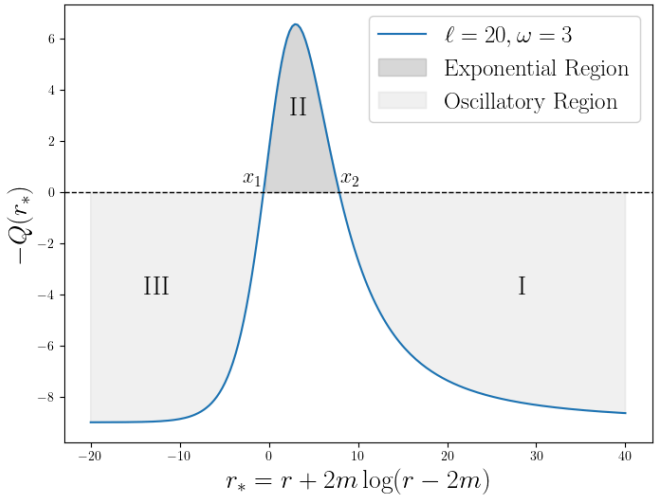

Figure 1: Plot of the exponential region II and the oscillatory regions I and III of the Schwarzschild wave potential. Note that the graph shows $-Q(r_*)$ so that $\mathcal{V}$ appears with positive sign.

The WKB solution in the regions I and III, with quasinormal boundary conditions imposed, is given by

$$\psi(r_*) \sim \begin{cases} \exp\left(-i\int^{r_*}\sqrt{Q(x)}\,dx\right), & r_* < x_1, \\ \exp\left(i\int^{r_*}\sqrt{Q(x)}\,dx\right), & r_* > x_2. \end{cases} \tag{4.1.17}$$

Following an argument given in more detail in Appendix A, it is generally not possible to match these solutions from regions I and III continuous-differentiably across the region boundaries x_1 and x_2 onto a general WKB solution in region II. However, there is one case for which it is possible to find a continuously differentiable solution, namely when the minimum of $Q(x)$ is exactly zero—i.e. when $x_1 = x_2$ and we have a second order turning point. Since the WKB solution is only approximate, we can allow for a narrow region (x_1, x_2) around the maximum at x_0 where $Q(x)$ is negative (cf. Appendix A).

In general, this region is too narrow for the WKB approximation to work. We can, however, proceed differently. Instead of using the exact function $Q(x)$ and approximating the solution, we can approximate $Q(x)$ up to quadratic order around the minimum at $x_0 \in (x_1, x_2)$, and solve the equation exactly. This approximation is valid since the region (x_1, x_2) is narrow. The expansion for $Q(x)$ around x_0 is

$$Q(x) = Q_0 + \frac{1}{2}Q_0''(x - x_0)^2 + \mathcal{O}(x - x_0)^3, \tag{4.1.18}$$

where we defined $Q_0 = Q_0(x_0)$, $Q_0'' = Q_0''(x_0)$ and the term linear in $(x - x_0)$ drops out by minimality. Thus, the approximate radial wave equation in region II reads

$$\psi''(x) + \frac{1}{2}Q_0''(x - x_0)^2\psi(x) = -Q_0\psi(x), \quad x \in (x_1, x_2) \tag{4.1.19}$$

which is a Schrödinger equation for an inverted harmonic oscillator with eigenvalue $-Q_0$. Using the spectrum of the inverted harmonic oscillator with outgoing boundary conditions

derived in Appendix B, we find the quantisation condition[12]

$$i\frac{Q_0}{\sqrt{2Q_0''}} = n + \frac{1}{2}, \quad n \in \mathbb{N}_0. \tag{4.1.20}$$

Since Q_0 contains the term ω^2, this is a condition on the quasinormal mode frequencies, and allows one to determine their approximate values. We note here that ω depends on both the angular quantum number ℓ as well as n. More explicitly, inserting $Q = \omega^2 - \mathcal{V}$ and solving for ω, we find

$$\omega = \sqrt{\mathcal{V}_0 - i\sqrt{-2\mathcal{V}_0''}\left(n + \frac{1}{2}\right)} \tag{4.1.21}$$

where $\mathcal{V}_0$ and $\mathcal{V}_0''$ are the values of $\mathcal{V}$ and $\mathcal{V}''$ at the maximum of the potential. For the case at hand, i.e. Schwarzschild, the maximum of the potential (4.1.6),

$$\mathcal{V}(r_*) = f(r)\left[\frac{\ell(\ell+1)}{r^2} + \frac{2M}{r^3}\right], \tag{4.1.22}$$

is located at

$$\tilde{r} = \frac{M}{2\lambda}\left(3\lambda + \sqrt{9\lambda^2 + 14\lambda + 9} - 3\right) = 3M + \mathcal{O}(\lambda^{-1}) \tag{4.1.23}$$

where $\lambda = \ell(\ell+1)$. For large ℓ and hence large λ, the position of the maximum, $\tilde{r}$, approaches the photon sphere radius at $r_0 = 3M$. In this limits, the $\frac{2M}{r^3}$ term in equation (4.1.22) becomes negligible. When writing $\omega = \omega_R + i\omega_I$ and using the associations $L = \left(\ell + \frac{1}{2}\right)$, $E = \omega_R$, we can identify

$$\omega^2 - \mathcal{V}(r) \approx E^2 - 2V_{\text{eff}}(r). \tag{4.1.24}$$

This creates a first link between wave-related objects on the left and geodesic-related objects on the right hand side.

For large ℓ, we can approximate

$$\begin{aligned} \mathcal{V}_0 &\approx \mathcal{V}(3M) \approx f(3M)\frac{\ell(\ell+1)}{(3M)^2} \approx \frac{1}{27M^2}\left(\ell + \frac{1}{2}\right)^2 = \Omega^2\left(\ell + \frac{1}{2}\right)^2, \\ \mathcal{V}_0'' &\approx \partial_{r_*}^2\left[f(r)\frac{\ell(\ell+1)}{r^2}\right]_{r=3M} = -2\frac{\ell(\ell+1)}{27^2M^4} \approx -2\left(\ell + \frac{1}{2}\right)^2\left(\frac{1}{27M^2}\right)^2 \end{aligned} \tag{4.1.25}$$

which further implies

$$\frac{\sqrt{-2\mathcal{V}_0''}}{\mathcal{V}_0} \approx \frac{2}{\ell + \frac{1}{2}} \ll 1. \tag{4.1.26}$$

For $n \ll \ell$, this allows us to approximate the quasinormal mode frequency spectrum as

[12]The upshot of the derivation is that the spectrum of the inverted harmonic oscillator with outgoing boundary conditions is simply the analytic continuation of the spectrum of the simple harmonic oscillator.

$$\begin{aligned}\omega &= \sqrt{\mathcal{V}_0}\sqrt{1 - i\frac{\sqrt{-2\mathcal{V}_0''}}{\mathcal{V}_0}\Big(n+\frac{1}{2}\Big)} \approx \sqrt{\mathcal{V}_0} - \frac{i}{2}\sqrt{\frac{-2\mathcal{V}_0''}{\mathcal{V}_0}}\Big(n+\frac{1}{2}\Big) \\ &= \Omega\Big(\ell+\frac{1}{2}\Big) - \frac{i}{3\sqrt{3}M}\Big(n+\frac{1}{2}\Big).\end{aligned} \tag{4.1.27}$$

Let us now take a step back to interpret the result. The quantisation condition (4.1.20), which determines the approximate quasinormal mode spectrum, depends on only two key pieces of information of the spacetime; the value of $Q(r_*) = \omega^2 - \mathcal{V}(r_*)$ at its minimum, Q_0, and the corresponding second derivative, Q_0''.
This observation has a striking implication: to approximate the quasinormal mode spectrum, it is sufficient to consider the behaviour of the potential $\mathcal{V}(r_*)$ in a small neighbourhood around its maximum. Specifically, expanding $\mathcal{V}(r_*)$ to second order near this maximum provides all necessary information. Thus, the determination of the approximate quasinormal mode frequencies relies solely on the local properties of the potential in this region, while the outgoing boundary conditions[13] ensure that the solutions match onto asymptotically outgoing waves. Moreover, since this minimum lies close to $r = 3m$, the present discussion motivates the study of the so-called near-ring region—roughly speaking, the vicinity of the photon sphere—which we will explore further in Section 4.2 below to clarify this relationship.

4.2 Geometric Optics Approximation and the Near Ring Region

This section is concerned with the geometric optics approximation of solutions to the wave equation. After introducing it in a general setting, we consider our recurring example, the Schwarzschild geometry, and impose the QNM boundary conditions on a particular solution. This naturally leads to the emergence of the photon sphere. We then use our insight gained from the WKB approximation and define a class of solutions close to the bound photon orbits, following the publications [6] and [4], which captures the significant information for the QNM spectrum. The subsequent analysis of the geometric optics solution in the near-ring region allows us to determine the QNM spectrum in the so-called eikonal limit, revealing the geodesic quantities that appear as parameters in it.

4.2.1 Geometric Optics Approximation

The geometric optics approximation provides a systematic method for constructing approximate solutions Φ to the massless wave equation

$$\Box_g \Phi = 0. \tag{4.2.1}$$

This approach assumes that Φ can be expressed as $\Phi(x) = A(x)e^{iS(x)}$, a rapidly oscillating phase e^{iS} modulated by a slowly varying complex-valued amplitude A. We define the phase gradient as $\ell_\mu = \partial_\mu S$, with which we can state the validity condition explicitly as

$$\frac{|\partial_\mu A(x)|}{|A(x)|} \ll |\ell_\mu(x)|. \tag{4.2.2}$$

This condition reflects the assumption that the amplitude $A(x)$ varies slowly compared to the rapid oscillations of the phase $S(x)$. Inserting the ansatz into the wave equation (4.2.1), we find

[13] at the boundary of this region

$$-A\ell^\mu\ell_\mu + i\Big[2\ell^\mu\partial_\mu A + A\underbrace{\nabla^\mu\ell_\mu}_{=\Box_g S}\Big] + \Box_g A = 0. \tag{4.2.3}$$

By the separation of scales (4.2.2), we can solve this equation by order in ℓ. At leading order, we recover the Hamilton-Jacobi equation

$$0 = \ell^\mu\ell_\mu = g^{\mu\nu}\partial_\mu S\partial_\nu S. \tag{4.2.4}$$

From Section 2.2, we know that hence, ℓ^μ represents the tangent field of a geodesic congruence. Therefore, the vector $\ell = \ell^\mu\partial_\mu$ is a directional derivative along the congruence, which we denote by $\ell = \partial_u$ where u is an affine parameter along the congruence.
At next-to-leading order, we find the transport equation

$$\partial_u \log A = -\frac{1}{2}\Box_g S = -\frac{1}{2}\Theta, \tag{4.2.5}$$

where, using equation (2.4.31), we identify the expansion $\Theta = \Box_g S$ of the congruence generated by S. From the discussion in Section 2.4.2 we know that Θ quantifies the focusing and dispersing of the null geodesic congruence. From this we infer that the amplitude is transported along the congruence, appropriately decreasing and increasing in magnitude as the congruence expands and contracts, respectively, i.e. as the wavefronts get dispersed and focused.

In summary, the geometric optics solution $\Phi = Ae^{iS}$ has wavefronts (level surfaces of S) that are transported along a null geodesic congruence with tangent ℓ^μ (i.e. $\ell^\mu\partial_\mu S = 0$). The amplitude is transported along the congruence as well, scaling in magnitude with the focusing and dispersing of the wavefronts.

4.2.2 QNM Boundary Conditions for Geometric Optics

In Section 3.1.3, we have derived a solution to the Hamilton-Jacobi equation. To it, we can associate an approximate geometric optics solution to the wave equation, $A(x)e^{iS(x)}$, with some amplitude function $A(x)$ subject to the transport equation (4.2.5). In this section, we investigate what implications the quasinormal mode boundary conditions have in the case of a polar congruence, i.e. for $L_3 = 0$. That is, we consider the Hamilton-Jacobi function

$$S(t, r_*, \theta, \varphi) = -Et + \int \varepsilon(r)\sqrt{E^2 - 2V_{\text{eff}}(r)}\, dr_* + L\theta, \tag{4.2.6}$$

with $L = \sqrt{\boldsymbol{L}^2}$, which will lead us to find the photon orbit emerge naturally from outgoing boundary conditions.

Quasinormal boundary conditions require $\Phi = Ae^{iS} \sim e^{\pm i\omega r_*}$ as $r_* \to \pm\infty$. From the separation of scales (4.2.2) we find

$$\frac{\partial_\mu\Phi}{|\Phi|} = \frac{\partial_\mu A}{|A|}e^{iS} + i\partial_\mu S\frac{\Phi}{|A|} \approx i\partial_\mu S\frac{\Phi}{|A|} \tag{4.2.7}$$

or equivalently

$$|\partial_\mu\Phi| \approx |\partial_\mu S|\ |\Phi|, \tag{4.2.8}$$

where we are allowed to drop $\partial_\mu A/|A|$ terms as they are small in comparison to $\partial_\mu S$. We infer that the variation of Φ is dominated by the variation of the e^{iS} term and hence the phase information of $\Phi(x)$ in the geometric optics limit is dominated by e^{iS}. Therefore the quasinormal boundary conditions turn into a condition on $S(x)$. More specifically, S must be monotone increasing as $r_* \to \infty$ and monotone decreasing for $r_* \to -\infty$ to reproduce the $\Phi \sim e^{\pm i\omega r_*}$ boundary condition. Since S appears as $\Phi = Ae^{iS}$, this can be rephrased into

$$\lim_{r_*\to\pm\infty} \partial_{r_*} S \begin{cases} > 0 \text{ for } r_* \to \infty, \\ < 0 \text{ for } r_* \to -\infty \end{cases} \tag{4.2.9}$$

which is to say that $\partial_{r_*} S = \varepsilon(r)\sqrt{E^2 - 2V_{\text{eff}}(r)}$ has at least one root and $\lim_{r_*\to\pm\infty} \varepsilon(r) = \pm 1$. Equivalently, the term $E^2 - V_{\text{eff}}(r)$ must have a double root, i.e. there must exist an r_0 for which $V_{\text{eff}}(r_0) = E^2$, $V'_{\text{eff}}(r_0) = 0$. These are exactly the conditions for the unstable photon orbit we found in Section 3.1.2 which are solved by $r_0 = 3m$ and $L = 3\sqrt{3}ME$. This turns the Hamilton-Jacobi function into

$$S(t, r_*, \theta, \varphi) = -Et + \int \operatorname{sgn}(r - 3m)\sqrt{E^2 - 2V_{\text{eff}}(r)}\, dr_* + 3\sqrt{3}ME\theta. \tag{4.2.10}$$

Here we chose $\varepsilon(r) = \operatorname{sgn}(r - 3m)$ to guarantee the correct asymptotic behaviour and simultaneously provide continuous differentiability of S.

Let us take a moment to further analyse and interpret this Hamilton-Jacobi function and the geodesic congruence it produces. We have seen that imposing the QNM boundary conditions led to the requirement that $L = 3\sqrt{3}ME$, which informs us that the generated congruence embeds photon ring geodesics. To see this explicitly, consider the tangent field $\ell^\mu = g^{\mu\nu}\partial_\nu S$ of the congruence produced by the H-J function (4.2.10), i.e.

$$\ell = \ell^\mu \partial_\mu = f(r)^{-1} E\partial_t + \operatorname{sgn}(r - 3m)\sqrt{E^2 - 2V_{\text{eff}}(r)}\partial_r + \frac{3\sqrt{3}ME}{r^2}\partial_\theta. \tag{4.2.11}$$

Its restriction to $r = 3m$ reads

$$\ell|_{r=3m} = 3E\partial_t + \frac{E}{\sqrt{3}M}\partial_\theta, \tag{4.2.12}$$

which is the tangent of the polar photon ring geodesic from equation (3.1.8). Hence, the Hamilton-Jacobi function (4.2.10) generates a congruence that embeds this geodesic. Moreover, we should note the effect the $\operatorname{sgn}(\ell^r) = \operatorname{sgn}(r - 3M)$ has—geodesics closer to the origin than $r = 3M$ travel inwards towards the horizon, while geodesics with $r > 3M$ move towards spatial infinity. This reflects both the unstable nature of the photon ring orbit as well as the intuitive picture of outgoing boundary conditions imposed by the quasinormal mode problem—moving away from the potential barrier towards $r_* = \pm\infty$. Moreover, due to the relationship $\Phi = Ae^{iS}$, we can see that the association $E = \omega_R$ from earlier produces a factor $e^{-i\omega_R t}$, as expected for the real part of the quasinormal mode frequency.

4.2.3 The Near-Ring Region

Following [6] and [4], we define the so-called near-ring region for mode solutions of the wave equation by

$$\begin{cases} \left|\frac{\ell}{\omega_R} - \frac{1}{\Omega}\right| \ll M, & \text{near-critical,} \\ \frac{1}{\omega_R} \ll M, & \text{high-energy,} \\ |r - 3M| \ll M, & \text{near-peak,} \end{cases} \tag{4.2.13}$$

and analogously, for geodesics, by

$$\begin{cases} \left|\frac{L}{E} - \frac{1}{\Omega}\right| \ll M, & \text{near-critical,} \\ \frac{1}{E} \ll M, & \text{high-energy,} \\ |r - 3M| \ll M, & \text{near-peak,} \end{cases} \tag{4.2.14}$$

where again, the analogy is given by the association $L = \left(\ell + \frac{1}{2}\right) \approx \ell$, $E = \omega_R$. The near-peak condition ensures that we are in the vicinity of $r = 3M$. The near-critical condition selects nearly bound geodesics/waves and the high-energy condition is what allows us to apply the geometric optics approximation. Notice that the near-criticality and high-energy conditions for waves impose constraints on the solution space of the wave equation. Since this space can be parameterised as a superposition of modes,

$$\Phi(t, r, \theta, \varphi) = \sum\!\!\!\!\!\!\int_{\omega\ell m} c(\omega, \ell, m)\Phi_{\omega\ell m}(t, r, \theta, \varphi), \quad |r - 3M| \ll M, \tag{4.2.15}$$

the coefficient function $c(\omega, \ell, m)$ is supported only in a restricted region of parameter space, allowing contributions exclusively from near-critical and high-energy modes. In addition, the near-peak condition restricts the radial coordinate to the vicinity of the photon sphere. This effectively defines a subregion in the space of wave solutions near $r = 3M$.

This definition of the near-ring region is motivated by the findings of the WKB treatment of the quasinormal mode problem in Section 4.1, as well as the conditions under which the geometric optics approximation is valid. The WKB analysis predicts that quasinormal modes exist at frequencies where $Q(\tilde{r}_*) \approx 0$, leading to $\omega_R^2 \approx \mathcal{V}(\tilde{r}_*)$. Here, $\tilde{r}_*$ is the position of the maximum of the potential $\mathcal{V}$, which resides near $r = 3M$ for large ℓ.
For both WKB and the geometric optics approximation to be valid, the wave frequency must be large with respect to the curvature scale of the metric, i.e. $\omega_R \gg \frac{1}{M}$. This high-energy condition ensures the separation of scales required by equation (4.2.2). Consequently, ℓ must also be large, implying that $\tilde{r} = 3M + \mathcal{O}(\ell^{-1})$ is close to $3M$, and the wave potential is approximated as

$$\mathcal{V}(r) \approx f(r)\frac{\ell(\ell + 1)}{r^2}. \tag{4.2.16}$$

Evaluating the potential at $\tilde{r} \approx 3M$, we find $\omega_R^2 \approx \mathcal{V}(3M) \approx \frac{\ell(\ell+1)}{27M^2} = \Omega^2\ell(\ell + 1)$, which leads directly to the near-criticality condition. Furthermore, the near-peak condition arises from the observation that the quasinormal mode spectrum can be approximated by considering only a small region around the maximum of the potential. This region is centred near $r = 3M$ in the high-ℓ limit, which establishes the near-peak condition.

At this stage, let us determine the radial behaviour of geodesics in the near-ring region to identify a geodesic parameter that will appear in the following. We define the deviation from the photon ring by $\delta r = r - 3M$. From equation (3.1.4) we infer that

$$\frac{d\delta r}{dt} = \frac{\delta\dot{r}}{\dot{t}} = \frac{f(r)}{E}\sqrt{E^2 - 2V_{\text{eff}}(r)}. \tag{4.2.17}$$

Making use of the near-peak and near-criticality conditions for geodesics, we deduce[14]

$$\frac{d\delta r}{dt} \approx \frac{1}{3E}\sqrt{-V''_{\text{eff}}(r_0)}\delta r \equiv \gamma_L \delta r, \tag{4.2.18}$$

which admits solutions $\delta r \sim e^{\gamma_L t}$. This demonstrates that $\gamma_L = (3\sqrt{3}M)^{-1}$ takes the role of a Lyapunov-exponent, quantifying the exponential divergence of geodesics in the near-ring region. In hindsight, it is clear that the Lyapunov-exponent, being a quantity that captures the divergence of trajectories, must be tied to the second derivative of the potential. This is because we have

$$\ddot{r} = -V'_{\text{eff}}(r) \quad \Longrightarrow \quad \partial_r \ddot{r} = -V''_{\text{eff}}(r) \tag{4.2.19}$$

- a difference in acceleration between neighbouring paths causes a tidal force, which changes the separation between them. Notice here that this is geodesic deviation around the photon ring geodesic—together with the orbital frequency Ω, this is *the* covariant information of the original spacetime preserved by the Penrose limit, as we have seen in Section 3.2.3. These quantities will reappear as we derive the eikonal Schwarzschild QNM spectrum in the following sections. This will establish a first indication of the fact that the Penrose limit contains the necessary information to determine the QNM spectrum.

4.2.4 Eikonal QNM Spectrum from Geometric Optics

The goal of this section is to derive the QNM spectrum in the near-ring limit using geometric optics. Specifically, we determine a solution corresponding to the $n = 0$ mode of the spectrum previously derived via WKB in (4.1.27). The subsequent construction of the overtones ($n > 0$) using conserved quantities along the congruence follows the approach of [4].

We begin with the $n = 0$ mode. Notice that the associations $E = \omega_R$ and $L = \ell + \frac{1}{2}$ already yield

$$\omega_R \approx \Omega\left(\ell + \frac{1}{2}\right) \tag{4.2.20}$$

due to the near-critical condition. Expanding the Hamilton-Jacobi function from Section 4.2.2 to second order in δr in the near-ring limit leads to

$$\begin{aligned} S &\approx -\omega_R t + \int 3\,\text{sgn}(\delta r)\sqrt{-V''_{\text{eff}}(r_0)\delta r^2}\, d\delta r + L\theta \\ &\approx -\omega_R t + \frac{9}{2}\omega_R \gamma_L \delta r^2 + L\theta \end{aligned} \tag{4.2.21}$$

where $L \approx \omega_R/\Omega$. The corresponding congruence has the expansion[15]

[14] We expand the expression within the square root to second order around $\delta r = 0$, making use of the fact that it has a double root at r_0 due to the near-critical condition.

[15] Up to the $\cot\theta$ term, this result aligns with that of Kapec and Sheta [4], who neglected this term by employing a Hamilton-Jacobi function valid only in the equatorial plane. The omission likely arises because the associated factor in the amplitude, $(\sin\theta)^{-1/2}$ in equation (4.2.24), does not affect the quasinormal mode spectrum.

$$\begin{aligned}\Theta = \Box_g S &= \frac{1}{r^2}\partial_r(r^2 f(r) 9\omega_R\gamma_L\delta r) + \frac{L}{r^2}\cot\theta \\ &\approx 3\omega_R\gamma_L + \frac{L}{9M^2}\cot\theta\end{aligned} \tag{4.2.22}$$

for $|\delta r| \ll M$. The transport equation (4.2.5) for the amplitude thus reads, assuming $\partial_r A = 0$,

$$\left(3\omega_R\partial_t + \frac{L}{3M^2}\partial_\theta\right)\log A \approx -\frac{3}{2}\omega_R\gamma_L - \frac{1}{2}\frac{L}{9M^2}\cot\theta \tag{4.2.23}$$

which is solved by

$$A = \frac{1}{\sqrt{\sin\theta}}e^{-\gamma_L t/2}. \tag{4.2.24}$$

The $e^{-\gamma_L t}$ factor accounts for the loss in amplitude as neighbouring geodesics diverge away radially from $r_0 = 3M$, whereas the $(\sin\theta)^{-1/2}$ quantifies the convergence of geodesics at the poles, reaching singular points at $\theta = 0, \pi$. Putting this back together with the phase, we get

$$\Phi = Ae^{iS} = \frac{1}{\sqrt{\sin\theta}}e^{-\gamma_L t/2}e^{-i\omega_R t}e^{i\frac{3}{2}\omega_R\gamma_L\delta r^2}e^{iL\theta}, \tag{4.2.25}$$

from which we can read off the quasinormal mode frequency

$$\omega = \Omega\left(\ell + \frac{1}{2}\right) - i\frac{\gamma_L}{2} \tag{4.2.26}$$

which we recognise as the $n = 0$ mode from equation (4.1.27).

We now move to the construction of the overtone modes with $n > 0$. We make the observation that for a quantity $q(x)$ which is conserved along the congruence, i.e. for which

$$\partial_u q = g^{\mu\nu}\partial_\mu S\partial_\nu q = 0, \tag{4.2.27}$$

the product $F(q(x))A(x)$ solves the transport equation (4.2.5) as well for any arbitrary function F. By means of Taylor expansion of F it is sufficient to consider monomials, using which we can generate an infinite family of wave profiles by setting

$$\Phi_n(x) = q(x)^n A(x)e^{iS(x)}, \tag{4.2.28}$$

identifying equation (4.2.25) as Φ_0.
One way to construct a conserved quantity is to make use of Killing vectors, as in Section 3.1.3, i.e. by taking a Killing vector K and setting $q(x) = K[S(x)]$. Since we imposed that $K_{(0)}[S] = -E$, $K_{(3)}[S] = L_3 = 0$, these two Killing vectors lead to constant conserved quantities, meaning that they take on the same value for each geodesic. Thus, equation (4.2.28) does not provide us with a distinct wave profile, but rather with a rescaled version of $\Phi_0 = Ae^{iS}$. Although the Killing vectors $K_{(1)}$ and $K_{(2)}$ would lead to a non-constant conserved quantity, let us entertain another approach. Recall from equation (4.2.18) that geodesics near the photon ring behave as $\delta r \sim e^{\gamma_L t}$, diverging from it exponentially. This means that for each such geodesic, in the near ring region,

$$e^{-\gamma_L t}\delta r = \text{const.} \tag{4.2.29}$$

and hence we may set $q(x) = e^{-\gamma_L t}\delta r$, leading to the overtone wave profiles

$$\Phi_n(x) = \frac{1}{\sqrt{\sin\theta}} e^{-\gamma_L(n+\frac{1}{2})t} e^{-i\omega_R t}\, \delta r^n e^{i\frac{3}{2}\omega_r \gamma_L \delta r^2}\, e^{iL\theta}. \tag{4.2.30}$$

From these, we can read off the *eikonal quasinormal mode* spectrum to be

$$\omega = \Omega\left(\ell + \frac{1}{2}\right) - i\gamma_L\left(n + \frac{1}{2}\right), \tag{4.2.31}$$

as anticipated from the WKB analysis in Section 4.1.3.

4.2.5 Conserved Quantities from Emergent Symmetries

In this section, we contextualise the conserved quantity q introduced in the previous section to generate QNM overtones and extract insights from it. To this end, we begin by reviewing a general method for constructing new solutions of the wave equation by exploiting symmetries. This will lead us to find that the generation of solutions by multiplication with the previous sections' conserved quantity q does not fit into this scheme, which will motivate the loose definition of *emergent symmetries*.

A well-known result in differential geometry is that the Lie derivative along a Killing field K commutes with the covariant derivative,

$$[\nabla, \mathcal{L}_K] = 0. \tag{4.2.32}$$

Together with $\nabla g = \mathcal{L}_K g = 0$, this immediately implies that $\left[\Box_g, \mathcal{L}_K\right] = 0$. To leverage this, consider a solution Φ of the wave equation, i.e. $\Box_g \Phi = 0$. Acting with $\mathcal{L}_K$ on Φ yields a new function for which

$$\Box_g(\mathcal{L}_K\Phi) = \mathcal{L}_K\big(\Box_g\Phi\big) + \left[\Box_g, \mathcal{L}_K\right]\Phi = 0, \tag{4.2.33}$$

implying that $\mathcal{L}_K\Phi$ also solves the wave equation. Consequently, new solutions can be constructed systematically, by acting on existing ones with a symmetry of the metric. For scalar fields, the Lie derivative reduces to the directional derivative along the vector field, $\mathcal{L}_K\Phi = K[\Phi]$.

To connect this symmetry-based construction to geometric optics and the conserved quantity q, we examine the action of $\mathcal{L}_K$ on a geometric optics solution. Explicitly, we find

$$\mathcal{L}_K\Phi = K\left[Ae^{iS}\right] = K[A]e^{iS} + iK[S]Ae^{iS} \approx iK[S]Ae^{iS}, \tag{4.2.34}$$

where the last approximation follows from the separation of scales (4.2.2). Recall from the construction of Hamilton-Jacobi solutions in Section 3.1.3 that $K[S]$ is conserved along the congruence due to the Killing property of K. Therefore, at leading order in $\ell_\mu = \partial_\mu S$, the action of a symmetry on a geometric optics solution reduces to multiplying the amplitude A by the conserved quantity $Q_K = K[S]$ associated with K.

From equation (3.1.12), we know that $\partial_u Q_K = 0$, confirming that the amplitude $Q_K A$ satisfies the same transport equation (4.2.5) as A. This aligns with the construction of q in the previous section, which relies on the multiplication of the amplitude by a conserved quantity. However, a closer examination reveals an important subtlety—the explicit form

$$q(x) = e^{-\gamma_L t}\delta r \tag{4.2.35}$$

shows that there exists no Killing field K such that $q(x) = K[S]$. This implies that certain conserved quantities, such as q, cannot be generated by any spacetime symmetry.

To explore this further, suppose there exists a vector field X such that $q = X^\mu \ell_\mu$. In this case, we have

$$q = \mathcal{L}_X S \quad \Rightarrow \quad \mathcal{L}_X \Phi \sim q\Phi, \tag{4.2.36}$$

for a particular solution $\Phi = Ae^{iS}$. In other words, there might exist vector fields X whose action generates new solutions from *specific* but *not all* existing solutions, even if X is not Killing. For the $q(x)$ defined above, one such vector field is $X = e^{-\gamma_L t}\partial_r$, as it satisfies

$$X[S] = e^{-\gamma_L t}\partial_r S = 3i\omega_R \gamma_L e^{-\gamma_L t}\delta r \sim q. \tag{4.2.37}$$

Although this will turn out not to be the full emergent symmetry, we now know that such non-Killing yet solution-generating vectors X exist. It is important to note that the region of solution validity is restricted to a small portion of the spacetime and will only generate new solutions on *certain* existing solutions; in the specific example of the approximate geometric optics solution, this is limited to the near-ring region.

In the following, we call such vector fields X—operators that generate new approximate solutions of the wave equation from *certain* existing solutions in a region of spacetime—*emergent symmetries*. The term reflects the fact that, while these transformations are not exact symmetries of the full spacetime, they act analogously to global (Killing) symmetries within a restricted subset of both the solution space and the spacetime. Their emergent nature will become clearer in Section 5.3.2, where we will see how these vector fields can be promoted to exact Killing vectors in the Penrose limit. In this sense, they "emerge" as symmetries in an appropriate regime. While this thesis focuses on the Schwarzschild case, a thorough generalisation of emergent symmetries to more general spacetimes would certainly go beyond the current analysis.

5 QNM Spectrum from the Penrose Limit Wave Equation

This section establishes a correspondence between the wave equation and its solutions in the Penrose limit and the near-ring quasinormal mode analysis presented in Section 4. We first identify the wave solutions that remain well-defined under the Penrose limit. Subsequently, we derive a complete classification of the QNM solutions of the wave equation in the plane wave geometry (3.2.8), revealing a double ladder structure generated by the plane wave isometry operators $a_\pm$ and $b_\pm$ introduced in Section 3.2.4. This structure is then shown to emerge as the $\lambda \to 0$ scaling limit of a corresponding ladder structure in the Schwarzschild near-ring region, derived via the coordinate transformation (3.2.11). Importantly, the Schwarzschild ladder structure involves not only exact isometry generators but also emergent symmetries specific to the near-ring region, which all become isometries of the Penrose limit. This section builds upon the findings of [4] and [3], with a stronger emphasis on the background of emergent symmetries established in Section 4.2.5.

5.1 Penrose Limit and Near Ring Region

In Section 4.2.4, we observed that the two geometric quantities determining the eikonal quasinormal mode spectrum are the orbital frequency Ω, normalised to the coordinate time t, and the Lyapunov exponent γ_L, which is related to $V''_{\text{eff}}(r_0)$ via equation (4.2.18). Notably, up to normalisation factors, these are precisely the quantities preserved by the Penrose limit (3.2.8) in its wave profile[16], where $A_{11} = -V''_{\text{eff}}(r_0)$ and $A_{22} = -\dot{\varphi}_\gamma^2$. This provides an initial indication that wave solutions of the plane wave equation, with appropriate boundary conditions imposed, could reproduce the eikonal QNM spectrum (4.2.31).

Before attempting to establish this connection rigorously, we first examine which wave solution modes of the original spacetime carry over nonsingularly to the Penrose limit, identifying the modes that remain well-defined. In this, we follow [4] and analyse the t- and φ-dependence of the modes (4.1.5) of Schwarzschild wave solutions, i.e. we study the limiting behaviour of

$$f_{\omega m}(x) = e^{-i\omega t + im\varphi}. \tag{5.1.1}$$

where $Y_{\ell m}(\theta, \varphi) \sim P_{\ell m}(\theta) e^{im\varphi}$ gives us the form of the φ-dependence. The radial and angular dependencies on r and θ are studied in detail in Section 5.3. To derive the conditions for a mode to remain non-singular in the Penrose limit, we rewrite this using the coordinate transformation (3.2.11) that relates the Schwarzschild to Brinkmann coordinates. This yields

$$f_{\omega m}(x) = e^{-i\omega \cdot 3u + im(3\Omega u + \Omega\lambda^2 v)} \equiv e^{-i\bar{\omega}u + ip_v v} \tag{5.1.2}$$

where

$$\bar{\omega} \equiv 3(\omega - m\Omega), \quad p_v \equiv m\Omega\lambda^2. \tag{5.1.3}$$

[16]Two subtleties should be noted here: Firstly, the eikonal QNM spectrum referenced above was derived using a polar congruence, where $\Omega = \dot{\theta}/\dot{t}$, whereas the Penrose limit (3.2.8) was constructed using an equatorial geodesic, leading to $\Omega = \dot{\varphi}/\dot{t}$. Due to the spherical symmetry of the Schwarzschild metric, however, these two settings are equivalent under a rotation. Secondly, while equation (4.2.18) may suggest that γ_L depends on E, for the Penrose limit, E was fixed to 1. Importantly, the $\frac{1}{E}$ factor in the definition of γ_L cancels the E^2 factor in $V''_{\text{eff}}(r)$, rendering γ_L independent of E.

These relationships can be inverted for ω and m, leading to

$$m = \frac{1}{\lambda^2}\frac{p_v}{\Omega}, \quad \omega = \frac{1}{3}\bar{\omega} + m\Omega = \frac{1}{3}\bar{\omega} + \frac{1}{\lambda^2}p_v \tag{5.1.4}$$

Their ratio is hence given by

$$\frac{\omega}{m} = \Omega + \lambda^2 \frac{\Omega}{3}\frac{\bar{\omega}}{p_v}. \tag{5.1.5}$$

For the modes (5.1.2) to remain non-singular in the limit $\lambda \to 0$, $\bar{\omega}$ and p_v must remain finite. The first equation in (5.1.4) hence requires

$$m \sim \frac{1}{\lambda^2} \gg 1. \tag{5.1.6}$$

In this limit, the $m\Omega$ term in the second equation of (5.1.4) dominates, and because of the relation $\Omega = (3\sqrt{3}M)^{-1} \sim 1/M$ this mandates

$$\omega \sim \frac{m}{M} \gg \frac{1}{M}. \tag{5.1.7}$$

Lastly, equation (5.1.5) translates to

$$\frac{\omega}{m} - \Omega \sim \frac{\lambda^2}{M} \ll \frac{1}{M}. \tag{5.1.8}$$

Recall that the integer m has its origin as a quantum number of the spherical harmonics $Y_{\ell m}$, and must hence satisfy $|m| \leq \ell$. Thus, equation (5.1.6) dictates that also $\ell \gg 1$. Moreover, for $m \approx \ell$, the last two equations reproduce the near-criticality and high-energy conditions of the near-ring region (4.2.13). We conclude that the modes studied in the derivation of the eikonal QNM spectrum in Section 4.2.4 are exactly those that remain non-singular in the limit $\lambda \to 0$, i.e. those that carry over to the Penrose limit. The Penrose limit thus naturally "zooms into" the near-ring region of the scalar wave solutions. In other words, the near-ring quasinormal solutions of the Schwarzschild wave equation remain solutions of the wave equation in the Penrose limit. We thus expect to be able to reproduce the eikonal QNM spectrum using the Penrose limit wave equation.

5.2 Quasinormal Mode Spectrum from Brinkmann Wave Equation

In the previous section, we demonstrated that wave solutions in the Schwarzschild spacetime which have non-singular Penrose limits are precisely those which lie in the near-ring region. This leads us to expect the eikonal quasinormal mode spectrum (4.2.31) to emerge from the wave equation in the Penrose limit, when imposing appropriate boundary conditions. In this section, we verify this through an analysis similar to that of [4] and [3]. More precisely, we will identify a fundamental mode from which the entire quasinormal mode spectrum can be generated by acting with the isometry algebra of the Penrose limit. This algebraic structure is essential for connecting the modes in the Penrose limit to the corresponding objects in the Schwarzschild spacetime.

The wave equation of a general plane wave metric in Brinkmann coordinates, (1.2.8), reads

$$0 = 2\partial_v\partial_u\Phi - A_{ab}(u)x^a x^b \partial_v^2\Phi + \delta^{ab}\partial_a\partial_b\Phi. \tag{5.2.1}$$

The form of this equation is already considerably simpler than the corresponding wave equation in the original Schwarzschild spacetime, (4.1.4), and is amenable to analytical solutions. In particular, the v-independence of equation (5.2.1) allows for a mode decomposition of solutions into modes of the form

$$\Phi(u, v, x^a) = e^{ip_v v}\Psi(u, x^a), \tag{5.2.2}$$

turning it into a time-dependent Schrödinger equation given by

$$ip_v\partial_u\Psi = -\frac{1}{2}\Delta\Psi - \frac{p_v^2}{2}A_{ab}(u)x^a x^b\Psi \tag{5.2.3}$$

where $\Delta = \delta^{ab}\partial_a\partial_b$ denotes the transverse Laplacian and u takes on the role of the time parameter. Due to the quadratic potential term, involving A_{ab} as a frequency matrix, we recognise this as a two-dimensional quantum harmonic oscillator problem with a time-dependent potential.

In our specific case, A_{ab} is u-independent and diagonal, enabling the separation of Ψ into modes as

$$\Psi(u, x^a) = e^{-i\bar{\omega}u}\phi_1(x_1)\phi_2(x_2). \tag{5.2.4}$$

This yields the separated equations

$$\begin{aligned} -\frac{1}{2}\phi_1'' - \frac{p_v^2}{2}A_{11}x_1^2\phi_1 &= E_1\phi_1, \\ -\frac{1}{2}\phi_2'' - \frac{p_v^2}{2}A_{22}x_2^2\phi_2 &= E_2\phi_2 \end{aligned} \tag{5.2.5}$$

for ϕ_1 and ϕ_2. The "energy eigenvalues" E_1 and E_2 are related to $\bar{\omega}$ via

$$\bar{\omega} = \frac{1}{p_v}(E_1 + E_2). \tag{5.2.6}$$

Ultimately, we want to form a connection between the spectrum arising from these equations and the isometry algebra from Section 3.2.4, as this will enable us to link the result to the Schwarzschild spacetime. Since the isometry generators depend on the parameter β, we recall that $A_{11} = -A_{22} = \beta^2$, which turns the one-dimensional harmonic oscillator equations (5.2.5) into

$$\begin{aligned} H_1\phi_1 &\equiv \frac{1}{2}(-\partial_1^2 - \beta^2 p_v^2 x_1^2)\phi_1 = E_1\phi_1, \\ H_2\phi_2 &\equiv \frac{1}{2}(-\partial_1^2 + \beta^2 p_v^2 x_2^2)\phi_2 = E_2\phi_2. \end{aligned} \tag{5.2.7}$$

At this stage, let us take a moment to interpret the result obtained so far. From Section 3.2.2, we know that the coordinates x_1 and x_2 correspond to the radial (r) and angular (θ) directions, respectively. Consequently, the functions ϕ_1 and ϕ_2 capture the radial and angular dynamics of the wave solution.
Examining the equations in (5.2.7), we observe a significant contrast between the two directions. The radial equation exhibits an inverted harmonic oscillator potential, indicative of instability in the r-direction. This reflects the divergent nature of radial geodesic motion near the photon ring, consistent with the physical interpretation of the Penrose limit. In

contrast, the angular equation features a simple harmonic oscillator potential, leading to stable oscillatory behaviour in the θ-direction.

5.2.1 Stable Angular Direction

We begin by analysing the x_2-direction, where the dynamics reduce to a familiar harmonic oscillator potential. This simpler case will serve as a basis for the treatment of the more complex radial x_1-direction. Notably, the θ-dependence of the exact wave solution in the Schwarzschild geometry, equation (4.1.5), is L^2-integrable. To remain consistent, we impose the same condition on ϕ_2.

There are several methods available for deriving the harmonic oscillator spectrum and its corresponding wavefunctions within L^2-spaces. Among these, the algebraic method —using raising and lowering operators—is particularly suited for our purposes. This method not only simplifies the derivation but also establishes a direct connection to the isometry algebra of the underlying plane wave spacetime we discussed in Section 3.2.4. For a thorough discussion of the algebraic method of constructing the harmonic oscillator spectrum, see e.g. section 2.3 of Griffiths [13].

We begin by defining the raising and lowering operators

$$\tilde{a}_\pm = \frac{1}{\sqrt{2\beta}}(\mp\partial_2 + \beta p_v x_2) \tag{5.2.8}$$

which satisfy the commutator relation

$$[\tilde{a}_-, \tilde{a}_+] = p_v. \tag{5.2.9}$$

Moreover, we can write the harmonic oscillator equation for ϕ_2 in (5.2.7) as

$$\beta\left(\tilde{a}_+\tilde{a}_- + \frac{1}{2}p_v\right)\phi_2 \equiv H_2\phi_2 = E_2\phi_2. \tag{5.2.10}$$

From the commutator

$$[H_2, \tilde{a}_\pm] = \pm\beta p_v \tilde{a}_\pm \tag{5.2.11}$$

we conclude that $\tilde{a}_\pm$ shifts the energy eigenvalue of an eigenfunction[17] ϕ_2 by $\pm\beta p_v$. To construct a ladder of L^2-solutions, we solve for the ground state, which must satisfy $\tilde{a}_-\phi_2 = 0$. A non-normalised ground state solution reads

$$\phi_2^0(x_2) = e^{-\frac{1}{2}\beta p_v x_2^2} \tag{5.2.12}$$

which has the energy

$$H_2\phi_2^0 = \frac{1}{2}\beta p_v \phi_2^0 \equiv E_2^0\phi_2^0. \tag{5.2.13}$$

[17] unless $\tilde{a}_-\phi_2 = 0$. To see the claimed shift in eigenvalues, consider $H_2\tilde{a}_\pm\phi_2 = \tilde{a}_\pm H_2\phi_2 + [H_2, \tilde{a}_\pm]\phi_2 = (E_2 \pm \beta p_v)\tilde{a}_\pm\phi_2$.

[18] There are no other solutions, since these would have to constitute their own ladder with a corresponding lowest energy state in the ladder, which would also need to satisfy $\tilde{a}_-\phi_2 = 0$, but this first order equation has a one-dimensional solution space.

The ground state solution ϕ_2^0 represents the fundamental oscillatory mode in the x_2-direction. It allows us to generate the full set[18] of L^2-eigenfunctions $\phi_2^{n_2}$ and eigenvalues $E_2^{n_2}$, given by

$$\phi_2^{n_2}(x_2) = (\tilde{a}_+)^{n_2}\phi_2^0(x_2), \quad E_2^{n_2} = \beta p_v\Big(n_2 + \frac{1}{2}\Big). \tag{5.2.14}$$

To see how this relates to the isometry algebra from Section 3.2.4, let us examine what the action of $\tilde{a}_\pm$ on $\phi_2(x_2)$ amounts to for the full wave function Φ from equation (5.2.2). Firstly, we note that E_2 gets shifted by $\pm\beta p_v$, which by equation (5.2.6) shifts $\bar{\omega}$ by $\pm\beta$. Thus,

$$\phi_2 \mapsto \tilde{a}_\pm\phi_2 \quad \Longrightarrow \quad \Phi \mapsto e^{\mp i\beta u}\tilde{a}_\pm\Phi \tag{5.2.15}$$

Since Φ depends on v only through $e^{ip_v v}$, in the expression

$$e^{\mp i\beta u}\tilde{a}_\pm = \frac{1}{\sqrt{2\beta}}e^{\mp i\beta u}(\mp\partial_2 + \beta p_v x_2), \tag{5.2.16}$$

we may replace the occurrence of p_v by a derivative with respect to v, $p_v \to -i\partial_v$. Notice that this reproduces the isometry generators $a_\pm$ from Section 3.2.4 —hence, for a given wave function Φ with the ϕ_2 component in its ground state, we can move between modes of the x_2 direction simply by acting on it with the isometry generators $a_\pm$.

5.2.2 Unstable Radial Direction

In general, the second equation in (5.2.7) allows for solutions for any eigenvalue E_1. The only solutions of interest to us, however, are those which satisfy outgoing QNM boundary conditions, as the x_2-coordinate is associated with the radial direction r in the original spacetime. In Appendix B we show that the spectrum of the inverted harmonic oscillator subject to these boundary conditions is simply the analytic continuation $\beta \to -i\beta$ of the simple harmonic oscillator. By this, we are led to define the ladder operators

$$\tilde{b}_\pm = \frac{1}{\sqrt{2\beta}}(\mp\partial_1 - i\beta p_v x_1) \tag{5.2.17}$$

which are simply the analytic continuation of equation (5.2.8) (except for the normalisation factor $1/\sqrt{2\beta}$), now acting on ϕ_1 instead of ϕ_2. We expect that these ladder operators allow us to construct the eigenstates to the eigenvalue spectrum

$$E_1^{n_1} = -i\beta p_v\Big(n_1 + \frac{1}{2}\Big), \tag{5.2.18}$$

which we now verify.

Firstly, we note that we can express the radial Hamiltonian H_1 as

$$H_1 = \beta\Big(\tilde{b}_+\tilde{b}_- - \frac{i}{2}p_v\Big) \tag{5.2.19}$$

From the commutators

$$\big[\tilde{b}_-, \tilde{b}_+\big] = -ip_v, \quad \big[H_1, \tilde{b}_\pm\big] = \mp i\beta p_v\tilde{b}_\pm, \tag{5.2.20}$$

we infer by the same reasoning as for the simple harmonic oscillator that the action of $\tilde{b}_\pm$ on an eigenstate of H_1 yields a new eigenstate with an eigenvalue shifted by $\mp i\beta p_v$. In

analogy to the simple harmonic oscillator, the solution of the first-order equation $\tilde{b}_-\phi_1 = 0$ serves as a "ground state" with eigenvalue $E_1^0 = -\frac{i}{2}\beta p_v$. It is a seed solution from which we can produce all eigenfunctions by means of repeatedly applying $\tilde{b}_+$, i.e.

$$\phi_1^{n_1}(x_1) = \big(\tilde{b}_+\big)^{n_1}\phi_1^0(x_1) \quad \text{at eigenvalue} \quad E_1^{n_1} = -i\beta\Big(n_1 + \frac{1}{2}\Big). \tag{5.2.21}$$

We can again analyse how the action of $\tilde{b}_\pm$ on an eigenfunction ϕ_1 affects the full wave function Φ. Similar to the stable direction, the operators $\tilde{b}_\pm$ shift E_1 by $\mp i\beta p_v$, which by equation (5.2.6) shifts $\bar{\omega}$ by $\mp i\beta$. Consequently,

$$\phi_1 \mapsto \tilde{b}_\pm\phi_1 \quad \Longrightarrow \quad \Phi \mapsto e^{\mp\beta u}\tilde{b}_\pm\Phi = \frac{1}{\sqrt{2\beta}}e^{\mp\beta u}(\mp\partial_1 - i\beta p_v x_1)\Phi, \tag{5.2.22}$$

in analogy to equation (5.2.16). Rewriting $ip_v \to \partial_v$, we find that the action of $\tilde{b}_\pm$ on ϕ_1 is reproduced on the full wave function Φ by acting on it with the isometry generators $b_\pm$ from Section 3.2.4.

5.2.3 Summary

In the above, we derived the QNM solutions of the wave equation equation (5.2.1) under outgoing boundary conditions in the radial direction x_1 and L^2-normalisability in the angular direction x_2. These solutions can be constructed systematically from the fundamental mode, whose wave function is given by

$$\Phi_{0,0}(x) = e^{-i\bar{\omega}u + ip_v v}e^{\frac{i}{2}\beta p_v x_1^2}e^{-\frac{1}{2}\beta p_v x_2^2} \quad \text{with} \quad \bar{\omega} = \frac{1}{2}\beta - \frac{i}{2}\beta. \tag{5.2.23}$$

Higher order modes are generated by repeatedly applying the isometry generators a_+ and b_+ to $\Phi_{0,0}$, yielding

$$\Phi_{n_1,n_2}(x) = (b_+)^{n_1}(a_+)^{n_2}\Phi_{0,0}(x), \tag{5.2.24}$$

where the corresponding eigenvalues $\bar{\omega}$ read

$$\bar{\omega}_{n_1,n_2} = \beta\Big(n_2 + \frac{1}{2}\Big) - i\beta\Big(n_1 + \frac{1}{2}\Big). \tag{5.2.25}$$

These results form a double-ladder structure for the QNM solutions, linking the spectrum to the isometry algebra discussed in Section 3.2.4. By the relationship to the frequency ω in the original spacetime from equation (5.1.4), we find the Schwarzschild QNM spectrum

$$\omega_{n_1,n_2} = \frac{1}{3}\bar{\omega}_{n_1,n_2} + m\Omega = \Omega\Big(m + n_2 + \frac{1}{2}\Big) - i\gamma_L\Big(n_1 + \frac{1}{2}\Big), \tag{5.2.26}$$

Here, we use the fact that β is associated with the second derivative of the effective geodesic potential in the original spacetime, $\beta = \sqrt{V''_{\text{eff}}(r_0)}$, for the unstable x^1-direction corresponding to n_1, and $\beta = 3\Omega$ for the stable x_2-direction (see Section 3.2.3). This leads to the identification

$$\frac{1}{3}\beta = \gamma_L = \Omega, \tag{5.2.27}$$

with γ_L corresponding to the x_1-part and Ω corresponding to the x_2-part of $\bar{\omega}$.

While equation (5.2.26) shares a similar structure with the eikonal QNM spectrum (4.2.31), a rigorous demonstration of their equivalence requires justifying the identifications $\ell = m + n_2$ and $n = n_1$. These identifications will be addressed in the following sections.

5.3 Plane Wave Isometries and (Emergent) Symmetries in Schwarzschild

In this section, we relate the double-ladder structure of the plane wave QNM solutions and associated ladder operators derived in the above to corresponding objects in the Schwarzschild geometry. This leads us to identify exact as well as emergent symmetries in the Schwarzschild spacetime whose scaling limits constitute the plane wave isometry generators $a_\pm$ and $b_\pm$. Moreover, the plane wave fundamental mode $\Phi_{0,0}$ is identified as the scaling limit of certain functions in the Schwarzschild spacetime, which establishes the correspondence between a double ladder structure of near-ring QNM solutions in Schwarzschild and the solution structure in the plane wave spacetime.

5.3.1 Scaling Limit of Spherical Harmonics and Ladder Operators

We now investigate the relationship between the isometry generators $a_\pm$ from Section 3.2.4 and their counterparts in the Schwarzschild spacetime. Recall from Section 5.2 that the $a_\pm$ generate higher-order modes when acting on the fundamental mode of the wave solution in the Penrose limit. Our first goal is to identify a wave solution in the Schwarzschild geometry whose scaling limit corresponds to the fundamental mode (or ground state) in the x_2-direction. Since higher-order modes in the Penrose limit are obtained by applying $a_\pm$ to the fundamental mode, we expect a similar ladder structure in the Schwarzschild spacetime to emerge from the correspondent of the plane wave ground state, generated by operators that scale into the $a_\pm$. To proceed, we first identify the fundamental mode correspondent.

In Section 5.1, we found that the Schwarzschild wave modes with non-singular scaling limits are precisely those that satisfy the near-ring conditions with $m \approx \ell$, motivating the study of wave modes with $m = \ell$. Moreover, the relationship

$$m = \frac{1}{\lambda^2}\frac{p_v}{\Omega} \quad \Longleftrightarrow \lambda^2 = \frac{1}{m}\frac{p_v}{\Omega} \tag{5.3.1}$$

was established, allowing us to rephrase the scaling limit $\lambda \to 0$ as $m \to \infty$. Since the $a_\pm$ are associated to the angular direction $x^2 \sim \theta$, we focus on the scaling limit of the (t, θ, φ)-dependence of the Schwarzschild wave modes (4.1.5). Using the coordinate transformation (3.2.11) and the explicit expression of the spherical harmonic $Y_{mm}(\theta, \varphi) = \sin^m\theta\, e^{im\varphi}$ we find

$$\begin{aligned} e^{-i\omega t}Y_{mm}(\theta,\varphi) &= e^{-i\omega t + im\varphi}\sin^m\theta \\ &= e^{-i\bar{\omega}u + ip_v v}\left(\cos\frac{\lambda}{3M}\psi\right)^m \end{aligned} \tag{5.3.2}$$

By our findings from Section 5.1, the $e^{-i\bar{\omega}u+ip_v v}$ term remains invariant under the scaling limit $m \to \infty$. However, the ψ-dependence undergoes a noteworthy transformation. Specifically, when expanding the cosine, we obtain

$$\begin{aligned}\left(\cos\frac{\lambda}{3M}\psi\right)^m &= \left(1-\frac{1}{2}\frac{\lambda^2}{9M^2}\psi^2+\mathcal{O}(\lambda^4)\right)^m \\ &= \left(1-\frac{\frac{1}{2}\beta p_v\psi^2}{m}+\mathcal{O}\Big(\frac{1}{m^2}\Big)\right)^m \xrightarrow{m\to\infty} e^{-\frac{1}{2}\beta p_v\psi^2}.\end{aligned} \tag{5.3.3}$$

This is immediately recogniseed as the ground state $\phi_2^0(x_2)$ from Section 5.2 under the identification $\psi = x_2$. Thence, the near-ring solutions of the Schwarzschild wave equation with $\ell = m$ scale into the fundamental mode of the Penrose limit's wave equation for the x_2-direction.

In the Penrose limit, higher order modes in the x_2-direction are generated by acting on the fundamental mode with the isometry generators $a_\pm$, resulting in a ladder structure of solutions. Each solution corresponds to a wave solution in the Schwarzschild spacetime which scales into it, forming a ladder structure in the geometry of origin. The algebraic structure behind spherical harmonics is a prime candidate for this ladder structure—to see this, let us briefly review the necessary background, with further details deferred to Appendix C. We define the operators

$$J_a = \frac{1}{i}K_{(a)}, \quad J_\pm = J_1 \pm iJ_2, \quad \boldsymbol{J}^2 = \delta_{ab}J_aJ_b. \tag{5.3.4}$$

Explicitly, the relevant differential operators are

$$J_\pm = e^{\pm i\varphi}\big(\mp\partial_\theta - i\cot\theta\partial_\varphi\big), \quad J_3 = \frac{1}{i}\partial_\varphi, \qquad \boldsymbol{J}^2 = -\Delta_{S^2}. \tag{5.3.5}$$

Their action on the spherical harmonics is given by

$$\boldsymbol{J}^2Y_{\ell m} = \ell(\ell+1)Y_{\ell m}, \quad J_3Y_{\ell m} = mY_{\ell m}, \quad \ell, m\in\mathbb{N}, \quad |m|\le\ell \tag{5.3.6}$$

$$J_+Y_{\ell m} = \begin{cases}0, & m=\ell,\\ Y_{\ell,m+1}, & m<\ell,\end{cases} \qquad J_-Y_{\ell m} = \begin{cases}Y_{\ell,m-1}, & m>-\ell,\\ 0, & m=-\ell.\end{cases} \tag{5.3.7}$$

Thus, $Y_{\ell m}$ are simultaneous eigenvectors of $\boldsymbol{J}^2$ and J_3 at eigenvalues $\ell(\ell+1)$ and m, respectively. The operators $J_\pm$ act as raising and lowering operators for the eigenvalue m, altering it by ±1. Any arbitrary spherical harmonic can be generated from $Y_{\ell\ell} = \sin^\ell\theta\, e^{i\ell\varphi}$ by repeatedly applying J_-. Note here that this "seed solution", $Y_{\ell\ell}$, is nothing other than the polar part of the wave solution we identified to scale into the fundamental mode in the Penrose limit. Since $J_+Y_{\ell\ell} = 0$, there is a "downward" ladder structure emerging from repeated action of J_- on $Y_{\ell\ell}$, establishing $J_\pm$ as candidates for scaling into $a_\mp$. This intuition is further validated by examining the explicit forms of $J_\pm$ in equation (5.3.7) and recalling the scaling coordinate transformation (3.2.11). Roughly speaking, the ∂_θ-derivative will scale into $\partial_\psi = \partial_2$, $\cot\theta$ into $\psi = x_2$, and ∂_φ is replaced by a term proportional to ∂_v. This indicates that $a_\pm$ might be reproduced as the scaling limit of $J_\pm$—let us now establish this rigorously. Explicitly, we have

$$\begin{aligned}\partial_\theta &= 3M\lambda^{-1}\partial_\psi, \quad & \cot\theta &= -\frac{\lambda}{3M}\psi+\mathcal{O}(\lambda^3),\\ \varphi &= \beta u+\Omega\lambda^2 v, \quad & \partial_\varphi &= \lambda^{-2}\Omega^{-1}\partial_v,\end{aligned} \tag{5.3.8}$$

which assembles into

$$J_{\pm} = \lambda^{-1} 3M e^{\pm i(\beta u + \lambda^2 \Omega v)} \big(\mp \partial_{\psi} + i\beta\psi\partial_{v}\big) + \mathcal{O}(\lambda). \tag{5.3.9}$$

Up to a normalisation factor and the singular behaviour of λ^{-1} in the scaling limit $\lambda \to 0$, this result aligns well with expectations. The normalisation factor presents no issue due to the linearity of the Killing equation, which permits arbitrary scaling. Regarding the singular factor λ^{-1}, a straightforward remedy is to consider the scaling limit of $\lambda J_{\pm}$ instead, analogous to the Penrose limit's rescaling of the metric, $g \to \lambda^{-2} g$. With this, we can see that $\lambda J_{\pm} \to a_{\mp}$ as $\lambda \to 0$, up to a normalisation constant. Notice that $\lambda J_{\pm}$ is a Killing vector for all finite $\lambda > 0$, due to the linearity of the Killing equation.

To illustrate the correspondence of the ladder operators and ladder structure, consider the commuting diagram in Figure 2 below:

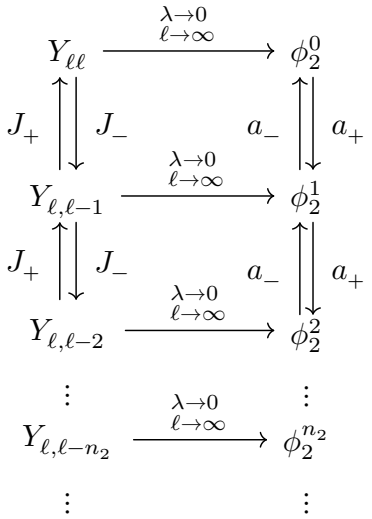

Figure 2: Ladder structure of the angular dependence of Schwarzschild wave modes, i.e. spherical harmonics (left) and the corresponding scaling limits (right).

In particular, we infer that $m = \ell - n_2$, i.e. n_2 represents the amount of ladder steps taken from the seed solution $\Phi_{0,0}$ and its lift[19] $Y_{\ell\ell}$, respectively. With this relation, the QNM spectrum from the Penrose limit we derived in Section 5.2, equation (5.2.26), becomes

$$\omega_{n_1,\ell} = \Omega\left(\ell + \frac{1}{2}\right) - i\gamma_L\left(n_1 + \frac{1}{2}\right), \tag{5.3.10}$$

leaving us to identify n_1 with the overtone number n to reproduce the eikonal QNM spectrum from Section 4.2.4. We investigate this second relationship, $n_1 = n$, in the next section.

5.3.2 Emergent Symmetries of the Near-Ring Wave Equation

The previous section demonstrated how the isometry generators $a_{\pm}$ of the plane wave geometry correspond to the scaling limits of the Schwarzschild isometry generators $J_{\pm}$. A natural question arises: can the $b_{\pm}$ generators similarly emerge as scaling limits of vector fields in the Schwarzschild geometry?

Unlike $a_{\pm}$, which act on the angular direction x_2, the $b_{\pm}$ generators are associated with the radial x_1-direction in the plane wave geometry. This suggests that their Schwarzschild

[19] In this context, a lift of an object X in the plane wave spacetime refers to an object in Schwarzschild that has X as its scaling limit.

lifts must act on the radial coordinate r. However, none of the Killing vectors of the Schwarzschild geometry, (3.1.18), exhibit dependence on r nor contain an r-component. Consequently, the $b_\pm$ cannot arise as scaling limits of exact isometry generators in the Schwarzschild spacetime.

However, recall from Section 5.1 that the wave solutions in the plane wave spacetime correspond precisely to the near-ring solutions in Schwarzschild. This implies that the ladder structure generated by $b_\pm$ needs to be reproduced only within the near-ring region, not globally across the Schwarzschild spacetime and wave solution space. Thus, we seek operators in the Schwarzschild spacetime that act as symmetry transformations on near-ring solutions, i.e. emergent symmetries as introduced in Section 4.2.5.

To construct the emergent symmetries $X_\pm$, we review the near-ring limit of the radial wave equation

$$0 = \partial_{r_*}^2\psi + [\omega^2 - \mathcal{V}(r_*)]\psi, \quad \mathcal{V}(r_*) = f(r)\left[\frac{\ell(\ell+1)}{r^2} + \frac{2M}{r^3}\right] \tag{5.3.11}$$

which we derived in Section 4.1.1. Specifically, we consider high-energy near-critical weakly damped ($\omega_R \gg \omega_I$) modes in the near-ring region, which is to say that

$$r \approx 3M, \quad \omega^2 \approx \omega_R^2 + 2i\omega_R\omega_I, \quad \ell(\ell+1) \approx 27M^2\omega_R^2 \tag{5.3.12}$$

Expanding the potential to second order in $\delta r = r - 3M$ with the above approximations leads to

$$\mathcal{V}(r_*) \approx \omega_R^2 - 9\gamma_L^2\omega_R^2\delta r^2. \tag{5.3.13}$$

Together with $\partial_{r_*} = f(r)\partial_r \approx \frac{1}{3}\partial_{\delta r}$, this reduces the radial wave equation to

$$\mathcal{H}\psi(\delta r) = \frac{1}{2\omega_R}\left[\frac{1}{9}\partial_{\delta r}^2 + 9\gamma_L^2\omega_R^2\delta r^2\right]\psi(\delta r) = -i\omega_I\psi(\delta r). \tag{5.3.14}$$

This is an inverted harmonic oscillator equation that can be treated in analogy to Section 5.2.2. In particular, the "Hamiltonian" operator $\mathcal{H}$ on the left-hand side can be rewritten as

$$\mathcal{H} = \tilde{X}_+\tilde{X}_- + \frac{i}{2}\gamma_L, \quad \tilde{X}_\pm \equiv \frac{1}{\sqrt{2\omega_R}}\left[\frac{1}{3}\partial_{\delta r} \pm i3\gamma_L\omega_R\delta r\right]. \tag{5.3.15}$$

We have the commutators

$$\left[\tilde{X}_-, \tilde{X}_+\right] = i\gamma_L, \quad \left[\mathcal{H}, \tilde{X}_\pm\right] = \pm\gamma_L\tilde{X}_\pm. \tag{5.3.16}$$

Because of this, we may construct the ladder of solutions to equation (5.3.14) as

$$\psi_n(\delta r) = \tilde{X}_+^n\psi_0(\delta r) \quad \text{with} \qquad \omega_I^n = -\gamma_L\left(n + \frac{1}{2}\right). \tag{5.3.17}$$

from the "ground state"

$$\psi_0(\delta r) = e^{\frac{i}{2}3\gamma_L\omega_R\left(\sqrt{3}\delta r\right)^2} = e^{\frac{i}{2}\beta\omega_R\left(\sqrt{3}\delta r\right)^2} \tag{5.3.18}$$

which satisies $\tilde{X}_-\psi_0 = 0$ and has the "energy" eigenvalue $\mathcal{H}\psi_0 = \frac{i}{2}\gamma_l\psi_0$. The action of $\tilde{X}_\pm$ on a radial eigenfunction ψ thus shifts ω_I by $\mp\gamma_L$, which translates to

$$\psi \mapsto \tilde{X}_\pm\psi \quad \Longrightarrow \quad e^{-i\omega t}\psi \mapsto e^{\mp\gamma_L t}\tilde{X}_\pm[e^{-i\omega t}\psi]. \tag{5.3.19}$$

From this, we want to derive two vectors $X_\pm$ which generalise this action onto the full wave function Φ from equation (4.1.5). To this end, we define

$$X_\pm \equiv \frac{1}{\sqrt{2\omega_R}}e^{\mp\gamma_L t}\left[\frac{1}{3}\partial_{\delta r} \pm 3\gamma_L^2\delta r\,\partial_\varphi\right] = \frac{1}{3\sqrt{2\omega_R}}e^{\mp\gamma_L t}\left[\partial_{\delta r} \pm \beta^2\delta r\,\partial_\varphi\right] \tag{5.3.20}$$

The introduction of $\gamma_L\partial_\varphi$ to replace $i\omega_R$is justified by the fact that for Schwarzschild wave modes with $m \approx \ell \gg 1$, we have

$$\gamma_L\partial_\varphi Y_{\ell m} = \gamma_L im Y_{\ell m} \approx i\gamma_L\ell Y_{\ell m} \approx i\omega_R Y_{\ell m}. \tag{5.3.21}$$

for near-critical solutions. The action of $X_\pm$ on a near-ring mode

$$\Phi_{\omega n\ell m} = e^{-i\omega t}\frac{\psi_n(r)}{r}Y_{\ell m}(\theta,\varphi) \tag{5.3.22}$$

is hence given by

$$X_\pm\Phi_{\omega n\ell m} \approx e^{-i(\omega\mp i\gamma)t}Y_{\ell m}\frac{\tilde{X}_\pm\psi_n}{r} = e^{-i(\omega\mp i\gamma)t}\frac{\psi_{n\pm1}}{r}Y_{\ell m} \approx \Phi_{\omega,n\pm1,m\ell} \tag{5.3.23}$$

for $r \approx 3M$. We neglect the action of $\tilde{X}_\pm$ on the $1/r$ factor as it is suppressed by $\frac{1}{M^2}$,

$$\left|\tilde{X}_\pm\frac{1}{r}\right| = \left|\partial_r\frac{1}{r}\right| = \frac{1}{3M}\left|\partial_r\left[1 - \frac{\delta r}{3M} + \mathcal{O}\left(\frac{\delta r^2}{3M^2}\right)\right]\right| \ll \frac{1}{M^2} \quad \text{for } |\delta r| \ll M. \tag{5.3.24}$$

We have thus shown that $X_\pm\Phi$ is a near-ring solution provided that Φ is as well, and hence verified that $X_\pm$ is an emergent symmetry of the Schwarzschild near-ring limit.

To verify the correspondence between the $X_\pm$ and $b_\pm$ ladder structures, we need to check two things. Firstly, the ground state $\psi_0(\delta r)$ must scale into the ground state $\phi_1^0(x_1)$ of the plane wave geometry, and the $X_\pm$ operators must have the $b_\pm$ as their scaling limits. To check the former, we make use of the coordinate transformation (3.2.11) as well as the relationships (5.1.4), expressed through which the ground state equation (5.3.18) reads

$$\psi_0(\delta r) = e^{\frac{i}{2}\beta\left(\frac{1}{3}\bar{\omega}+\frac{1}{\lambda^2}p_v\right)\lambda^2\rho^2} \xrightarrow{\lambda\to0} e^{\frac{i}{2}\beta p_v\rho^2}. \tag{5.3.25}$$

By identifying $\rho = x_1$, we recognise the ground state ϕ_1^0 of the x_1-direction in the plane wave geometry, and have hence verified the scaling limit of ϕ_0. Repeating the same procedure for the emergent symmetries $X_\pm$, employing the relations (5.3.8) as well as $\partial_{\delta r} = \lambda^{-1}\sqrt{3}\,\partial_\rho$ we find

$$X_\pm \sim \lambda^{-1}e^{\mp\beta u}\left[\,\partial_\rho \pm \beta\rho\partial_v\right], \tag{5.3.26}$$

from which we infer that $\lambda X_\pm$ has a scaling limit proportional to the isometry generators $b_\pm$ from Section 3.2.4. This establishes the correspondence between the radial ladder structures in the Schwarzschild and plane wave geometries, as depicted in Figure 3 below. To conclude this section, we note that in addition to the near-ring conditions, we made use of $\ell \approx m$,

which does not hold in general. From the previous section, we know that $n_2 = \ell - m$, which means that the radial ladder structure's correspondence is only valid for small values of n_2. Notice that this is consistent with the requirement $n \ll \ell$ necessary to obtain the eikonal QNM spectrum from the WKB approximation, as seen in equation (4.1.27).

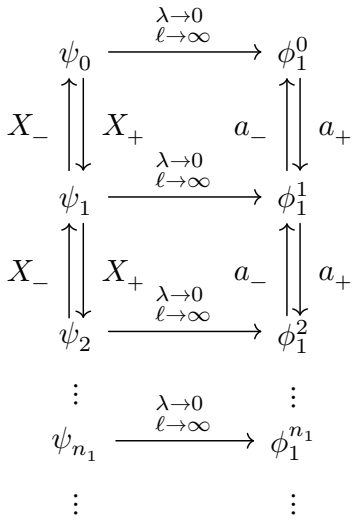

Figure 3: Ladder structure of the radial near-ring Schwarzschild solutions (left) and the corresponding scaling limits (right).

5.3.3 Completing the Isometry Algebra

Besides the ladder operators $a_\pm$ and $b_\pm$, the Penrose limit of the Schwarzschild spacetime along the equatorial photon ring (3.2.8) has two additional isometry generators,

$$Z = -i\partial_v, \quad H = \frac{i}{\beta}\partial_u. \tag{5.3.27}$$

In this section we identify their lifts in the Schwarzschild spacetime and summarise the (emergent) symmetries in the Schwarzschild geometry that reproduce the plane wave isometry algebra as their scaling limit.

The ladder operators $a_\pm$ are linked to the angular momentum generators $J_\pm$, which span the same subspace of the complexified tangent space as the Schwarzschild Killing vectors $K_{(1)}$ and $K_{(2)}$. Given this, is is natural to conjecture that the remaining Killing vectors of the Schwarzschild spacetime, $K_{(0)} = \partial_t$ and $K_{(3)} = \partial_\varphi$, should also exhibit meaningful scaling limits.

To confirm this intuition, we consider the coordinate transformation (3.2.11), under which the Killing vectors $K_{(0)}$ and $K_{(3)}$ transform as

$$K_{(0)} = \partial_t = \frac{du}{dt}\partial_u = \frac{1}{3}\partial_u, \quad K_{(3)} = \partial_\varphi = \frac{\partial v}{\partial \varphi}\partial_v = \lambda^{-2}\Omega^{-1}\partial_v \tag{5.3.28}$$

From these results, it is evident that the Kiling vector $K_{(0)}$ scales into an operator proportional to H, while the scaled Killing vector $\lambda^2 K_{(3)}$, or equivalently $\lambda^2 J_3$ with a different normalisation constant, reproduces Z.

A summary of the plane wave isometry algebra and their lifts in the Schwarzschild geometry is provided in Table 1. Any entry in the "Schwarzschild" column has its counterpart in the "Plane Wave" column as its scaling limit, making it a lift of the plane wave

correspondent. The correspondence is to be understood as up to normalisation factors. Here, we should point out that all plane wave isometry generators except for $b_\pm$ emerge as scaling limits of isometry generators in the Schwarzschild spacetime. The $b_\pm$ however result from the scaling limits of the $X_\pm$ operators, which are emergent symmetries of the near-ring region, i.e. they act as symmetry transformations on near-ring solutions around $r = 3M$.

Spacetime	**Schwarzschild**	**Plane Wave**
Time Transl. Gen.	$K_{(0)} = \partial_t$	$H = \frac{i}{\beta}\partial_u$
Rotation Gen.	$K_{(3)} = \partial_\varphi$	$Z = -i\partial_v$
Angular Ladder Op.	$J_\pm = e^{\pm i\varphi}\big(\mp\partial_\theta - i\cot\theta\partial_\varphi\big)$	$a_\pm \sim e^{\mp i\beta u}(\mp\partial_2 - i\beta x_2\partial_v)$
Radial Ladder Op.	$X_\pm \sim e^{\mp\gamma_L t}\big(\partial_{\delta r} \pm \beta^2\delta r\,\partial_\varphi\big)$	$b_\pm \sim e^{\mp\beta u}(\mp\partial_1 - \beta x_1\partial_v)$

Table 1: Overview of the plane wave isometry generators and their lifts in Schwarzschild.

At this stage, we can also study a consequence of the additional scalings required to obtain the non-singular scaling limits $a_\pm$ and Z from their lifts $J_\pm$ and J_3. Recall that the operators $J_\pm$ and J_3 span the (complexified) $\mathfrak{so}(3)$ isometry subalgebra corresponding to the spherical symmetry of the Schwarzschild geometry, satisfying the commutator relations

$$[J_-, J_+] = 2J_3, \quad [J_3, J_\pm] = \pm J_\pm. \tag{5.3.29}$$

We now define

$$a_\pm^{(\lambda)} \equiv \lambda J_\mp, \quad Z^{(\lambda)} \equiv \lambda^2 J_3, \tag{5.3.30}$$

so that the scaling limit

$$\lim_{\lambda\to 0} a_\pm^{(\lambda)} \sim a_\pm, \quad \lim_{\lambda\to 0} Z^{(\lambda)} \sim Z \tag{5.3.31}$$

reproduces the plane wave isometry generators $a_\pm$ and Z. Notice that for each finite $\lambda > 0$, $a_\pm^{(\lambda)}$ and $Z^{(\lambda)}$ satisfy the same $\mathfrak{so}(3)$ algebra as $J_\pm$ and J_3 up to normalisations, i.e.

$$\begin{aligned}\big[a_+^{(\lambda)}, a_-^{(\lambda)}\big] &= \lambda^2[J_-, J_+] = 2\lambda^2 J_3 = 2Z^{(\lambda)},\\ \big[Z^{(\lambda)}, a_\pm^{(\lambda)}\big] &= \lambda^3[J_3, J_\mp] = \mp\lambda^3 J_\mp = \mp\lambda^2 a_\pm^{(\lambda)}\end{aligned} \tag{5.3.32}$$

Taking the limit $\lambda \to 0$ on the first equation yields, as expected from Section 3.2.4, the commutator

$$[a_-, a_+] \sim Z. \tag{5.3.33}$$

For the second commutator, although expected as well, something more interesting happens. In the limit $\lambda \to 0$, we find

$$[Z, a_\pm] \sim \mp 0 \cdot a_\pm = 0. \tag{5.3.34}$$

Remarkably, this alters the algebraic structure of the isometry algebra. For all finite $\lambda > 0$, the set $\left\{a_{\pm}^{(\lambda)}, Z^{(\lambda)}\right\}$ spans $\mathfrak{so}(3)$, but in the limit $\lambda \to 0$, the algebra is deformed such that Z becomes a central element, aligning with the Heisenberg algebra structure of the plane wave geometry, as discussed in Section 3.2.4. This process of the limiting deformation of a group/algebra is called a *group/algebra contraction*. The above considerations show that the additional scalings of $J_{\pm}$ by λ and J_3 by λ^2 are not only necessary to keep their scaling limits non-singular, but also to ensure that the algebraic structure of $\mathfrak{so}(3)$ contracts into a Heisenberg algebra.

To close this chapter, the following section provides an overview over the foregoing derivations and highlights essential insights.

5.4 Summary

This section summarises the calculation-heavy preceding parts and interprets the derived results.

In Section 5.1, we analysed the behaviour of solutions to the wave equation in Schwarzschild spacetime under the Penrose limit, i.e. under the limit $\lambda \to 0$ following the coordinate transformation (3.2.11). This analysis revealed that near-ring solutions—solutions subject to the conditions (4.2.13)—are precisely those that scale non-singularly under the Penrose limit. These solutions determine the eikonal quasinormal mode spectrum of the Schwarzschild black hole, further substantiating the utility of the Penrose limit for deriving this spectrum.

To confirm this connection, in Section 5.2 we proceeded to derive the QNM solutions of the wave equation in the plane wave geometry. These solutions, satisfying outgoing boundary conditions in the radial direction and consisting of decaying L^2-functions in the angular direction, revealed a double-ladder structure originiating from the fundamental mode $\Phi_{0,0}$. The plane wave isometry generators $a_{\pm}$ and $b_{\pm}$ (introduced in Section 3.2.4) act as ladder operators for this structure. Moreover, the resulting spectrum, equation (5.2.26), remarkably mirrors the eikonal QNM spectrum (4.2.31) determined through geometric optics in the Schwarzschild near-ring region, up to identification of the integers that appear in it.

Given that the near-ring Schwarzschild wave solutions scale non-singularly into wave solutions of the plane wave geometry (3.2.8), one would expect the same double ladder structure to be present for the near-ring quasinormal wave solutions in the Schwarzschild geometry. Section 5.3 examined this in detail, starting with identifying Schwarzschild isometries $J_{\pm}$, which act as ladder operators on the spherical harmonics, as lifts of the angular isometry generators $a_{\pm}$ in Section 5.3.1. Moreover, the scaling limit of Y_{mm} was identified to reproduce the ground state $\phi_2^0(x_2)$ of the angular direction in the plane wave geometry. This established a complete identification of the angular ladder structure between the plane wave and Schwarzschild wave solutions. For the radial direction, studied in Section 5.3.2, a similar structure was identified—the vectors $X_{\pm}$, defined in equation (5.3.20), have $b_{\pm}$ as their scaling limits and produce a ladder structure of solutions in the Schwarzschild near-ring region. The ground state of this ladder structure, ψ_0, was verified to scale into the ground state ϕ_1^0 of the radial wave equation of the plane wave geometry, completing the association between the plane wave- and near-ring Schwarzschild solutions' ladder structures.

However, the $J_\pm$ and $X_\pm$ differ significantly: $J_\pm$ are exact isometry generators (Killing vectors), whereas $X_\pm$ are emergent symmetries (cf. Section 4.2.5)—vectors that locally act like symmetries on certain solutions, in this case the near-ring region. Nonetheless, under the Penrose limit, the $X_\pm$ are promoted to Killing vectors, generating exact isometries.

In conclusion, the Penrose limit onto equatorial photon ring geodesics effectively serves as a covariant prescription to implement the near-ring region and promotes its emergent symmetries to global isometries. This facilitates constructing the ladder structure of solutions and, consequently, deriving the QNM spectrum.

Appendix A - Argument for the WKB Schutz-Will Method

Consider the WKB solution for a three-region potential as introduced in Section 4.1.3, with QNM boundary conditions already applied. Such a solution looks like

$$\psi(x) = |Q(x)|^{-\frac{1}{4}} \begin{cases} B_- \exp\Big(-i\int^x \sqrt{|Q(z)|}dz\Big), & x < x_1 \\ C_+ \exp\Big(\int^x \sqrt{|Q(z)|}dz\Big) + C_- \exp\Big(-\int^x \sqrt{|Q(z)|}dz\Big), & x \in (x_1, x_2) \\ D_+ \exp\Big(i\int^x \sqrt{|Q(z)|}dz\Big), & x > x_2. \end{cases} \tag{A.1}$$

The solution must be C^1, which leads to four continuity conditions at the boundaries of region II, one for each of the function values of ψ at x_1 and x_2 as well as for the derivatives of ψ at x_1 and x_2. Although superficially, it looks like we have four degrees of freedom to satisfy these (the constants $B_-, C_\pm, D_+$), recall that the equation (4.1.8) that ψ has to satisfy is linear and hence we can always rescale ψ to set e.g. $B_- = 1$. This shows that we effectively only have three degrees of freedom to satisfy the four conditions, which in general will have no nontrivial solution.

However, there is at least one way out. Let us define

$$a = \int_{x_1}^{x_2} \sqrt{|Q(z)|}dz. \tag{A.2}$$

Then, continuity at x_1 and x_2 demands

$$B_- = C_+ + C_-, \quad D_+ = C_+ e^a + C_- e^{-a}. \tag{A.3}$$

Here we can see that in the case where $a = 0$, these conditions become linearly dependent and hence we only have three linearly independent conditions instead of four. Because of this, the three degrees of freedom in the constants in ψ are enough to make ψ a C^1 function. One way of achieving $a = 0$ is by having $x_1 = x_2$, i.e. to have the minimum of Q at $x_0 = x_1 = x_2$ with $Q(x_0) = 0$.

Since we are working with an approximate solution anyways, the exact QNM boundary conditions, demanding purely outgoing waves, do not need to be satisfied exactly. We could hence allow small ingoing components in our approximate solution and still be in the vicinity of the exact QNM solution in the vicinity of that frequency. Such small additional degrees of freedom (in the form of B_+ and D_- terms in the approximate solution (A.1)) could allow us to account for small positive values of a, which corresponds to a narrow region II, so x_1 and x_2 close together.

Appendix B - Spectrum of the Inverted Harmonic Oscillator

In this section, we derive the spectrum of the inverted harmonic oscillator with outgoing boundary conditions. Its dynamics are given by the Schrödinger equation

$$\psi''(\xi) + \xi^2\psi(\xi) = K\psi(\xi). \tag{B.1}$$

The equation (4.1.19) can be brought into this form by the substitutions

$$\xi = \left(\frac{Q_0''}{2}\right)^{\frac{1}{4}}(x - x_0), \quad K = -\sqrt{\frac{2}{Q_0''}}Q_0. \tag{B.2}$$

For $\xi \to \pm\infty$, the constant K becomes negligible and equation (B.1) turns into $\psi''(\xi) = -\xi^2\psi(\xi)$, which has the asymptotic solution

$$\psi(\xi) \sim e^{\pm i\frac{\xi^2}{2}} \tag{B.3}$$

where in the derivative we neglect terms of order lower than 2 in ξ. This motivates the ansatz

$$\psi_\pm(\xi) = h(\xi)e^{\pm i\frac{\xi^2}{2}}. \tag{B.4}$$

Before computing the equation that $h(\xi)$ should satisfy, we can make a choice for $\pm$. In the context of quasinormal modes, we are solely interested in outgoing solutions. This fixes the sign to $e^{+i\xi^2/2}$ to produce an increasing phase as ξ moves away from the origin. We now drop the $\pm$ notation, i.e. we consider

$$\psi(\xi) = h(\xi)e^{i\xi^2/2}. \tag{B.5}$$

To find the equation that h must fulfill, we insert this ansatz into equation (B.1) and multiply by $e^{-i\xi^2/2}$. This yields

$$\begin{aligned}(K - \xi^2)h(\xi) &= e^{-i\xi^2/2}\frac{d^2}{d\xi^2}\Big(h(\xi)e^{i\xi^2/2}\Big) \\ &= h''(\xi) + 2i\xi h'(\xi) + (-\xi^2 + i)h(\xi)\end{aligned} \tag{B.6}$$

Rearranging terms leads us to the equation

$$h''(\xi) + 2i\xi h'(\xi) + (-K + i)h(\xi) = 0. \tag{B.7}$$

To solve this, we employ a power series ansatz,

$$h(\xi) = \sum_{k=0}^{\infty} c_k \xi^k, \tag{B.8}$$

with which equation (B.7) becomes

$$\sum_{k=0}^{\infty}\Big[(k+2)(k+1)c_{k+2} + \Big(i(1+2k) - K\Big)c_k\Big]\xi^k = 0. \tag{B.9}$$

Comparison of coefficients then yields the recursion relation

$$c_{k+2} = \frac{K - i(1+2k)}{(k+2)(k+1)}c_k. \tag{B.10}$$

The function h should be such that the full solution $\psi(\xi) = h(\xi)e^{i\frac{\xi^2}{2}}$ still has the desired asymptotic behaviour. Let us analyse this more precisely. For large ξ, terms with large k dominate, with coefficients behaving as

$$c_{k+2} \approx \frac{-2i}{k+2}c_k \quad \Longrightarrow \quad c_k \approx \frac{(-2i)^{\lfloor k/2 \rfloor}}{k!!}\begin{cases} c_0, & k \text{ even}, \\ c_1, & k \text{ odd}. \end{cases} \tag{B.11}$$

Here, $k!!$ denotes the double factorial, for which $(2n)!! = 2^n n!$. Let us resum e.g. the even terms[20] for large ξ,

$$h(\xi) \sim \sum_{n\in\mathbb{N}} \frac{(-2i)^n}{(2n)!!}\xi^{2n} = \sum_{n\in\mathbb{N}} \frac{\left(-i\xi^2\right)^n}{n!} = e^{-i\xi^2}. \tag{B.12}$$

Hence, the full solution has asymptotic behaviour $\psi(\xi) \sim e^{-i\frac{\xi^2}{2}}$, which violates our boundary conditions. There is, however, a way out of this. We can require the series expansion (B.8) to terminate at a finite value, which is to say that we require the existence of an $n \in \mathbb{N}$ such that $c_{n+2} = 0$, $c_n \neq 0$. This yields a polynomial expression for h that does not interfere with the boundary conditions. Imposing this termination condition on the coefficients (B.10) requires the fractional factor to be zero, which in turn is satisfied if and only if

$$K = K_n = i(1 + 2n), \quad n \in \mathbb{N}_0. \tag{B.13}$$

Curiously, this is simply the analytic continuation $\omega \to i\omega$ of the result one finds for the regular, non-inverted harmonic oscillator. In particular, we find that the eigenfunctions $\psi_n(\xi)$ to the eigenvalues K_n behave as

$$\psi_n(\xi) \sim (\xi^n + (\text{terms of order } \xi^{n-2} \text{ and lower}))e^{i\xi^2/2} \tag{B.14}$$

Hence, asymptotically, we have

$$\psi_n(\xi) \sim \xi^n e^{i\xi^2/2} \tag{B.15}$$

Appendix C - Review: Spherical Harmonics

Spherical harmonics are eigenfunctions of the Laplacian on S^2,

$$\Delta_{S^2} = \partial_\theta^2 + \cot\theta\partial_\theta + \frac{1}{\sin^2\theta}\partial_\varphi^2, \tag{C.1}$$

i.e. functions satisfying $\Delta_{S^2} Y = \lambda Y$. This section provides the necessary definitions and background for spherical harmonics and serves as a refresher on how they work. We roughly follow the exposition given by Griffiths [13], adapted to our purposes.

C.1 Algebraic Structure and Eigenvalues

In this section we use the $\mathfrak{so}(3)$ algebra defined by the Schwarzschild Killing vectors $K_{(a)}$, $a = 1, 2, 3$ from equation (3.1.18) to derive the eigenvalue spectrum of the Laplacian on S^2. We begin by making the definitions

$$J_a = \frac{1}{i}K_{(a)}, \quad \boldsymbol{J}^2 = \delta_{ab}J_aJ_b, \quad J_\pm = J_1 \pm iJ_2 \tag{C.1}$$

and compute the commutators

$$[J_a, J_b] = i\varepsilon_{abc}J_c, \quad [\boldsymbol{J}^2, J_a] = 0, \quad [\boldsymbol{J}^2, J_\pm] = 0, \quad [J_3, J_\pm] = \pm J_\pm, \tag{C.2}$$

[20]The sum over the odd terms is more involved, and we refer to [14] which provides a closed form expression that turns into $h(\xi) \sim \operatorname{erf}\left(e^{-i\pi/4}\xi\right)e^{-i\xi^2}$ for the case at hand. The corresponding $\psi(\xi)$ violates the outgoing boundary conditions, leaving the argument for the series' termination intact.

where ε_{abc} denotes the Levi-Civita tensor in three dimensions with $\varepsilon_{123} = 1$. We further note that

$$\boldsymbol{J}^2 = -\Delta_{S^2}, \tag{C.3}$$

i.e. the problem of finding eigenfunctions of the Laplacian on S^2 boils down to finding eigenvectors of $\boldsymbol{J}^2$. Since $\boldsymbol{J}^2$ commutes with J_3, we can find simultaneous normalised eigenvectors $Z_{\lambda\mu}$ with

$$\boldsymbol{J}^2 Z_{\lambda\mu} = \lambda Z_{\lambda\mu}, \quad J_3 Z_{\lambda\mu} = \mu Z_{\lambda\mu}. \tag{C.4}$$

We now derive the eigenvalues λ and μ and subsequently define the $Y_{\ell m}$ in terms of the $Z_{\lambda\mu}$. We begin by noting that the $J_\pm$ act as raising and lowering operators for μ, i.e.

$$J_3 J_\pm Z_{\lambda\mu} = J_\pm J_3 Z_{\lambda\mu} + [J_3, J_\pm] Z_{\lambda\mu} = (\mu \pm 1) Z_{\lambda\mu} \quad \Rightarrow \quad J_\pm Z_{\lambda\mu} = Z_{\lambda,\mu\pm1}, \tag{C.5}$$

while leaving λ unchanged,

$$\boldsymbol{J}^2 J_\pm Z_{\lambda\mu} = J_\pm \boldsymbol{J}^2 Z_{\lambda\mu} = \lambda J_\pm Z_{\lambda\mu}. \tag{C.6}$$

From

$$\lambda = \int_{S^2} Z^*_{\lambda\mu} \boldsymbol{J}^2 Z_{\lambda\mu} = \mu^2 + \int_{S^2} Z^*_{\lambda\mu} (J_1^2 + J_2^2) Z_{\lambda\mu} \geq \mu^2 \tag{C.7}$$

we infer that $\lambda \geq |\mu|^2 \geq 0$. Hence, for a given λ, there exists maximal and minimal values $\mu_{\max}, \mu_{\min}$ that the eigenvalue μ can take, so that

$$J_+ Z_{\lambda\mu_{\max}} = 0, \quad J_- Z_{\lambda\mu_{\min}} = 0. \tag{C.8}$$

One can derive that

$$\boldsymbol{J}^2 = J_\pm J_\mp + J_3^2 \mp J_3, \tag{C.9}$$

from which it follows that

$$\lambda Z_{\lambda\mu_{\max}} = \boldsymbol{J}^2 Z_{\lambda\mu_{\max}} = (J_- J_+ + J_3^2 + J_3) Z_{\lambda\mu_{\max}} = \mu_{\max}(\mu_{\max} + 1) Z_{\lambda\mu_{\max}}. \tag{C.10}$$

Introducing the shorthand $\ell = \mu_{\max}$, we find $\lambda = \ell(\ell+1)$. Similarly, we have

$$\lambda Z_{\lambda\mu_{\min}} = \boldsymbol{J}^2 Z_{\lambda\mu_{\min}} = (J_+ J_- + J_3^2 - J_3) Z_{\lambda\mu_{\min}} = \mu_{\min}(\mu_{\min} - 1) Z_{\lambda\mu_{\min}}. \tag{C.11}$$

This implies that

$$\ell(\ell+1) = \mu_{\min}(\mu_{\min} - 1) \quad \Rightarrow \quad \mu_{\min} = -\ell. \tag{C.12}$$

Hence, the allowed values for μ lie between $-\ell$ and ℓ, with integer steps between them. Therefore, $\lambda = \ell(\ell+1)$ can only be an eigenvalue if the distance $\mu_{\max} - \mu_{\min} = 2\ell$ is integral, i.e. if ℓ is a half-integer. To summarise, we have the eigenvalues

$$\lambda = \ell(\ell+1) \quad \text{and} \quad \mu = m \in \{-\ell, -\ell+1, ..., \ell-1, \ell\} \tag{C.13}$$

where ℓ is a half-integer. We conclude by defining the spherical harmonics as

$$Y_{\ell m} = Z_{\ell(\ell+1),m} \tag{C.14}$$

As a last remark, note here that not necessarily all values of ℓ and m derived herein are eigenvalues of the operators $\boldsymbol{J}^2$ and J_3. Indeed, we have shown the converse: Any operators satisfying the algebra (C.2) have eigenvalues of the derived form, but by no means all values of this are eigenvalues. E.g. in the next section, for the representation on $L^2(S^2)$, non-integer values of ℓ and m are not allowed, as this would make the φ-dependence non-periodic and hence discontinuous. Nonetheless, the spectrum abides by the rules derived in this section.

C.2 Explicit Forms of the Eigenfunctions

In this section, we derive the explicit forms of spherical harmonics needed in this thesis. To begin, we need the explicit expressions for J_3 and $J_\pm$ as differential operators. These are given by

$$J_3 = -i\partial_\varphi, \quad J_\pm = e^{\pm i\varphi}\big(\mp\partial_\theta - i\cot\theta\partial_\varphi\big). \tag{C.1}$$

To derive expressions for $Y_{\ell m}(\theta,\varphi)$, we employ the separation ansatz

$$Y_{\ell m}(\theta,\varphi) = N_{\ell m}P_{\ell m}(\theta)f_{m(\varphi)}. \tag{C.2}$$

where $N_{\ell m}$ is a normalisation constant. The eigenvalue equation $J_3Y_{\ell m} = mY_{\ell m}$ fixes $f_m(\varphi) = e^{im\varphi}$. By periodicity, m must be an integer and cannot take on half-integer values - as a consequence, ℓ must be an integer as well. To find the θ-dependence $P_{\ell m}(\theta)$, we construct a solution $P_{\ell\ell}(\theta)$, from which the solutions of lower m are obtained via the lowering operator,

$$Y_{\ell m} = (J_-)^{\ell-m}Y_{\ell\ell} \quad \Rightarrow \quad P_{\ell m} = [\partial_\theta + (m+1)\cot\theta]...[\partial_\theta + \ell\cot\theta]P_{\ell\ell} \tag{C.3}$$

and so on. The solution $Y_{\ell\ell}$ is subject to the condition

$$J_+Y_{\ell\ell} = 0 \quad \Rightarrow \quad [-\partial_\theta + \ell\cot\theta]P_{\ell\ell} = 0, \tag{C.4}$$

which is solved by $P_{\ell\ell}(\theta) = \sin^\ell\theta$. Hence, an arbitrary spherical harmonic is given by

$$Y_{\ell m}(\theta,\varphi) = N_{\ell m}(J_-)^{\ell-m}\big[\sin^\ell\theta\, e^{i\ell\varphi}\big]. \tag{C.5}$$

Notably, the φ-dependence is always of the form $e^{im\varphi}$. Note here that $J_+Y_{\ell\ell} = 0$ is a sufficient condition for it to be an eigenfunction of $\boldsymbol{J}^2$, since

$$\boldsymbol{J}^2Y_{\ell\ell} = \big(J_-\underbrace{J_+}_{\to 0} + J_3^2 + J_3\big)Y_{\ell\ell} = \ell(\ell+1)Y_{\ell\ell}, \quad \ell, m \in \mathbb{N}, \quad |m| \leq \ell \tag{C.6}$$

The fact that then, $J_{\ell m}$ is an eigenfunction as well follows from the discussion in the previous section.

Bibliography

[1] K. D. Kokkotas and B. G. Schmidt, "Quasi-Normal Modes of Stars and Black Holes," *Living Reviews in Relativity*, vol. 2, 1999, [Online]. Available: https://arxiv.org/abs/gr-qc/9909058v1

[2] M. P. P. Closa, "The WKB Approximation: An application to the alpha decay," 2016.

[3] K. Fransen, "Quasinormal Modes from Penrose Limits," 2023, [Online]. Available: https://arxiv.org/pdf/2301.06999

[4] D. Kapec and A. Sheta, "PP-Waves and the Hidden Symmetries of Black Hole Quasionormal Modes," 2024, [Online]. Available: https://arxiv.org/pdf/2412.08551

[5] B. Schutz and C. Will, "Black hole normal modes - A semianalytic approach," *Astrophysical Journal*, vol. 291, pp. L33–L36, Apr. 1985, doi: 10.1086/184453.

[6] S. Hadar, D. Kapec, A. Lupsasca, and A. Strominger, "Holography of the Photon Ring," 2022, [Online]. Available: https://arxiv.org/pdf/2205.05064

[7] M. Blau, "Plane Waves and Penrose Limits," 2004, [Online]. Available: http://blau.itp.unibe.ch/lecturesPP.pdf

[8] R. Penrose, "Any Space-Time has a Plane Wave as a Limit," *Differential Geometry and Relativity*. Springer Netherlands, pp. 271–275, 1976. doi: 10.1007/978-94-010-1508-0_23.

[9] M. Blau, M. Borunda, M. O'Loughlin, and G. Papadopoulos, "Penrose Limits and Spacetime Singularities," *Class.Quant.Grav.*, vol. 21, p. L43, 2004, doi: 10.1088/0264-9381/21/7/L02.

[10] M. Blau, *Lecture Notes on General Relativity*. 2024. [Online]. Available: http://blau.itp.unibe.ch/newlecturesGR.pdf

[11] N. Slotboom, "veclib: Component-Based Differential Geometry/General Relativity Library for Python." [Online]. Available: https://github.com/TheVecGH/veclib

[12] E. W. Leaver, "An analytic representation for the quasi-normal modes of Kerr black holes," *Proc. R. Soc. Lond. A*, vol. 402, pp. 285–298, 1985.

[13] D. J. Griffiths, *Introduction to Quantum Mechanics*, 2nd ed. Pearson Education International, 2004.

[14] E. W. Weisstein, "Double Factorial.," *From MathWorld–A Wolfram Web Resource.*, [Online]. Available: https://mathworld.wolfram.com/DoubleFactorial.html